SERPENTINIZATION AND FRACTURE FORMATION IN PERIDOTITES ON OTRØY, WESTERN GNEISS REGION, NORWAY:

LATE STAGE PT-CONDITIONS AND IMPLICATIONS FOR TECTONIC DECOMPRESSION

- THESIS -

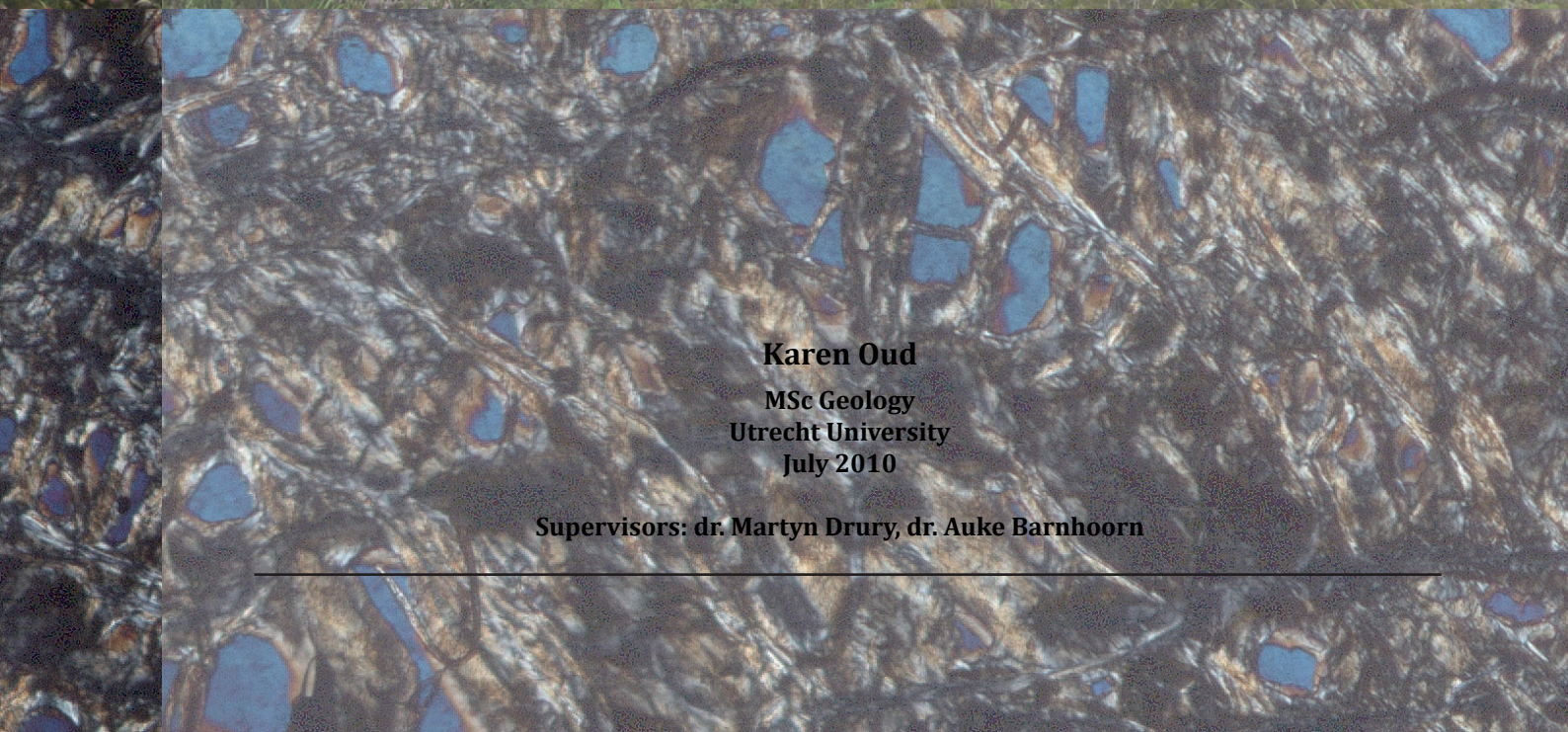

Karen Oud
MSc Geology
Utrecht University
July 2010

Supervisors: dr. Martyn Drury, dr. Auke Barnhoorn

Serpentinization and fracture formation in peridotites on Otrøy, Western Gneiss Region, Norway:

Late stage PT-conditions and implications for tectonic decompression

...or, joyfully unraveling the mes(s/h) that's called **serpentine**...

Dutch:

ser•pen•ti•ne lange, opgerolde strook van gekleurd papier waarmee men bij feesten gooit

English:

ser•pen•ti•ne complicated and difficult to understand

Karen Oud
Utrecht, July 2010

TABLE OF CONTENTS

ABSTRACT

Hydration reactions in mantle peridotites substituting olivine with serpentine causes a volume change of 20-55% in the rocks. This volume change is accompanied by fracturing at several scales. Fractures form sets according to a hierarchical fracture pattern or a kernel pattern, both characterized by fracture sets at 90° angles to each other. The main difference between both patterns is in the onset of fracturing. This is either caused by stress differences in the rock, which forms one set at first and other sets later on (hierarchical fracturing); or by a different degree of serpentinization within so-called kernels (blocks in the rock), which form fractures in three directions at the same time (kernel pattern).
To see whether other – larger scale – processes, like tectonic stresses, are also involved in fracture formation, two peridotite bodies on the island of Otrøy, WGR, Norway, are studied. The abundance of fractures and the mode of fracturing will be determined, as well as the pressure and temperature conditions of their formation, in order to place the hydration and fracturing of the peridotites in the larger scale tectonic history of the Western Gneiss Region.

Spatial analyses are performed determining the fracture form and orientation, on both large and small scale. A clear dominance of a set of early fractures in one direction would give implications for extensional tectonic stresses perpendicular to that, and similarity of fracture normals with orogen-normal extensional features in the surrounding rocks would show the influence of tectonic stress on fracture formation.
Both peridotite bodies show a fracture pattern with fracture sets having approximately 90° angles, but no relative timing between sets can be observed in the field. Stereographic projections of the normals to the fracture planes form a range between (W)NW-(E)SE, which is the same direction of the orogen-normal extension and exhumation of the peridotite bodies. One set clearly plots near the direction of the WNW-oriented orogen-normal lineations in the surrounding gneiss. This implies that the orientation of at least one set of fractures was caused by tectonic extension during exhumation.
Fracture orientation with respect to the compositional banding would be caused by anisotropy between the compositional layers and subsequent differentiation in volume change. Results from stereographic rotation of fracture poles to equal compositional bandings throughout the bodies show only minor dependence. However, it can explain the scatter between poles within sets, as well as the slight difference in orientation of the first formed fracture set between both bodies: Ugelvik has more NW directed poles in this set and Raudhaugene has more WNW directed poles.

Determination of fracture filling – e.g. serpentine polymorphs and their growth forms – and the mode of fracturing are used to quantify pressure and temperature conditions of serpentinization and fracturing in the latest stages of the tectonic history. This is done using electron microprobe and microscope observations.
Two generations of mesh formation are present; lizardite formed first and is later (partly) replaced by chrysotile. Mesh formation went on during fracturing and fracture filling in the rock. At least four generations of (ongoing) fracture filling are observed: a first filling by banded/kinked chrysotile changes to triangular lizardite, ribbon antigorite and micro-granular lizardite, followed by some cross-fractures of fibrous and banded/kinked chrysotile. Calcite is present in many fractures as a latest stage, but is probably not linked to the first fracture filling phase.
Early hydration occurs at about 530°C and 0.4-0.5 GPa through reaction of olivine (± orthopyroxene) + talc (± chlorite) + water to serpentine (lizardite). Later serpentine polymorphs are formed by ongoing reaction of mainly olivine and orthopyroxene with water, and by recrystallization of earlier forms of serpentine. Calcite forms after serpentinization, below 180°C and below 0.3 GPa, through infiltration of a CO_2-rich fluid in the system, which binds free Ca that has probably provided by Ca-rich garnet and amphibole in the rock.

1 INTRODUCTION

Serpentinized peridotites have been drawn much attention recently in different fields of research. The discovery of ultra-high pressure minerals like coesite and micro-diamond in peridotites has profoundly changed the ideas on their early evolution; their origin lies much deeper and earlier than always thought [Brueckner and Van Roermund, 2004]. The Western Gneiss Region (WGR) in Norway plays an important role in this matter. During the last two decades, it is found that the WGR preserves relicts of the Archaean mantle, which has led to conclusion that it was subjected to ultra-deep continental subduction [Spengler, 2006 and references therein].
The latest stages of evolution of these rocks has not been extensively researched in the past. However, the ongoing question on climate change has led to some revolutionary new ideas: it is believed that peridotites can provide large storage capacities for CO_2. For this, enhancement of the natural fracturing that takes place in the rock due to serpentinization would be necessary [Kelemen and Matter, 2008]. Serpentinization occurs during the latest stages of exhumation, due to hydration of the rock.

However, still not very much is known about the late stage processes in peridotites during their retrograde evolution, which will be needed for this CO_2 storage question. O'Hanley [1992, 1996] and Iyer et al. [2008] state that fracturing of peridotites at large and small scale is caused by the volume change in the rock during serpentinization. Iyer et al. [2008] also propose that the orientation of fracturing is mainly determined by anisotropy in rock properties or in stress in the rock. The question here is to what extent stresses can occur. Is the rock only affected by local anisotropy, or do large scale – tectonic – stresses, such as extension and subsequent exhumation of a peridotite body, also play a role?

In this study, I want to determine if there is a link between both phenomena, thus, what is the cause of fracturing in serpentinized peridotites. Two peridotite bodies on the island of Otrøy in the WGR will be subject of this research. Furthermore, I will try to give constraints on PT conditions during serpentinization and fracturing of the peridotites.
This will be done on the basis of determining different generations of fracturing, in both outcrop and thin sections. Chemistry and the mode of mineral growth within the serpentine mesh and fractures will be determined. Also, a spatial analysis of the fracture patterns in outcrop will be done. With these, implications will be made for the exact cause of fracturing in the peridotites, compared to the processes as described in literature.

2 GEOLOGICAL SETTING

2.1 TECTONICS OF THE SCANDINAVIAN CALEDONIDES

The Caledonian orogeny comprises a series of orogenic events during the Paleozoic, all contributing to the building of the Caledonian mountain belt. In the Mesozoic, the Caledonides broke up into the present-day Appalachian mountain belt, the Greenland Caledonides (east Greenland and Spitsbergen), the British Caledonides (Scotland, Ireland, Shetland Islands) and the Scandinavian Caledonides [Spengler, 2006].
The continents Laurentia, Baltica and Avalonia, which had been part of the supercontinent Gondwana until the late Precambrian, approached each other just south of the equator during the late Ordovician. First, Baltica and Avalonia were sutured together due to closure of the Tornquist Ocean. The merged continent Baltica-Avalonia became then sutured to Laurentia by closure of the Iapetus Ocean (figure 2.1).

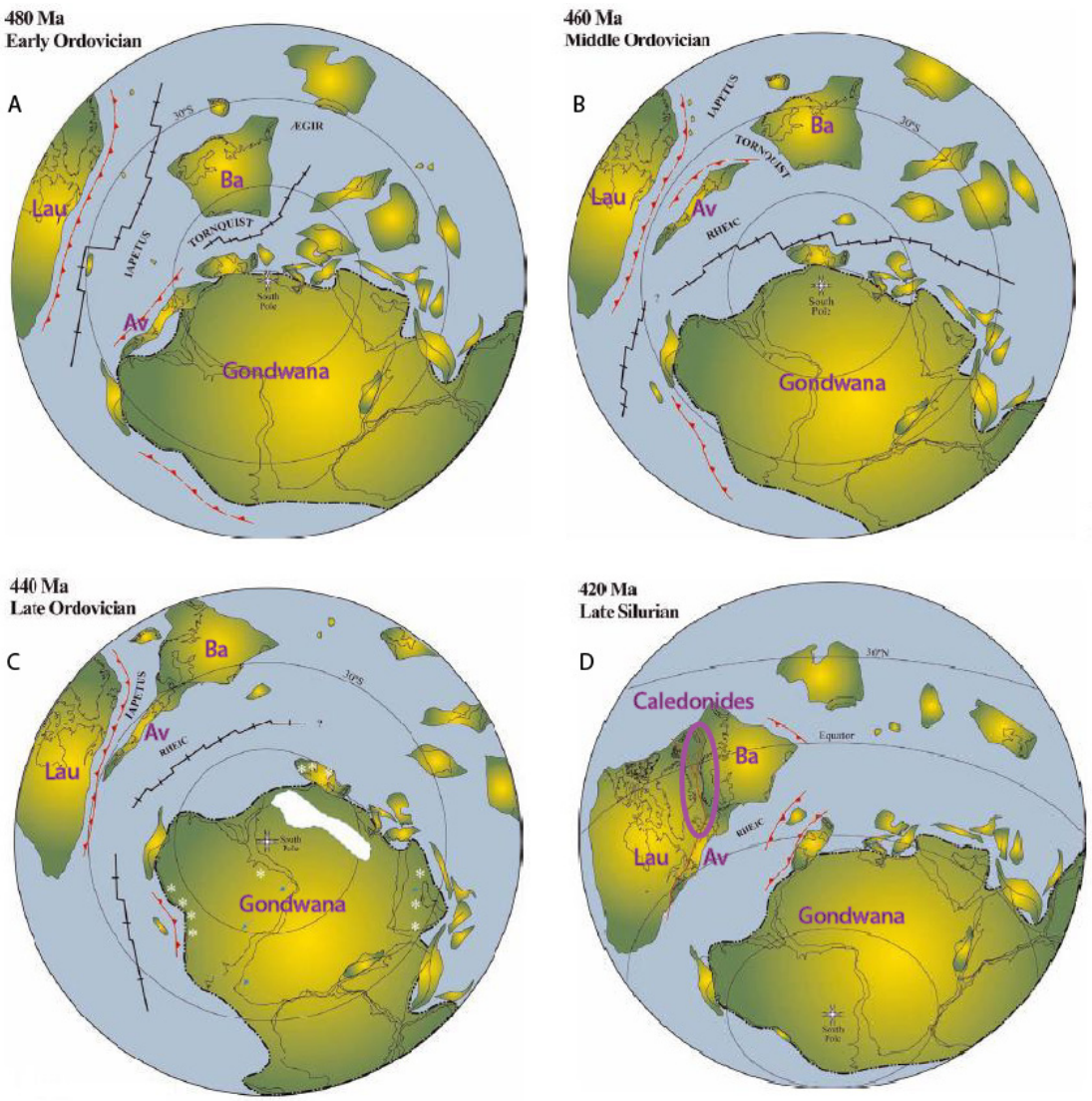

Figure 2.1. *Plate reconstructions of Gondwana, Baltica (Ba), Laurentia (Lau) and Avalonia (Av) from the Early Ordovician (A) till the Late Silurian (D). In (D), the position of the Caledonian Orogeny is shown. After Cocks and Torsvik [2006].*

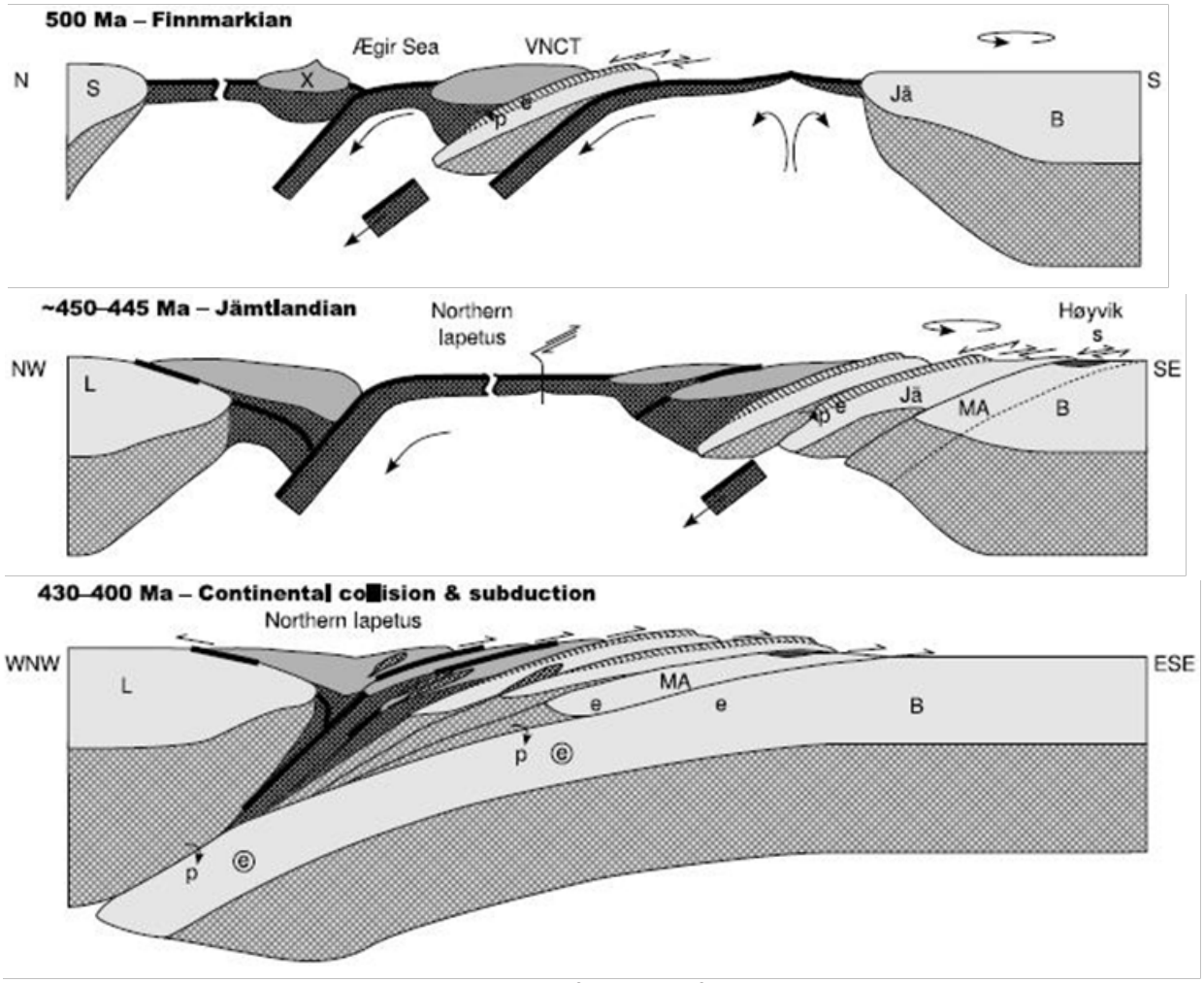

Figure 2.2. *Most important phases during the formation of the Caledonian orogeny. L – Laurentia, B – Baltica, S – Sibiria, X – volcanic arc, Jä – Jämtland continental margin, MA – Middle Allochthon, p – peridotite, e – HP eclogite, (e) – UHP eclogite, s – sediment. After Spengler [2006].*

Baltica (northeast) and Avalonia (southwest) merged together at the transition between the Ordovician and Silurian (440 Ma), due to southward, slightly oblique, subduction in the Tornquist Ocean. The merged continent moved further northward towards the equator, while rotating anticlockwise. The Iapetus Ocean, bounded by Baltica-Avalonia in the east and Laurentia in the west, was already closing since 480 Ma. This reached a climax during the Silurian: between 440 and 420 Ma, the onset of continental collision between Baltica-Avalonia and Laurentia took place due to westward intra-oceanic subduction. The eventual suture of both continents and closure of the Iapetus Ocean occurred between 430 and 420 Ma, starting in the north and forming the supercontinent Laurussia [Torsvik et al, 1996; Spengler, 2006]. Mountain building along the boundary of both former continents went on during the early Devonian (until about 400 Ma) due to subsequent subduction of the continental plate margin of Baltica-Avalonia beneath Laurentia.

The convergence of Baltica-Avalonia to Laurentia caused some island arcs that were present in between to accrete onto the continents through subduction. This accretion took place with several compressive and transpressive tectonothermal events, and subsequent local HP and UHP metamorphism within the involved terranes.

The most important phases and their corresponding rock assemblages that are recognized in this series of accretion are the following [Spengler, 2006], also shown in figure 2.2:
1) Finnmarkian (500 Ma). Subduction of the margin of the Norrbotten microcontinent beneath the Virisen (oceanic) volcanic arc; the composite terrane is called Virisen/Norrbotten (VNCT). This

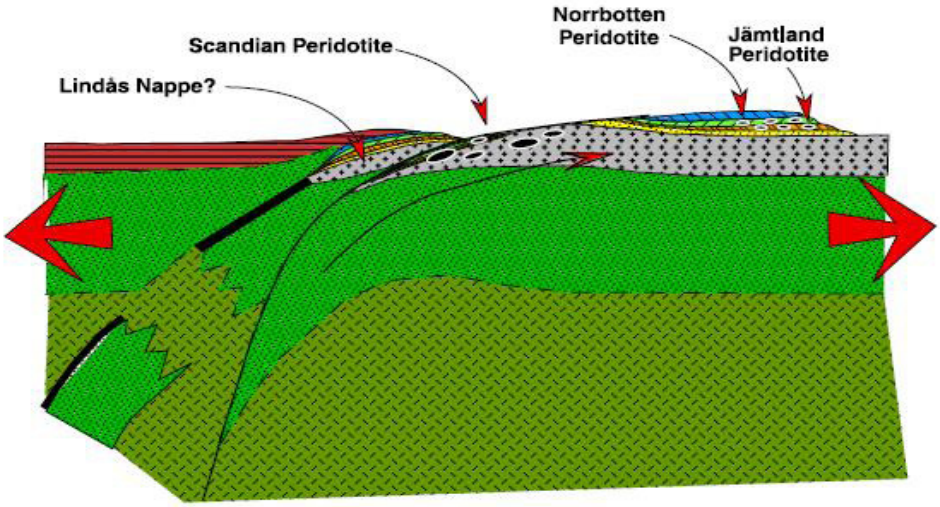

Figure 2.3. *Post-Scandian phase (400-380 Ma). Orogenic-normal extension without a basal thrust caused exhumation of the WGR and its UHP peridotites. After Brueckner and Van Roermund [2004].*

caused sub-oceanic peridotites to become emplaced into the continental crust.
2) Jämtlandian (450-445 Ma). The margin of Baltica subducts beneath the VNCT. Sub-continental peridotites are emplaced from the VNCT mantle wedge into the subducted Baltic crust. Subsequently, the subducted and HP metamorphosed Baltic crust was exhumed and delaminated from its sub-continental lithosphere.
3) Scandian (425-400 Ma). Westward subduction of the continental margin of Baltica into the mantle beneath Laurentia, up to 150 km depth. This yielded formation of (U)HP eclogite in the subducting Baltic crust and emplacement of UHP peridotites from the mantle wedge above (with sub-continental lithospheric mantle affinity of Baltica and Laurentia) into the subducted basement.
4) Post Scandian (400-380 Ma). Orogenic-normal extension without a basal thrust (buoyancy enhanced exhumation [Brueckner and Van Roermund, 2004], see figure 2.3) and subsequent exhumation of the UHP metamorphosed rocks in the southern Caledonides (Western Gneiss Region, WGR). The nappe pile which had been formed as a consequence of the earlier convergent stages was remodelled to a pile of extensional allochthons, bounded by low angle brittle and ductile shear zones.

During accretion of the oceanic arcs and continental terranes, several nappes of (U)HP crustal metamorphic rocks and upper mantle peridotite were stacked on top of each other in the present-day Scandinavian Caledonides, on top of the Precambrian basement. The nappes and Precambrian basement are subdivided into tectonic units (complexes): the Autochthon and Parautochthon and the Lower, Middle, Upper and Uppermost Allochthon.
The nappes that contain eclogitized subducted crust with peridotites incorporated from the hanging wall are the Köli and Seve Nappe Complex (Upper Allochthon) and the Western Gneiss Region (Parautochthon), shown in figure 2.4. The first two were subducted and metamorphosed during the Finnmarkian and Jämtlandian stage, and the Western Gneiss Region was subducted and metamorphosed during the Scandian stage.

2.2 Western Gneiss Region

The biggest exposure of parautochthonous basement in the Scandinavian Caledonides is formed by the Western Gneiss Complex in the Western Gneiss Region (WGR) in the southwest of Norway. The complex serves as a tectonic window through the pile of Caledonian thrust sheets that have been stacked around and on top of it. The Precambrian basement consists mainly of tonalitic to granodioritic ortho- and paragneisses, together with HT/HP granulites, amphibolites and anorthosites and widespread occurring bodies of eclogite and peridotite, all metamorphosed during Scandian (U)HP metamorphism.

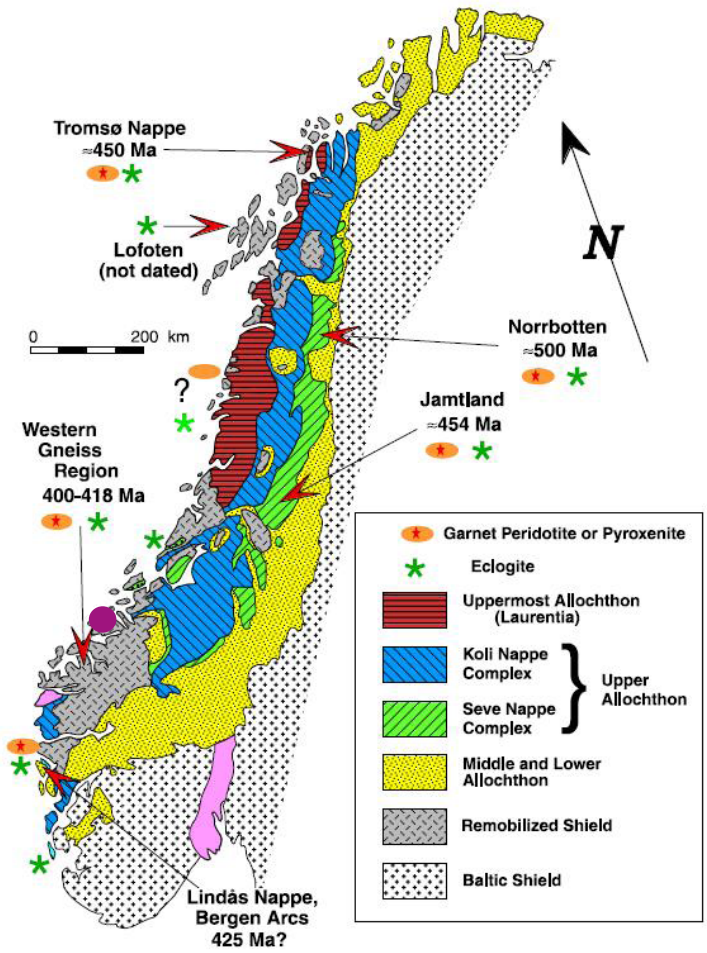

Figure 2.4. *Simplified overview of the Scandinavian Caledonides, showing the major (U)HP terranes, and the location of mantle-derived peridotites. The location of the island of Otrøy in the Western Gneiss Region is depicted with a purple dot. After Brueckner and Van Roermund [2004].*

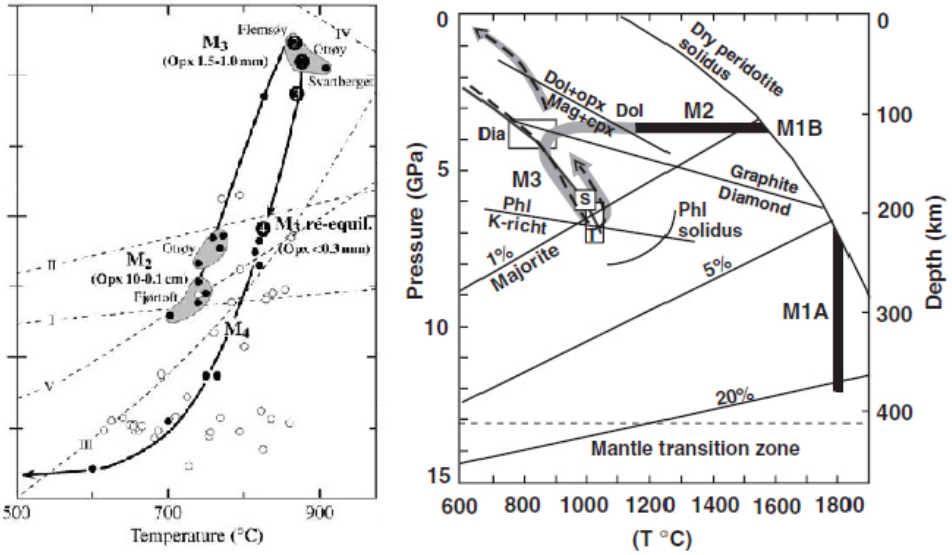

Figure 2.5. *PT paths for the early evolution of WGR peridotites. Left: from Spengler et al. [2009], pressure range at the vertical axis is 0-7 GPa (upward). Right: from Scambelluri et al. [2008]. Both paths clearly show peak metamorphic conditions of 6-7 GPa.*

Lens-shaped peridotite bodies have been incorporated in the eclogitized crust throughout the whole WGR. They are most abundant in the area between Nordfjord and Moldefjord (the north-western part) and range in size between a few metres and a few kilometres. These peridotites

can be divided into different groups. Most common are the chl-amph-peridotites. Gt-peridotites are less common. These can be subdivided into Fe-Ti gt-peridotites (crustal origin) and Mg-Cr gt-peridotites (originated from the sub-continental lithospheric mantle, SCLM). The first are believed to have been emplaced during the Proterozoic, and to have experienced Scandian metamorphism. The SCLM peridotites have originated and cooled in the upper mantle during the Archaean, and have been incorporated in the crustal gneisses of the subducting lithosphere during Scandian (U) HP metamorphism [Spengler, 2006].
It is shown that some of the latter have equilibrated at depths of about 130 km, at 700-950oC and 20-45 kbar, thus 2 to 4.5 GPa. Some of the northern gt-peridotite bodies in the WGR have relicts of majoritic garnet, which implies that these peridotites must have formed at depths of over 185 km and 6 GPa [Brueckner and Van Roermund, 2004]. PT paths for WGR peridotites (amongst which those at Otrøy) from Scambelluri et al. [2008] and Spengler et al. [2009] are shown in figure 2.5. They will be discussed later on, in subsection 8.1.3.
The eclogites in the WGR have been equilibrated at 600 to over 850°C, from southeast to northwest. This is consistent with northwestward subduction of the WGR into the mantle beneath Laurentia to depths of 200 km during Scandian continent-collision.

Brueckner and Van Roermund [2004] state that exhumation of the WGR was driven by buoyancy, instead of being driven by orogenic collapse and an associated large basal thrust. This theory is illustrated in figure 2.6. The first stage of exhumation, during the late Scandian and post Scandian phase, was relatively fast: approximately 10 mm/yr from 407-395 Ma. From 395-375 Ma, exhumation was slower with 1 mm/yr. Fast exhumation driven by buoyancy can explain why some of the HP and UHP mineral assemblages, as can be found in the Mg-Cr gt-peridotites, do not show extensive signs of retrograde metamorphism, and have many remains of their original (U)HP mineral assemblage.

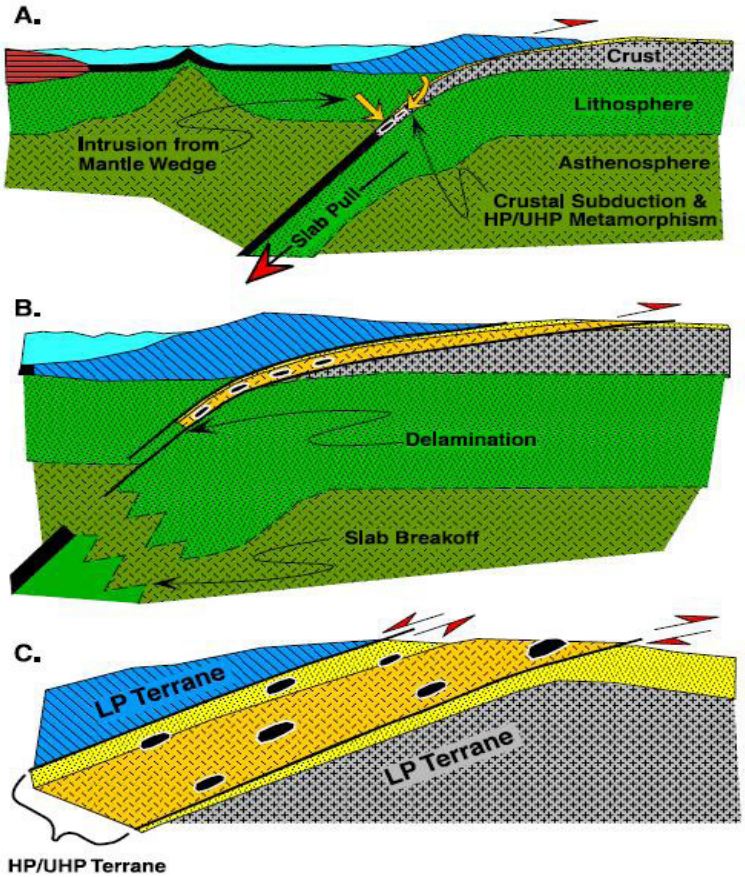

Figure 2.6. *The subduction/eduction model for HP/UHP metamorphic terranes from Brueckner and Van Roermund [2004]. Yellow arrows in (A) show the intrusion of UHP SCLM peridotites (black lenses) from the overriding plate into the subducting slab. The UHP terrane is subsequently exhumed by extension without a large basal thrust.*

2.3 Otrøy

The island of Otrøy, near the coast in the northwestern part of the WGR, mainly consists of Proterozoic basement. A simplified geologic map of the western part of the island is shown in figure 2.7. Banded dioritic gneiss and migmatitic or augen-orthogneiss are interlayered, they have mid-Proterozoic ages [Spengler, 2006]. Within the orthogneiss, lenses of eclogite, retro-eclogite and gt-amphibolite occur. The gneisses show a strong foliation, directed WNW-ESE, which is isoclinally folded with the axial planes having the same orientation.
In the western part of the island, two Mg-Cr gt-peridotite bodies are present, approximately 1 km from each other. One other peridotite body is present more to the south, which is only about 100m long, but this one is not considered in this study. The two bodies are both about 1 km in length, and about 500 m (Raudhaugene) to 700 m (Ugelvik) in width. Their long direction lies more or less along the foliation of the surrounding gneiss. An exposed contact between both rocks does not occur [Carswell, 1963], but the smallest distance of 10 m is found at the northern margin of the Raudhaugene peridotite body. Also, nowhere in the surrounding gneiss a high temperature contact aureole is found, and instead, strong shearing structures are observed [Carswell, 1963], which is evidence for tectonic emplacement of the peridotite bodies within the surrounding rocks.
The southern part of the island is separated with the northern part by a southward dipping thrust fault. The rocks above the thrust consist of allochthonous paragneisses, which are of considerable lower metamorphic grade than the northern part of the island. The paragneisses have been placed within the basement by thrusts, they are remnants of allochthonous thrust nappes. No eclogites are present within the paragneisses.

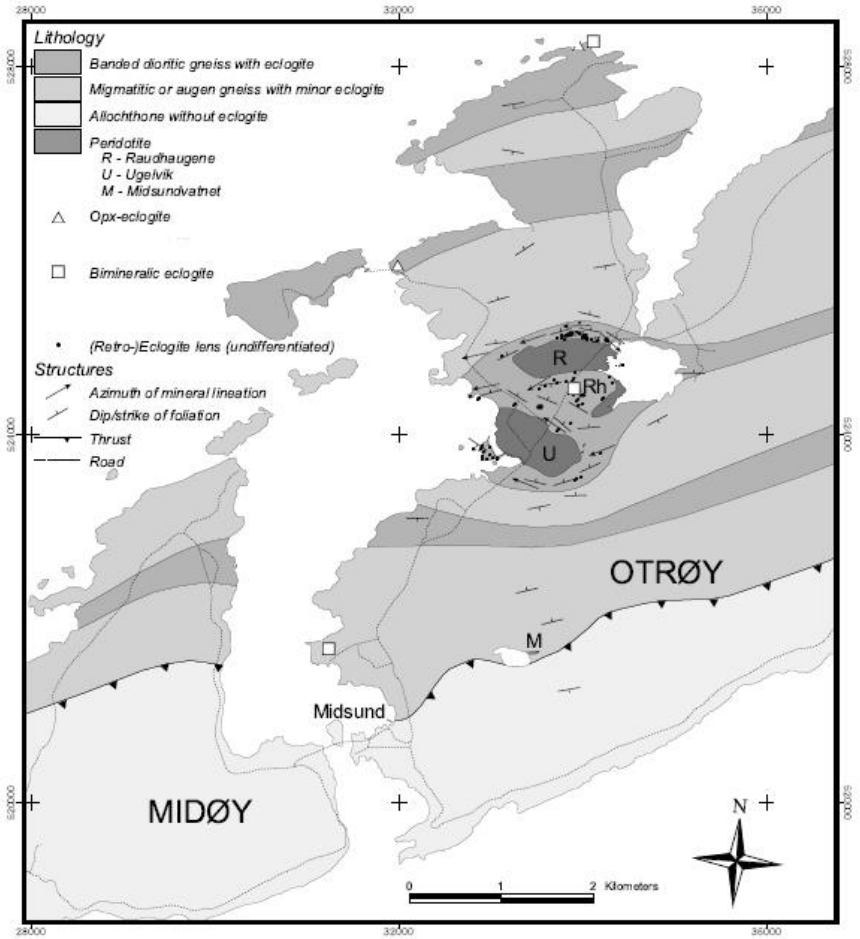

Figure 2.7. *Simplified geological map of the western part of Otrøy, with the peridotite bodies embedded in the basement gneiss and the foliation within these surrounding rocks clearly shown. After Spengler [2006].*

Both peridotite bodies are heavily serpentinized (over 60%). They have a composition ranging from dunite to harzburgite (see figure 2.8 for a classification of ultramafic rocks), which is shown within a strong compositional banding. The Raudhaugene peridotite body has somewhat less dunite and more lherzolite than Ugelvik [Drury et al., 2001]. Some harzburgite bands are rich in garnet or clinopyroxene, or both. Dunite bands are sometimes relatively rich in orthopyroxene.
Within the peridotites, lenses of gt-pyroxenites occur, which differ in thickness of some mm's up to about ten cm's. Some are richer in orthopyroxene, and some in clinopyroxene. In the Raudhaugene peridotite body, there are more pyroxenite lenses present compared to the Ugelvik peridotite body. These are especially abundant in the centre of the Raudhaugene body. The relative enrichment of the pyroxenite lenses in garnet is quite exceptional compared to other WGR peridotite bodies.
Medaris [1984] describes four mineral assemblages that are found on Otrøy and the area south of this, between Nordfjord and Storefjord. These are olivine-orthopyroxene-clinopyroxene-garnet (1), olivine-orthopyroxene-pargasitic amphibole-garnet (2), olivine-orthopyroxene-pargasitic amphibole-spinel (3) and a later formed assemblage of olivine-orthopyroxene-tremolite-chlorite (4). As will be discussed in subsection 7.1, this is quite consistent with what is found in the rocks in this study. Only pargasitic amphibole was not observed here, but this is probably due to a generalization of amphibole to tremolite under the microscope.
Mineral assemblages as mentioned in Spengler [2006] are quite similar. He presents an early assemblage of olivine-garnet-spinel-clinopyroxene-orthopyroxene. Late mineral phases are amphibole, serpentine, chlorite and magnetite; amphibole often in the vicinity of the kelyphite surrounding garnet, and often containing inclusions of spinel.

The compositional banding is folded with open to tight folds in both bodies. In Raudhaugene, this occurs more extensively than in Ugelvik. There, the compositional banding has a quite consistent orientation, whereas that of Raudhaugene shows quite some variation.

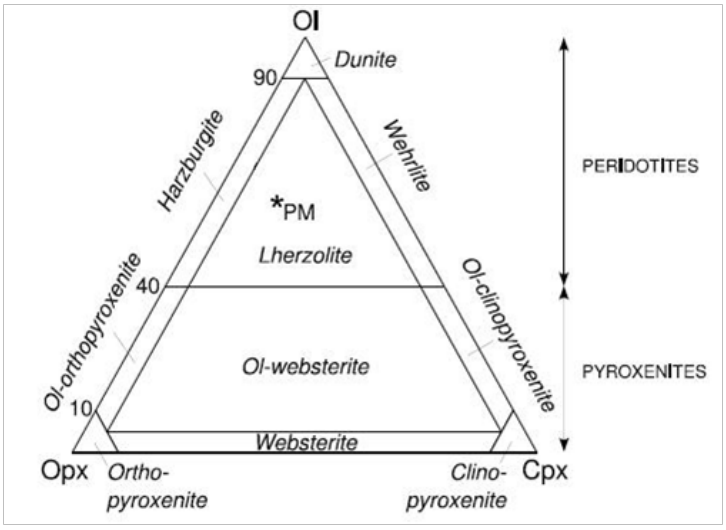

Figure 2.8. *Classification of ultramafic rocks in the ol-opx-cpx system. PM depicts the composition of the primary mantle. After Spengler [2006].*

3 SERPENTINE AND SERPENTINITE

3.1 PERIDOTITE

Serpentine rock, or serpentinite, originates from ultramafic peridotite, derived from the Earth's mantle. Serpentinization of peridotite is a retrograde metamorphic process, and occurs through fluid infiltration in the rock at the ocean floor or during exhumation. During this process, olivine is replaced by serpentine and orthopyroxene by so-called bastite, a serpentine as well. Bastites from clinopyroxene, amphibole, talc and phlogopite also occur, but are rare.

There are several types of peridotites, which originate in different ways from the Earth's lithospheric crust and mantle. Subsequently, serpentinites also originate in different ways. Serpentinization can cause difficulties in finding the exact origin of the peridotite.

Alpine type or orogenic peridotites are upper mantle peridotites found in orogenic belts and are tectonically emplaced into their present position. They can originate from either the oceanic lithosphere or from the sub-continental upper mantle:
- Peridotites from the oceanic lithosphere form part of an ophiolitic assemblage, in which the composition of the Earth's crust and upper mantle, as formed at oceanic ridges, is recorded in a sequence of mostly intrusive rocks. Oceanic peridotites (and other mafic intrusives in the sequence) are serpentinized by hydrothermal circulation through the young oceanic crust.
- The dominant rock type in the Earth's mantle above a depth of 400 km is peridotite. Pieces of this sub-continental lithospheric mantle can be emplaced into the crust along thrust faults. They are also orogenic peridotites, but have nothing to do with ophiolite complexes. Serpentinization of these peridotites occurs as a consequence of fluid infiltration during exhumation.

Ultramafic cumulates are rocks with a peridotitic composition, which are derived from mafic magma by accumulation of dense olivine and pyroxene crystals. They have intruded in the crust, and can form layered complexes associated with the root zone of volcanoes.

3.2 CHEMISTRY

The serpentine group consists of several polymorphs of the same mineral, composed from the chemical formula $Mg_3Si_2O_5(OH)_4$. The rock-forming types are lizardite, chrysotile (asbestos) and antigorite, which are often difficult to distinguish chemically. Some other forms exist, but are rare. Bastite exists as all three types mentioned here.

Serpentines are trioctahedral 1:1 layer silicates, which are built from alternating layers of 4-coordinated Si and 6-coordinated Mg. They differ in their crystallographic structure: lizardite is forms planar layers, whereas chrysotile consists of scrolled layers, which often roll up to form cylinders. Antigorite has a periodic reversal of the 1:1 layer, which causes a discontinuity in the octahedral sheet and loss of octahedral sites. This so-called modulated structure makes it not strictly a polymorph of the other two; it has less octahedral coordinated sites, which means loss of Mg and OH_4, and therefore enrichment in Si [O'Hanley, 1996; Mével, 2003]. Basic structures of the three major serpentine polymorphs are shown in figure 3.1.
Brucite ($Mg(OH)_2$) is a mineral that is often formed together with serpentine, it forms sheets that are interlayered with serpentine layers.

Quite some chemical variations exist between and within the different polymorphs. Substitutions of Si in the tetrahedral sites can occur by Al and Fe^{3+}. In the octahedral sites, Mg can be substituted

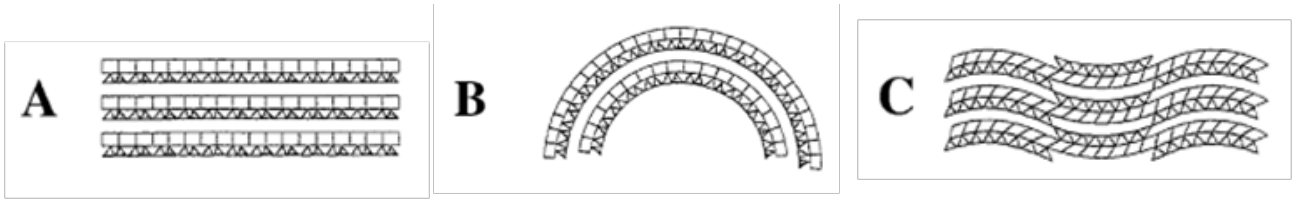

Figure 3.1. *Basic structure of the principal polymorphs of serpentine: A) planar lizardite; B) 'scrolled' chrysotile; C) reversing antigorite. After Mével [2003].*

by Fe^{2+}, Fe^{3+}, Al, and less often by Cr, Ni, Mn and Ti [Andreani et al, 2007].
Mével [2003] states that although lizardite and chrysotile have overlapping compositions, substitution in lizardite occurs more easily. Often it is more enriched in Al and Fe^{3+} [O'Hanley, 1996], and there even exist complete solid solutions with Al and Fe^{3+} end-members for lizardite, whereas chrysotile is typically poor in Al_2O_3. Antigorite tends to be high in SiO_2 and low in MgO and H_2O [Whittaker and Wicks, 1970].
Bastite is relatively rich in aluminium and chromium. Less substitutions are generally present within veins and in replacement-serpentine (which thus replaces another form of serpentine during ongoing serpentinization) [Mével, 2003].

3.3 Appearance

3.3.1 Extent of serpentinization

Serpentine can form throughout the peridotite rock, forming a mesh texture, as well as in veins and fractures that run through the rock.
Serpentinization in peridotites usually extends up to 60 to 100%, which is the percentage of the secondary minerals. Dunites (more than 90% olivine) are in general more serpentinized than harzburgites (with a considerable percentage of orthopyroxene, see figure 2.8).
Serpentinization most often occurs under static conditions, so that primary textures can still be seen after the deformation. Evidence for other types of deformation can be found in the abundance of vein networks, which occur in most of the rocks. These are evidence for fracturing and crack opening due to stresses that play a role during serpentinization.

3.3.2 Microstructures

Serpentinization is a pseudomorphic process, in which the texture of the protolith (the peridotite) is preserved. Olivine crystals react to serpentine due to fluid infiltration. It starts at the rim of the crystals, and continues towards the centre of the crystal upon further hydration. This kind of pseudomorphic texture is called a mesh texture, consisting of mesh cells and rims. In case of incomplete serpentinization, the unaltered remains of the olivine form the mesh centre; serpentine forms the mesh rim. Another type of texture is an hourglass texture, in which it is not possible anymore to distinguish between mesh centre and mesh rim. Both textures can occur together in one sample, as can be seen in figure 3.2.

The different serpentine polymorphs are often quite difficult to distinguish under the light microscope, because of overlapping features like refractive index and their very fine-grained nature. Although chrysotile is the only truly fibrous serpentine, all polymorphs can appear fibrous, because they show cross-sections of plates. In general, they all have first order colours under cross-polarized light.
In addition, serpentines and especially bastites are able to preserve features of the original crystal. They can show the original cleavage and for instance deformation lamellae. These can also have higher interference colours than first order. This can be up to third order, for instance in the case of serpentine after talc [O'Hanley, 1996].
The appearance (texture) of serpentine is thus more or less dependent on the crystal from which it

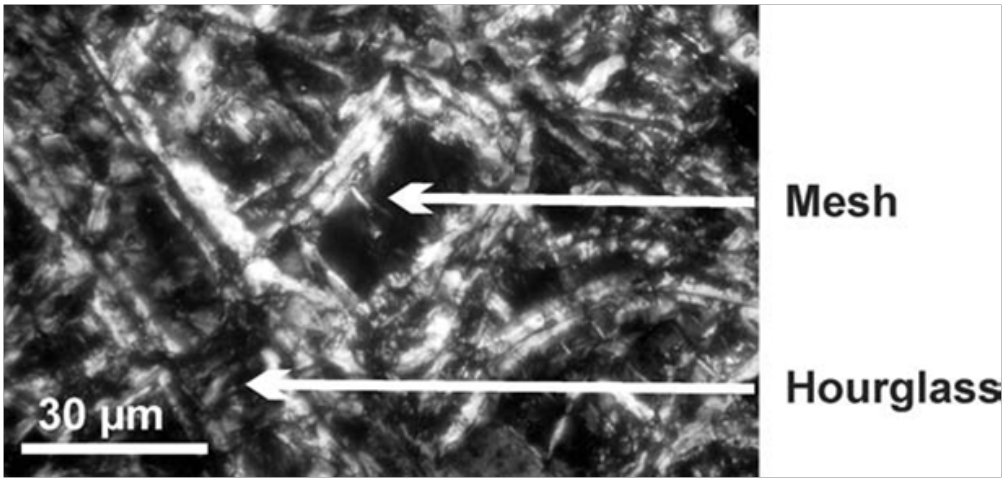

Figure 3.2. *XPL photograph of serpentine mesh and hourglass texture. From Caillaud et al. [2006].*

originates. This texture can be changed though; by recrystallization – which changes the grain size –, or by replacement – which changes the entire serpentine polymorph [O'Hanley, 1996].

In general, fibres in the mesh rims are orientated perpendicular to the edge between the rim and the centre of the cell. Furthermore, O'Hanley [1996] states that antigorite forms arrow-shaped crystals in the mesh, and that chrysotile forms knotted strings or feathers. Lizardite is usually fibrous or granular. The characteristics of serpentine in fractures will be discussed in subsection 6.2.2, where many of the microscope observations are compared to the fractures described by Andreani et al. [2007].
The determination of the different serpentine polymorphs in the thin sections in this study will be mainly based on the interpretations mentioned here, from Andreani et al. [2007], Mével [2003] and O'Hanley [1996], in pictures and chemistry.

To really distinguish between different types of serpentine, optical analysis is not enough. Powder X-ray diffraction, or microbeam X-ray diffraction patterns can determine the in situ optic orientation of the mineral in the texture, which can thus distinguish the polymorph.

3.3.3 Occurrence

There are records of quite a number of appearances of the different serpentine polymorphs in both the mesh and in veins. Serpentine in the mesh often looks different than the same polymorph in a vein. Some controversies exist about their tendency to grow in either the mesh or in fractures, or in both.

O'Hanley [1996] gives quite some detailed descriptions of textures and occurrences of different polymorphs in thin section. He makes a distinction between α-serpentine and γ-serpentine, which refers to length-fast fibres (negative elongation) and length-slow fibres (positive elongation), relatively. With this distinction, a subdivision is made of the occurrence of the serpentine polymorphs within pseudomorphic textures or in fractures. Lizardite with brucite would be the main α-serpentine in mesh rims, mesh centres and hourglass textures; and antigorite or chrysotile the main γ-serpentines. Bastites are generally lizardite.
In fractures and veins, chrysotile and/or lizardite (or antigorite) with brucite form the γ-serpentines; α-serpentines are rarely found.

Mével [2003] states that lizardite appears to be the dominant polymorph in seafloor samples, and is found in the mesh and in bastites. Chrysotile is the major fracture-filling mineral and also coexists with and replaces lizardite in the mesh. Antigorite – though more scarce – also occurs in fractures. Andreani et al. [2007] also find that lizardite and chrysotile are the main fracture-filling serpentines.

Figure 3.3. *Dunite from Otrøy with the typical brown weathering colour of peridotite, and the black colour of serpentinite on the inside. From Van Roermund [2009].*

3.3.4 Appearance in outcrop

Serpentinites in outcrop show various colours and textures, dependent on the basic rock composition. The colour varies due to the abundance of opaque iron-oxides like magnetite and hematite, and to the extent of hydration of the rock. These can weather the surface of serpentinite. Fresh serpentinite has a dark green to black colour, the weathered colour that shows at the surface however is a golden brown, shown in figure 3.3. Serpentine minerals itself can have various colours, ranging from white to (pale) green [Deer, Howie and Zussman, 1983].

3.3.5 Volume change

Exhumed serpentinized peridotites are fractured to a large extent. These fractures would be caused by volume changes due to the serpentinization reactions, and are often filled with serpentine.
There is some debate about whether or not serpentinization occurs at constant volume or at constant mass, but most studies assume a constant mass. If a constant volume was assumed, a significant amount of MgO and SiO_2 must be removed from the rock during serpentinization. The reaction describing the volume conservation is as follows [O'Hanley, 1992]:

$$6.15\ (Mg,Fe)_2SiO_4 + 6\ H_2O = 2\ (Mg,Fe)_3Si_2O_5(OH)_4 + 2\ Mg(OH)_2 + 4.3\ MgO_{(aq)} + 2.15\ SiO_{2\ (aq)}. \quad (3.1)$$

$$(865g;\ 271cm^3)\ forsterite + 90g\ water = (554g;\ 221cm^3)\ serpentine + (116g;\ 49cm^3)\ brucite + 173g\ MgO_{(aq)} + 129g\ SiO_{2(aq)}.$$

This reaction would yield significant MgO and SiO_2 metasomatism of the surrounding rock. In general, this is not observed in field studies [O'Hanley, 1992].

The following reaction has conservation of mass during serpentinization [O'Hanley, 1992]:

$$2\ Mg_2SiO_4 + 3\ H_2O = Mg_3Si_2O_5(OH)_4 + Mg(OH)_2. \quad (3.2)$$

$$(281g;\ 88cm^3)\ forsterite + 45g\ water = (277g;\ 111cm^3)\ serpentine + (5g;\ 25cm^3)\ brucite.$$

The percentage of volume change varies in different studies, but ranges between 25 and 55% [Iyer et al., 2008; O'Hanley, 1996]. Theories for volume change and subsequent fracturing during serpentinization will be discussed further in subsection 8.3.

4 METHODS

4.1 FIELD METHODS

4.1.1 Sampling and measurements

Samples were taken from both peridotite bodies, from the peridotite itself as well as from the pyroxenite lenses within. The goal was to compare the influence of serpentinization and serpentine fractures in both rock types, and on the boundaries between them. It was tried to sample as much as possible from fractures that still contained filling material, which was weathered away from many fractures.
Some fractures, as mentioned by Spengler [2006], show a thickening ('weathering out') of the fracture rim at the surface, probably caused by locally coarsened olivine. Some samples were taken from such rims to see if the cause of the thickening had anything to do with serpentinization, and if these were thus so-called reaction rims.

Measurements were done on the orientations of fracture planes and compositional banding. The latter was taken into account to serve as a reference plane for the fracture planes. The aim was to determine if there was some kind of relation between them. In the case of extensive fracture networks at one site, some of the most representative and abundant directions were taken.

4.1.2 Geometrical analyses

All measurements of fracture planes and compositional banding within the peridotites were analysed for spatial patterns throughout the bodies. To represent the data, the fracture planes were rotated with their compositional bandings acting as a reference plane, until those had the same orientations. This was to see if there was a relation between the fractures in different localities. For sites where the compositional banding could not be measured, the banding orientation was taken from measurements from Spengler [2006]. All original and rotated measurements were plotted with stereographic projections using the program Stereo32 [© Röller and Trepmann, 2003-2008]. The most abundant directions were determined through density distribution plots.

The angles of the fracture planes with their corresponding compositional bandings were calculated to see if a pattern between fractures and compositional banding was present. If so, this would give implications for the role of the compositional banding during fracturing.

4.2 ROCK ANALYTICAL METHODS

From a selection of samples, thin sections were made, which were analysed optically and chemically.

4.2.1 Light microscopy

The thin sections were studied on mineral content and degree of serpentinization. It was tried to distinguish different kinds of serpentines within the mesh and within veins, on the basis of their characteristic features, as mentioned in chapter 3. Structures, deformational features and different generations of growth between or within veins were recorded, as well as signs of reactions that had occurred during retrograde metamorphism of the rock.

4.2.2 Electron Microprobe

A chemical analysis of some of the thin sections was made with the microprobe. This was especially useful for minerals that were hard to define with the light microscope. Furthermore, it gave a quantitative result, and therefore a more exact definition of the mineral formula in terms of presence of

key elements, which could help determine past reactions in the sample.
Major element mineral compositions in the samples were determined with a JEOL JXA8600 Superprobe at Utrecht University. Both the five wavelength dispersive spectrometers and the energy dispersive spectrometer were used (in different runs). This yielded a (semi-)quantitative impression of major elements present in certain minerals.
Standard conditions were an acceleration voltage of 15 kV, a beam current of 20 nA and a beam diameter of 1 µm. Obtained data was corrected using the ZAF routine. The counting time in both WDS and EDS was 30s. External calibration occurred against international standards with a precision of ±0.5%.

5 FRACTURE NETWORKS AND FRACTURES

Both peridotite bodies on Otrøy show diverse fractures and fracture networks, having different scales and orientations. The Raudhaugene peridotite body has the most extensive and consistent fracture network throughout the whole body, whereas the Ugelvik peridotite body has somewhat more localized and diverse fracture networks. Even so, fractures that form the fracture networks show quite some variety in terms of length/width, filling and reaction rims.
In the following subsections, a division between fracture networks is made on the basis of their spacing and extent. Large scale fracture networks are those that contain wider spaced fractures (from about 10 cm onward) and occur in the largest part of an outcrop. Small scale fracture networks have narrow-spaced fractures (from a few up to tens of mm's) and usually occur in only a part of an outcrop.
A map of the sites visited in both bodies, with measurements and the locations of the samples that were used, is given in figure 5.1 and 5.2 (see next two pages).

5.1 LARGE SCALE NETWORKS

5.1.1 Raudhaugene

A larger scale fracture network that occurs throughout the largest part of the Raudhaugene peridotite body is formed by fractures with a spacing of about 10 cm to several tens of cm's. In all outcrops, fractures have varying lengths, ranging from 5 cm to tens of cm's. This network occurs at the eastern locality R2 (figure 5.3), in the centre localities R8 (figure 5.4) and R9 (figure 5.5) and at site R3.1 (figure 5.6). At site R9.2, which is close to the contact with the surrounding basement gneiss, there are also some fractures present in the gneiss, in the wall closest to the peridotite. Though not as extensive as in the peridotite at R9.2, the fractures make a network with blocks of tens of cm's, as is shown in figure 5.7.

Figure 5.3. *Fracture network at locality R2. View is at a vertical surface, to the north. Orientation of the compositional banding is 340/80 (dipdirection/dip). Hammer for scale.*

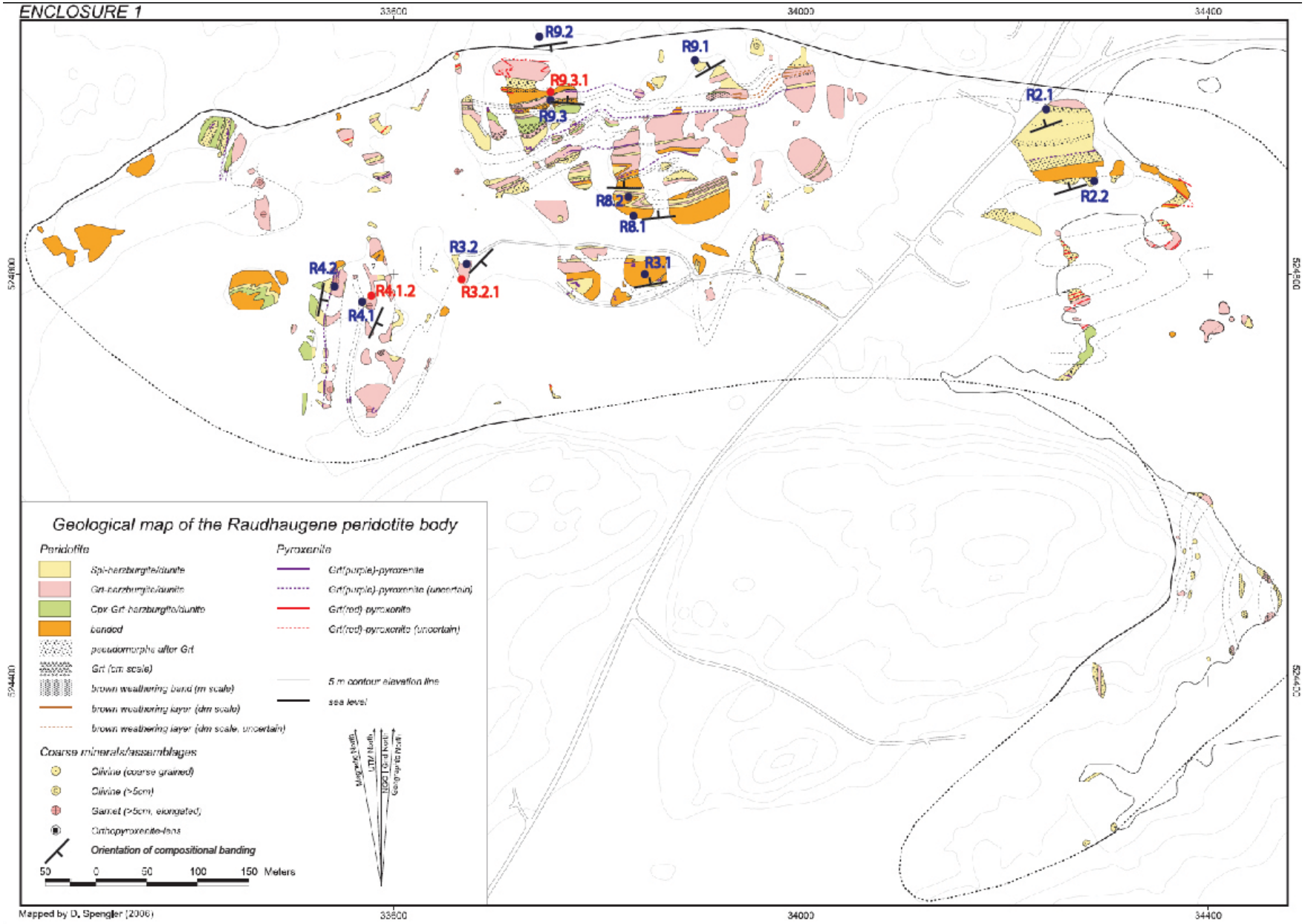

Figure 5.1. *Field map of Raudhaugene peridotite body, with the sites visited (blue), the used samples (red) and strike and dip of the compositional banding per site. Modified after Spengler [2006].*

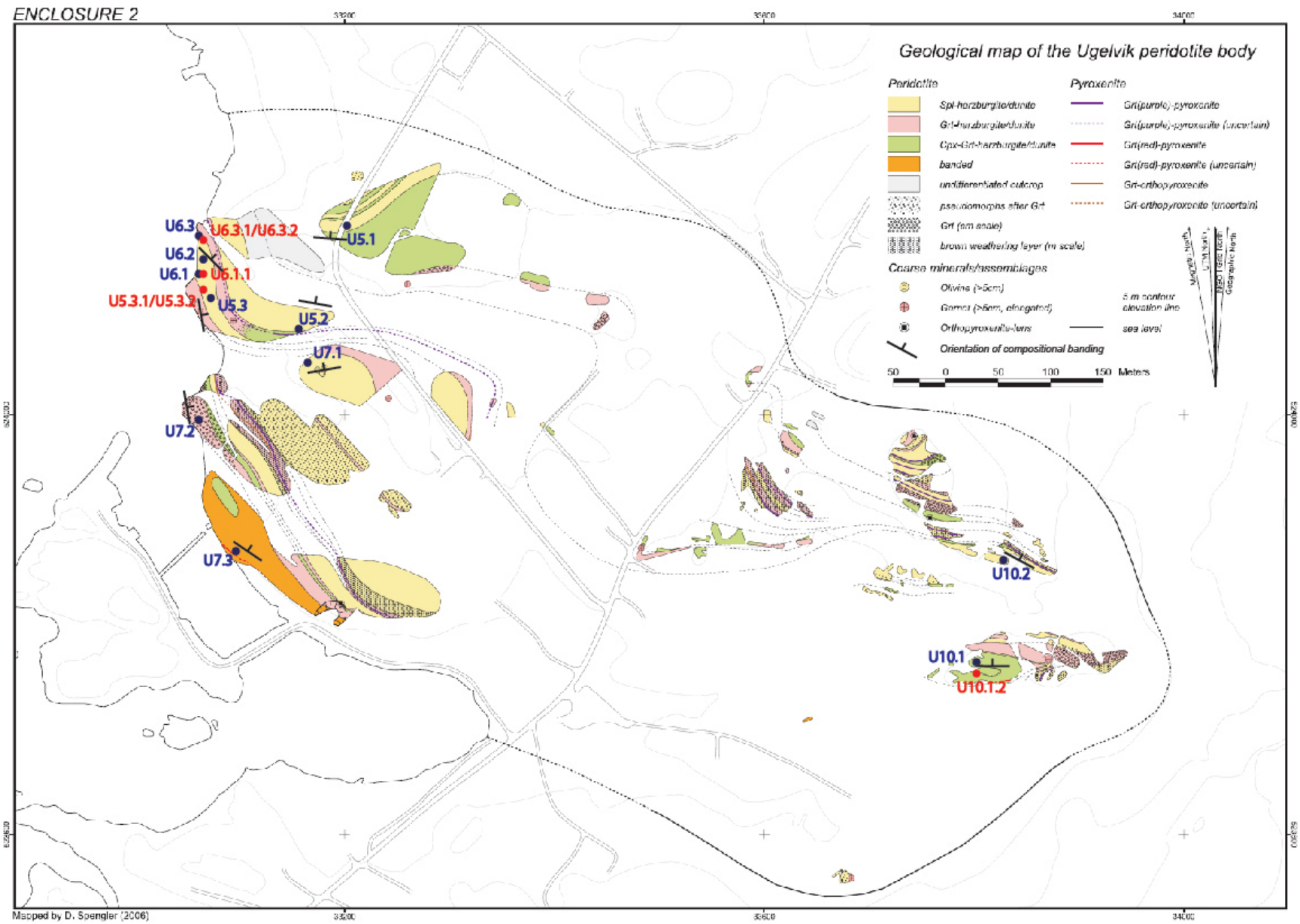

Figure 5.2. *Fieldmap of Ugelvik peridotite body, with the sites visited (blue), the used samples (red) and strike and dip of the compositional banding per site. Modified after Spengler [2006].*

Figure 5.4. *Fracture network at locality R8. Dashed lines are inferred fractures. Compositional banding can be seen, the orientation is 354/78. Oblique fractures seem to make a conjugate set. View is at semi-horizontal surface, plunge is to the south and view is to the northeast.*

Figure 5.5. *Fracture network at locality R9. Orientation of the compositional banding is 004/74. View is to the south.*

Figure 5.6. *Fracture network at site R3.1. Oblique fractures seem to make a conjugate set. Surface is semi-horizontal, plunge is to the south and view to the north. The compositional banding has orientation 350/73.*

The fractures that form the networks have various appearances. Most of the fractures at R2 show a rim (up to 2 cm wide) that has been weathered away. They often have a filled core of about 1 mm wide, consisting of white material that sticks out in the middle (figure 5.8A). At R2.2 the weathering

Figure 5.7. *Gneiss just outside the peridotite body, close to site R9.2. Some fractures can be seen. View is to the north.*

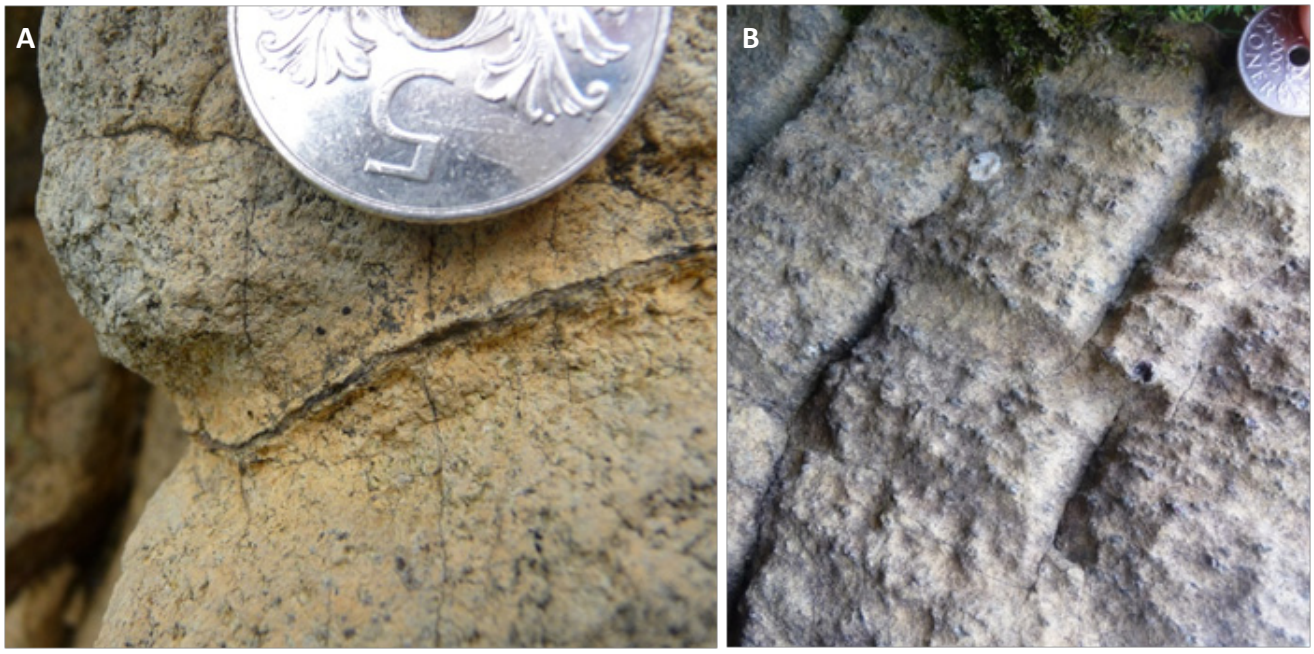

Figure 5.8. *Examples of fractures with weathered away rims at locality R2, with a filled core sticking out (A) and cores no longer to be seen (B).*

went relatively deep, up to a few cm's, and in figure 5.8 B, a core can no longer to be seen.

Only some of the larger fractures at R2 have a somewhat thicker rim (1-2 cm wide) that comes out of the surface for some mm's. This is in contrast with the fractures at localities R8 and R9. Here, many fractures have a thick (and up to 1-3 cm wide) rim. The core is sometimes a little bit weath-

ered inward, and sometimes not. The rim is less developed when a fracture crosses a pyroxenite layer (figure 5.9).
Many heavily weathered inward fractures seem to form the blocks in which the outcrops at R8 and R9 are fragmented (figure 5.10). The weathered away fractures form now fissures between the blocks, which are up to some cm's wide. Some fractures in the surrounding gneiss are also weathered away to some cm's deep and a few cm's wide.

At all these localities, most of the fractures that define the network form angles of about 90° with each other. However, oblique fractures are present everywhere, which make various angles with the other fractures. At site R3.1, one of the 'right angle' fracture sets follows the compositional banding. The oblique fractures there look like a conjugate set of fractures (see figure 5.6).

In none of the localities mentioned here, clear crosscutting relationships could be determined, which would give implications on a possible sequence of fracturing. An example of mutually crosscutting fractures is given in figure 5.11.

Figure 5.9. *A fracture with a thick rim that crosses a pyroxenite layer in locality R8. The rim is less developed in the pyroxenite layer.*

Figure 5.10. *Blocky outcrop due to heavily weathered away fractures in locality R9, which have the same orientation as non-weathered fractures. Coin for scale just left and above of the centre.*

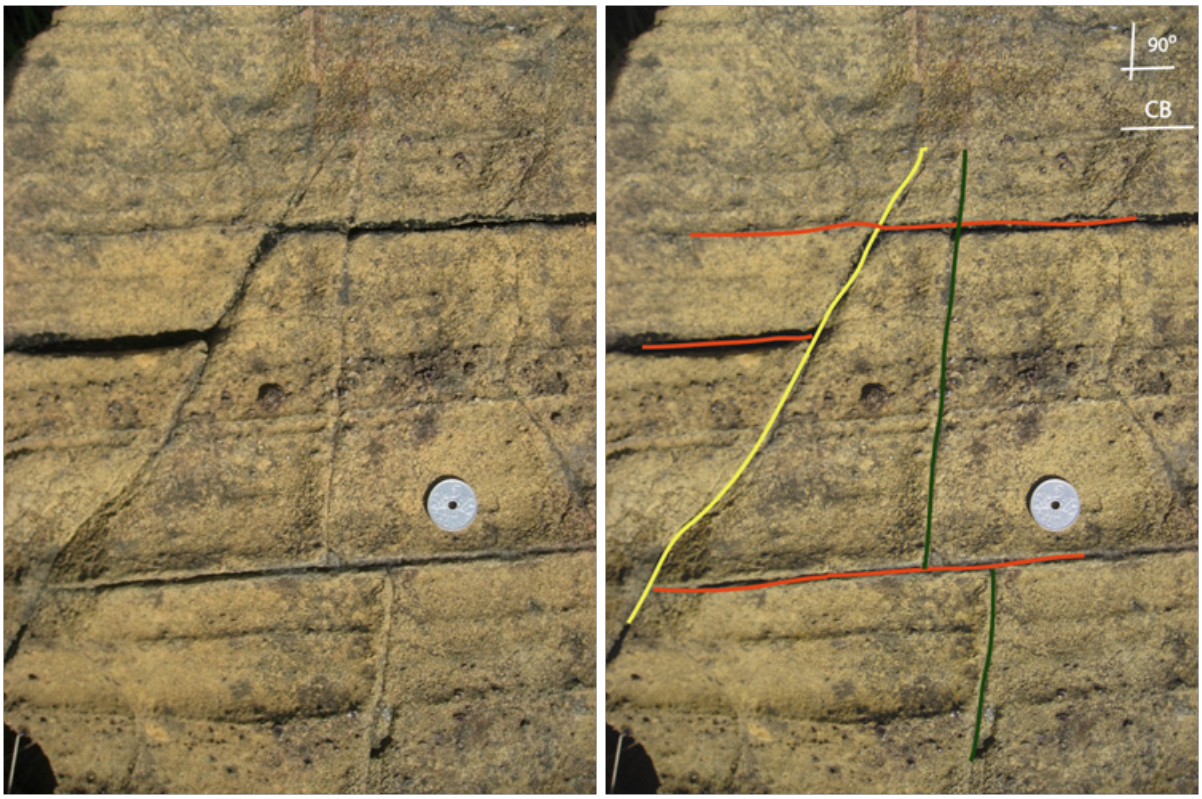

Figure 5.11. *No definite cross-cutting relationships can be determined in most of the fracture sets. An example of one fractures that seem to grow from another (thus later) but at other places just crosses it.*

Figure 5.12. *Weathered away fractures and resulting blocky outcrops at locality U10. Myself for scale. View to the north. Compositional banding has orientation 000/42.*

5.1.2 Ugelvik

In the Ugelvik peridotite body, a large fracture network as seen at locality R8 and R9 is also present, however a little less abundant throughout the body. At locality U10 (figure 5.12), there are some parts of the outcrops that have approximately the same appearance: blocks that seem to have fragmented at weathered away fractures. The fractures form blocks ranging from about 20 to tens of cm's. Fractures that have not been weathered away have a thick rim of a few mm's to 2 cm wide. Other parts of the outcrops at locality U10 have no large scale network, but show some other, more localized fracture appearances which will be discussed in subsection 5.3.

The coastal outcrops in the west of the body, at sites U5.3 and U7.2 and locality U6, have another large fracture network. Again, a blocky structure is present, but the blocks are closer spaced, as can be seen in figure 5.13 (up to a few mm's wide), rather than being separated by a 1-2 cm wide fissure, as was observed in R8 and R9. At site U7.2, some larger fractures occur that have a width of up

to 2-3 cm, fully filled with dark green material, which is sometimes layered parallel to the fracture and is sometimes fibrous perpendicular to the fracture (figure 5.14). At the other coastal sites, filling can be seen at only few of the fractures from the large network. Some fractures have remains of silvery white to greenish, flaky material.

The fracture network at U10.1 is more randomly orientated than in R8 or R9. However, at U10.2 they seem to make angles of approximately 60-90° with each other (figure 5.15). At the coastal outcrops, also quite some 90° fractures are observed, however with a few other directions present.

Figure 5.13. *Blocky outcrop with closer spaced blocks at the western coast of Ugelvik, site U5.3 and locality U6. The two lines depict two of the dominant fracture orientations; the orientation of the compositional banding is 080/36. View is to the west.*

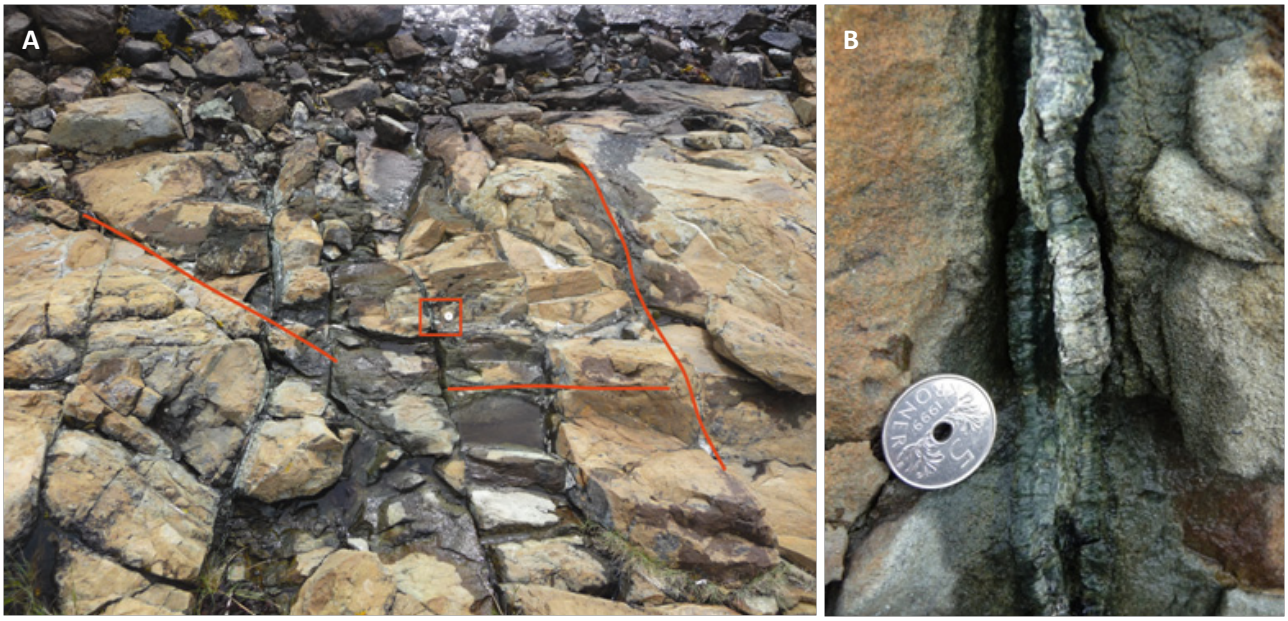

Figure 5.14. *Fracture pattern at site U7.2. Dominant directions and the area of close-up are shown (A). Coin for scale in the centre. The orientation of the compositional banding is 079/30. (B) is the close-up of a few cm's wide filled fracture, slightly layered, and fibrous perpendicular to the fracture. View is to the west, on a surface that slightly plunges to the west.*

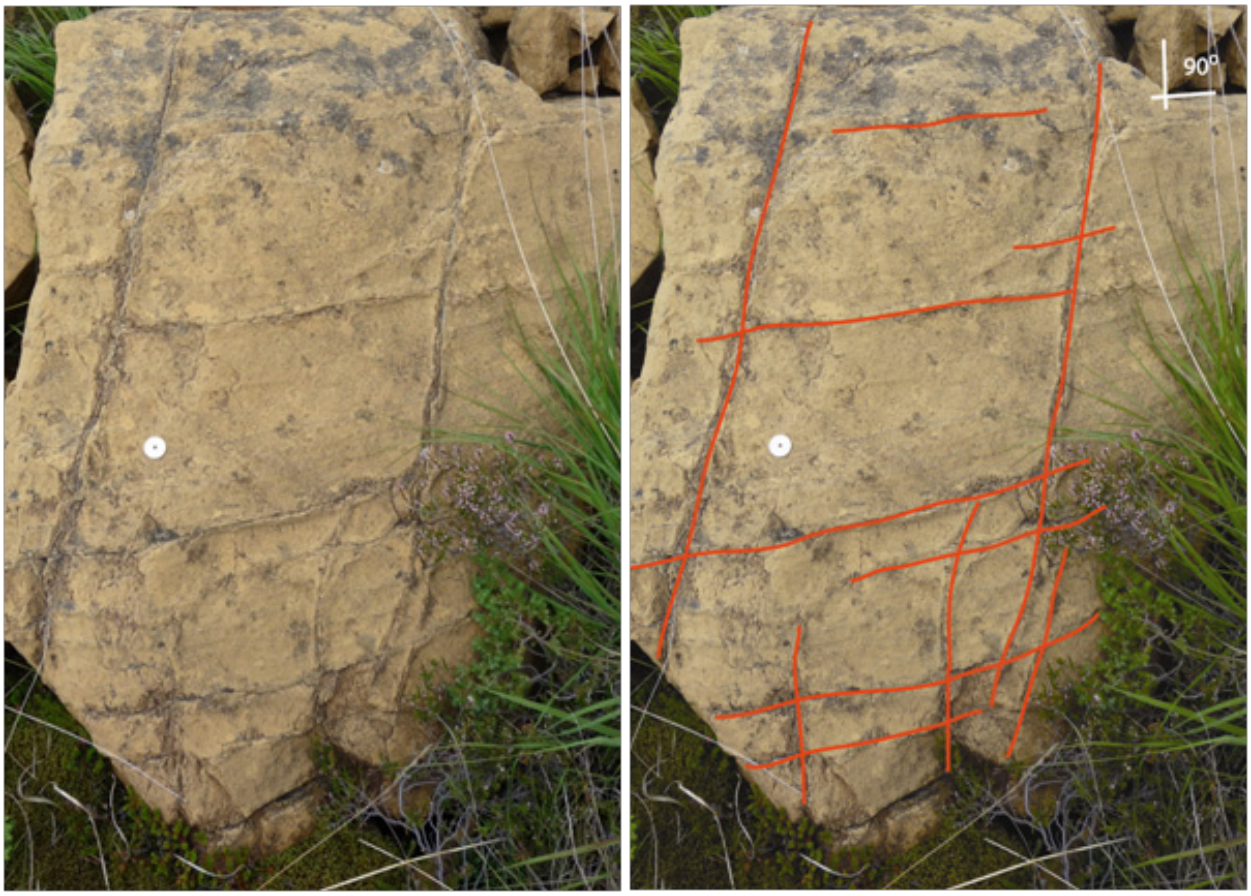

Figure 5.15. *Fracture network at site U10.2. View to the north, surface plunges quite steeply to the south. The compositional banding has orientation 028/45.*

5.1.3 Fracture orientations

A visualisation of the measurements done on the large scale networks in both peridotite bodies, using stereographic projections, are shown in figure 5.16 (A-D). These are the original measurements of the fracture planes; the poles are plotted. Figure 5.16 (E-H) gives plots of the rotated measurements. For the Raudhaugene peridotite body, the measurements have been rotated to a mean compositional banding of 343/48; for the Ugelvik peridotite body, a mean compositional banding of 045/30 is taken.

As can be seen in figure 5.16 A and C, the poles of the Raudhaugene fracture planes are grouped in three centres, of which two are the clearest. The angle between the centres is 63°, 76° and 100°. The poles of the Ugelvik fracture planes are less well centred, as shown in figure 5.16 B and D. Instead they form a range with some centres, however less dense than for the Raudhaugene data, and one centre offset from the range. Nonetheless, the angle between the clearest three 'centres' is 30°, 116° and 122°. The range has an approximate WNW-ESE orientation, which gives that the fracture planes have a strike varying between NW-SE and NE-SW.
When looking at the measurements of separate sites of Ugelvik (figure 5.17 D-F), a similar range can be seen in site U5.1 and U10.2. The data from site U6.2 is more scattered. The data for the separate sites of Raudhaugene shows no clear trends in figure 5.17 A-C. However, site R8.1 also shows a range having approximately the same orientation as those observed in Ugelvik.

The rotated data give the same trends: for Raudhaugene, three centres can be seen which are 60°, 75° and 110° apart (figure 5.16 E and G). For Ugelvik figure 5.16 F and H), there are less clear centres again, and a range of data. This range is more dispersed, however, with one clear centre. The other

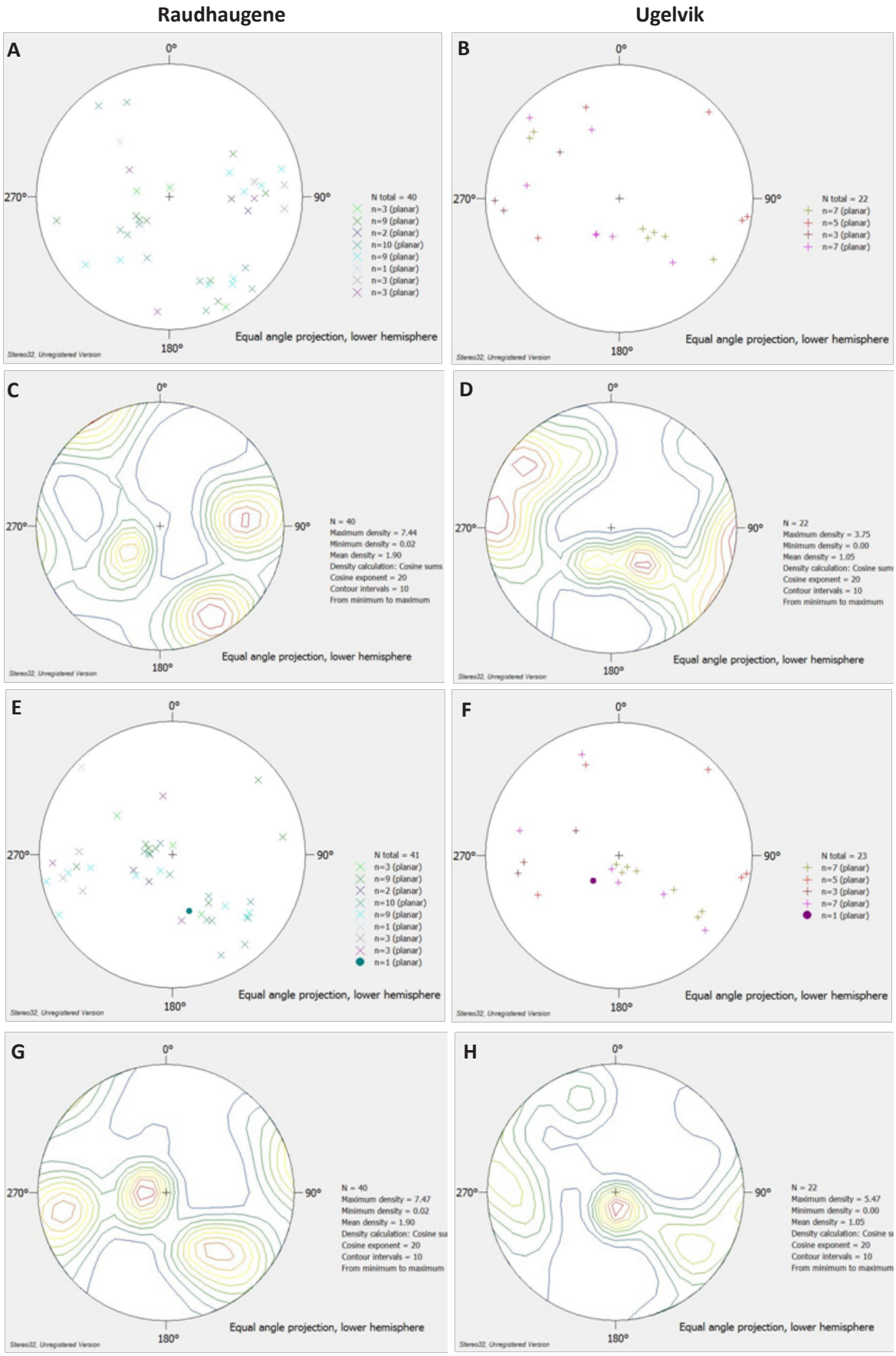

Figure 5.16. *Stereographic projections of the measurements on fracture planes. A and B: original data, poles to fracture planes. C and D: original data, density plots. E and F: rotated data, poles to fracture planes and pole to compositional banding (dot). G and H: rotated data, density plots.*

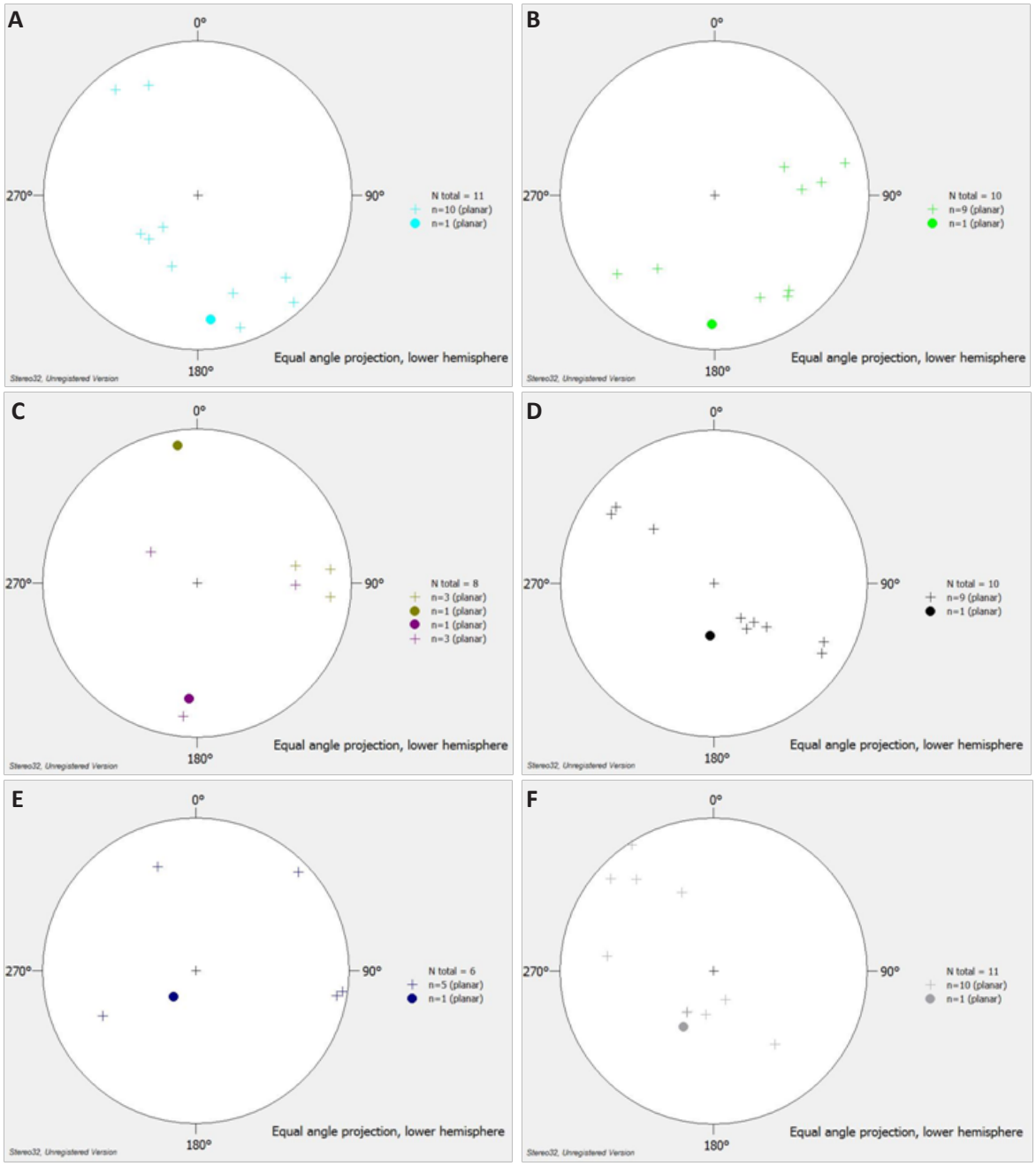

Figure 5.17. *Stereographic projections of the measurements for separate sites, poles to fracture planes (crosses) and pole to compositional banding (dots). A: R8.1. B: R8.2. C: R9. D: U5.1. E: U6.2. F: U10.2.*

'centres' have a density too small to be measured. The WNW-ESE orientation in this range is still present, which can be explained by the quite consistent orientation of the compositional banding in this body; most data was barely rotated.
Here, a striking similarity exists between both bodies. When looking at the density plots of the rotated data of both bodies, the areas that are covered by the data show comparable directions. The Raudhaugene data range shows a WNW-ESE orientation as well.

The poles to the fracture planes of both bodies have been put together in one plot as well (figure 5.18 A-D). The rotated plot (B and D) shows the data after rotation of all fracture planes to a mean compositional banding of 343/48. In both the original data and the rotated data much scatter can be seen, which is stronger than in the plots for the bodies separated.

The angles of all fracture planes with respect to the compositional banding (per site) is shown in figure 5.19. The Ugelvik peridotite body shows highs at around 70° and 90°. Furthermore, a majority

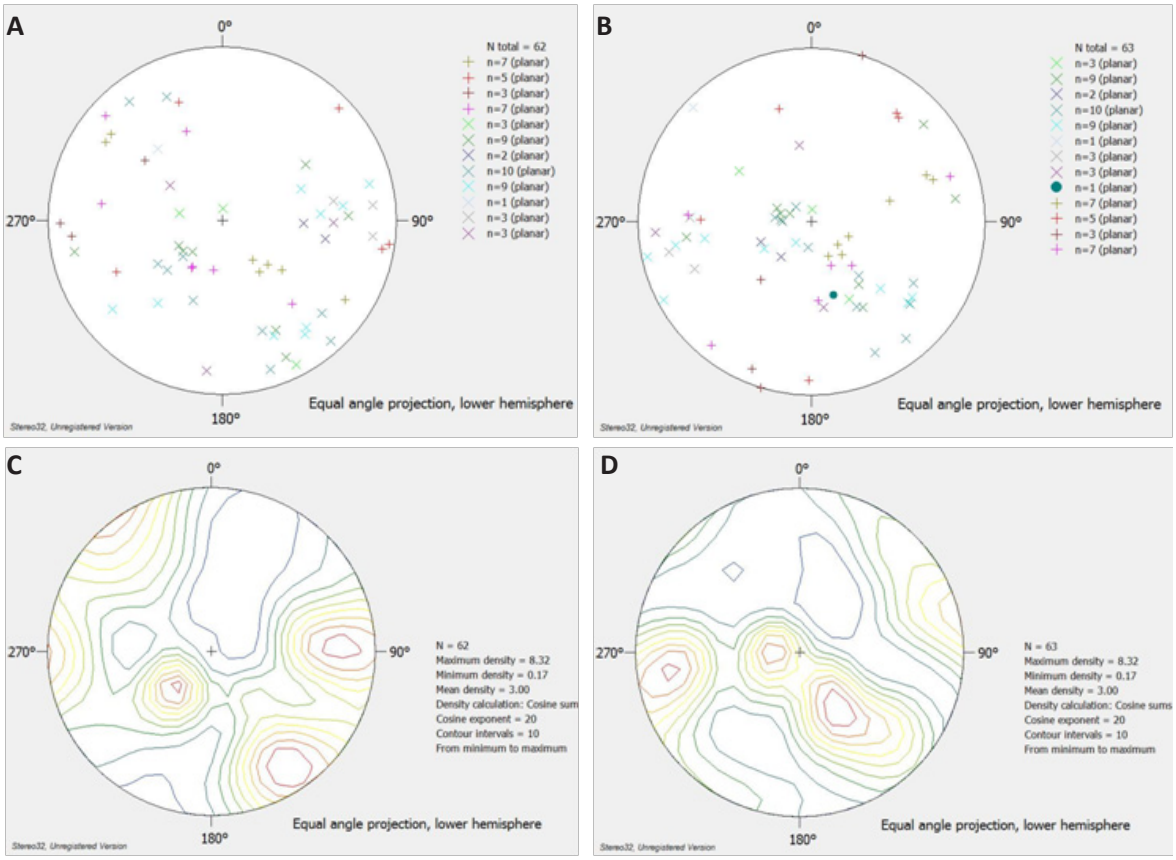

Figure 5.18. *Stereographic projections of the Raudhaugene and Ugelvik measurements together. A and C: original data; B and D: rotated data to a mean compositional banding of 343/48 (dot in B).*

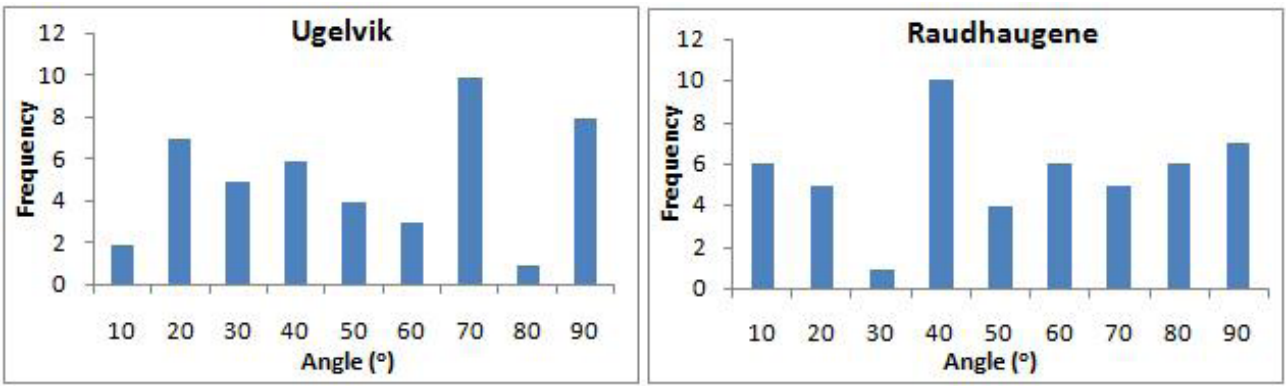

Figure 5.19. *Histograms of angles of fracture planes with respect to the compositional banding in both peridotite bodies.*

of the fractures shows a preference to occur at relatively low angles to the compositional banding (between 20° and 40°). The Raudhaugene peridotite body however shows different results. There is a high at 40°, and the second highest peak is 90°. In between, the fractures have quite some variation in their angle to the compositional banding. However, the data points are too few to really draw conclusive results here.

5.2 SMALL SCALE NETWORKS

5.2.1 Raudhaugene

Some smaller scale networks are observed at localities R2 and at sites R3.2 (figure 5.20) and R4.1.

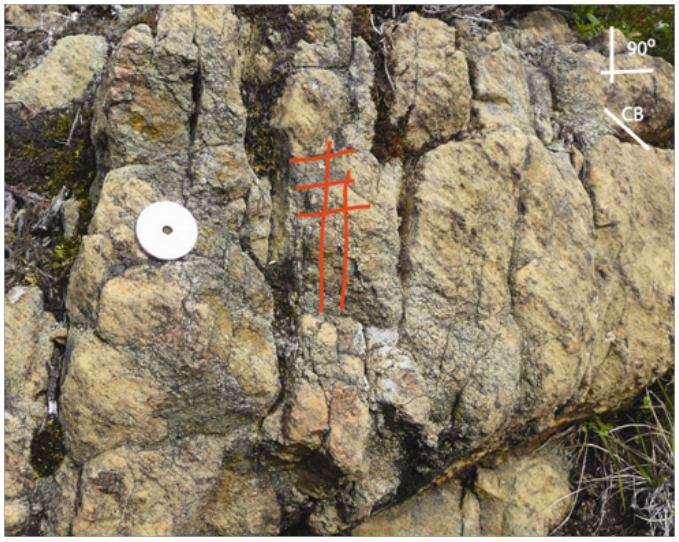

Figure 5.20. *Small scale fracture network at site R3.2.*

Figure 5.21. *Small scale fracture network, within larger network at site R2.1.*

In these networks, fractures have a mean spacing of 2 – 50 mm and they are a few cm's to a few tens of cm's long.
At locality R2 (figure 5.21), the smaller scale network is embedded in some of the blocks of the larger scale network, and sometimes some of the larger fractures have thin perpendicular side-fractures that are about 0.1 mm wide and are 0.5-1.5 cm apart. The fractures in site R4.1 are mainly formed by some side-fractures that branch of from the fractures that appear outside the pyroxenite band, as can be seen in figure 5.22.

The small scale fractures do not often show a weathered away or thicker rim. Some fractures at site R3.2 have a rim that is slightly weathered away, but no more than 1 mm deep. Only sporadically, a white core can be observed, because most of the fractures are just too narrow.
As in previously discussed sites, a roughly 90° angle pattern can be seen in all networks.

5.2.2 Ugelvik

The only fractures that are depicted as a small scale network in the Ugelvik peridotite body are those at sites U5.1 and U7.1. The fractures observed here are very narrow and quite long; they range from a few cm's to tens of cm's. At site U7.1 they form a network of small blocks of 0.5 cm to

Figure 5.22. *Small scale fracture network at site R4.1, partly formed from fractures that start in the pyroxenite lens beneath it that is also visible here.*

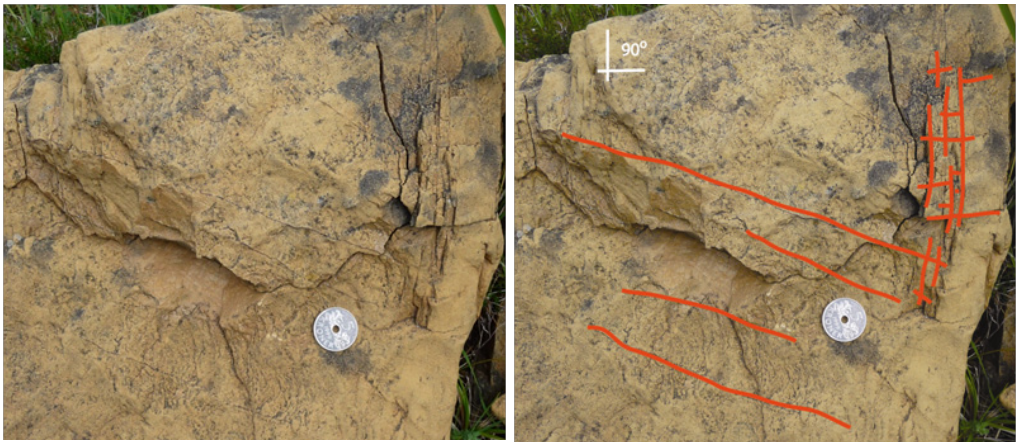

Figure 5.23. *Small scale fractures at site U7.1.*

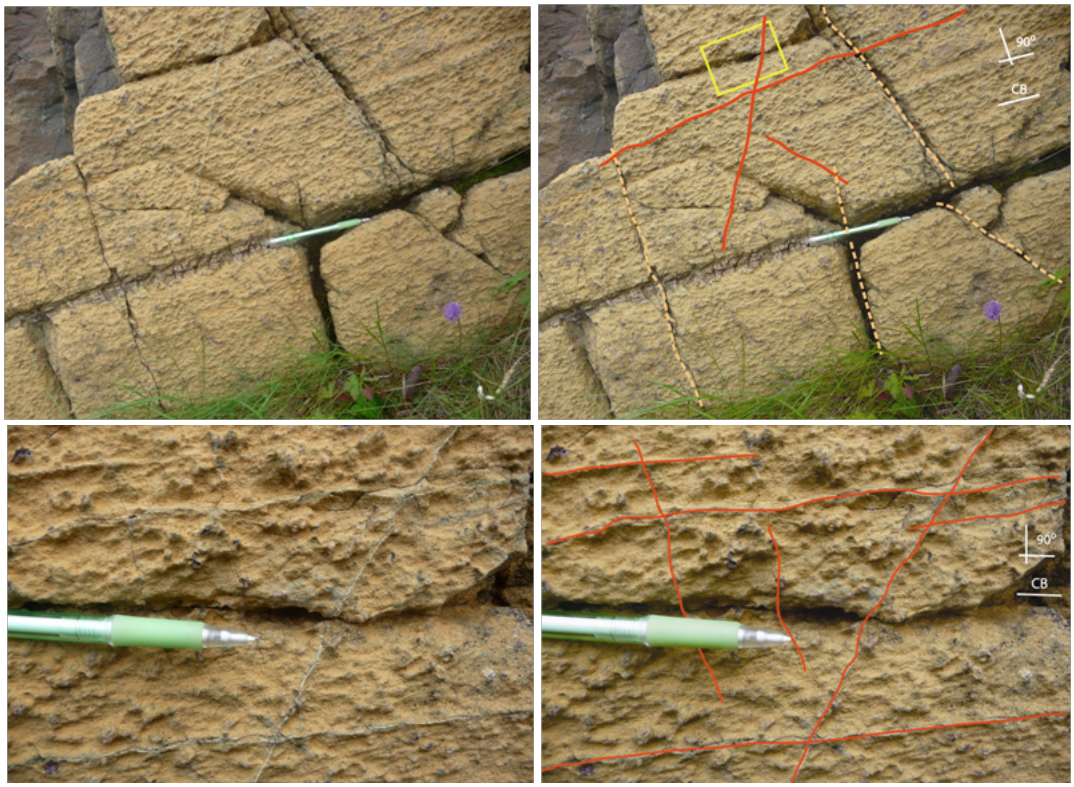

Figure 5.24. *Top row: Fracture network at site U5.1, with inferred fractures. The yellow frame depicts the close-up in the bottom row, which shows fractures at smaller scale.*

a few cm's (figure 5.23). Furthermore, there is no rim around most fractures at both sites, though some have a little rim of some mm's wide. Filling is hardly seen in most of the fractures, but some seem to be filled by white material (U5.1) or orange-brown material (U7.1).
At site U7.1, there are three sets of fractures, which make approximately 90° angles to each other. At site U5.1, the network most resembles that of site R3.1; containing fractures that approximately follow the direction of the compositional banding, fractures with a direction perpendicular to that, and some oblique fractures (figure 5.24).

5.3 Other fractures

Fracture sets that not have been depicted as part of a network – thus are only observed in that particular site – have only been described in the Ugelvik peridotite body.

Site U5.3 at the coast has two sets of fractures that do not belong as such to a network. One of those sets consists of some quite thick veins, 0.1-2 cm wide, filled with fibrous material (figure 5.25). The colour at the surface is orange-brown, but the fresh colour is silver-green. In two of the thicker veins, a second generation of fractures is present. The mode of fracturing resembles that of the pyroxenite bands, as will be discussed in subsection 5.4. These second generation fractures are perpendicular to the layering (the thick vein) and parallel to each other, and are filled with light green material. Some of the fractures do not stop at the boundary with the peridotite, but cross it by a few mm's.

Figure 5.25. *Orange-brown veins with light green cross-fractures at site U5.3.*

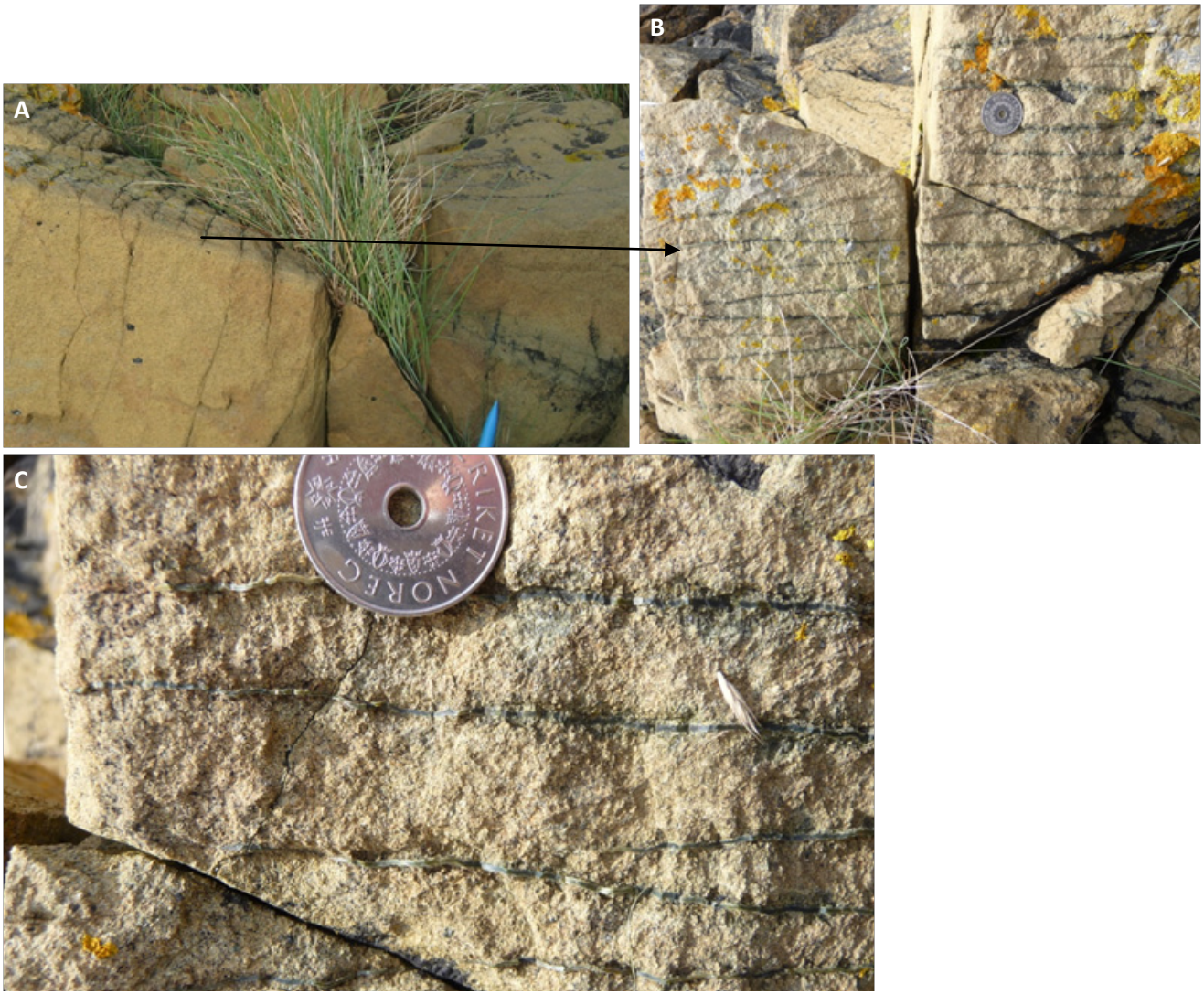

Figure 5.26. *A: Pyroxenite layer, with plane beneath showing regularly spaced parallel fractures (B), and close-up (C), showing banded light green and grey filling.*

The other set of fractures at site U5.3 occurs just underneath a pyroxenite layer, on a surface parallel to the pyroxenite layer (and thus to the compositional banding). Here, a set of regularly spaced semi-parallel fractures can be seen. The length of these fractures is unknown; the block is not large, as can be seen in figure 5.26 (A and B). The spacing is about 1-2 cm, and the fractures are filled with banded light green (outside) to grey (inside) material of about 1 mm wide (figure 5.26C).

Locality U10 has several other fracture sets that only occur locally. A first set at site U10.1 (figure 5.27) contains light pink veins that are up to 1-2m long, 1-15 mm wide and run semi-parallel to each other. The filling material is fibrous, with fibres perpendicular to oblique to the layering. Some of the veins are broken in half, parallel to the layering.
Another set of semi-parallel fractures is found at site U10.1, these fractures cross each other regularly. The fractures in this set are narrower (1-2 mm wide), have no rim and are filled with light green to white material (figure 5.28).

At site U10.2, a set of fractures with remarkable rims is found. The fractures are relatively short, only a few cm's up to 20 cm's long, and they all have rims of about 2 cm wide and 1-2 mm thick (figure 5.29). Some of them almost appear as real 'lips'. Most of the fractures are parallel to the compositional banding, some have an oblique orientation with an angle of about 30° to the compositional banding.

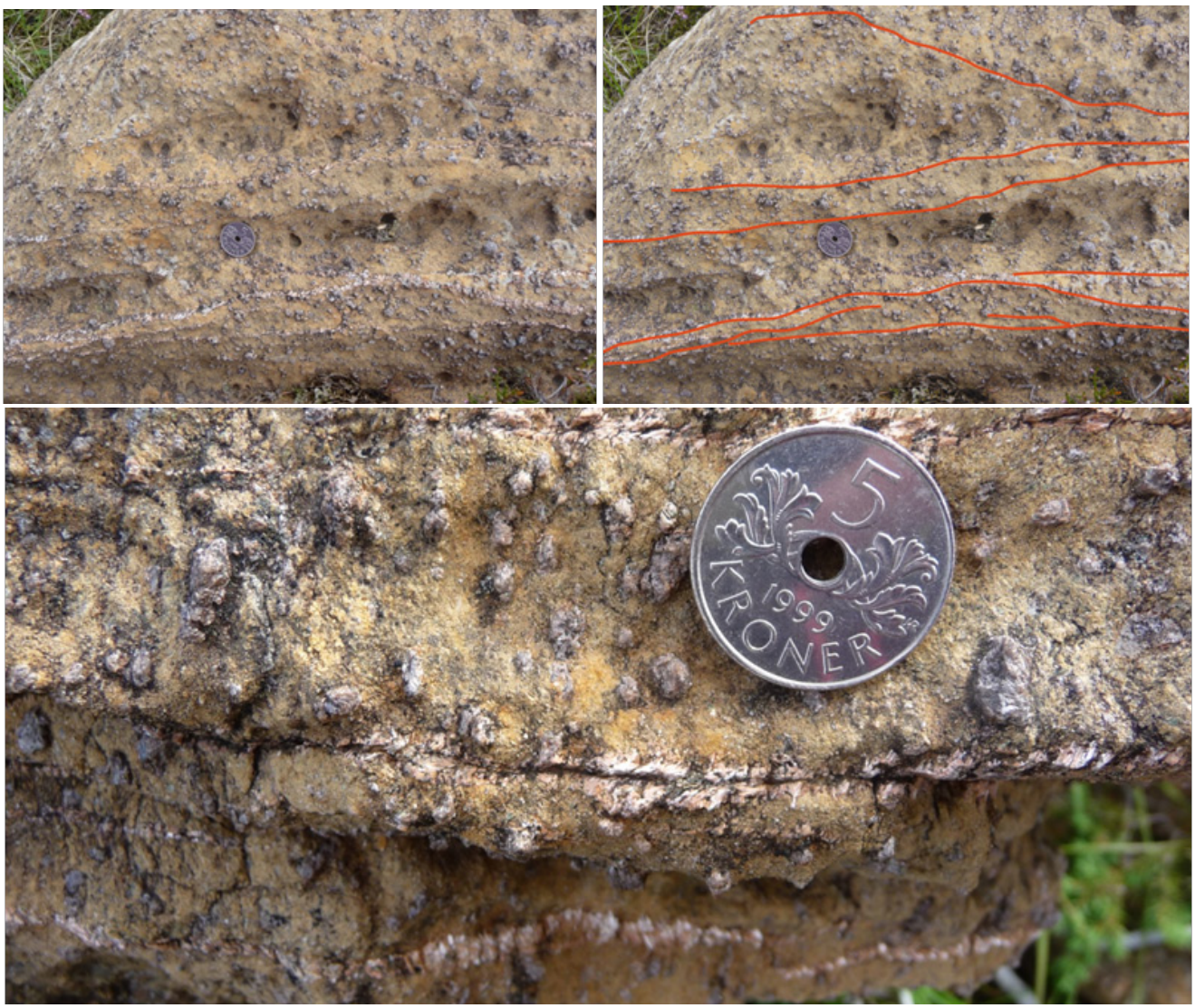

Figure 5.27. *Light pink fibrous veins at site U10.1 (top row) and magnification (bottom), in which can be seen that the fracture plane of one of the fractures is split.*

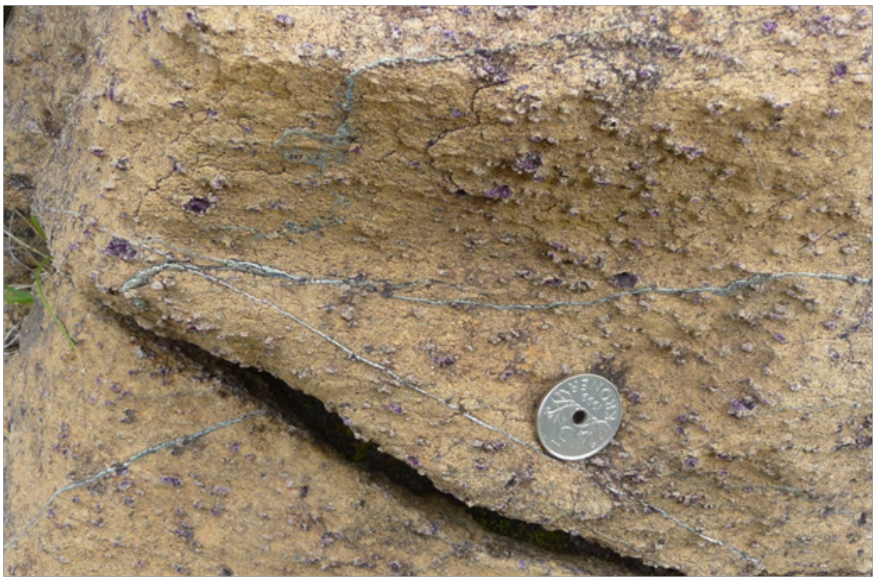

Figure 5.28. *Thin fractures crossing each other in site U10.1.*

Figure 5.29. *Fractures with a thick rim at site U10.2. Almost all follow the compositional banding, whereas some are oblique to it (top), and perpendicular (bottom).*

5.4 PYROXENITE FRACTURES

Throughout both peridotite bodies, fractures are observed within the many pyroxenite lenses/layers that are present. All fractures have a quite consistent appearance: they are regularly spaced, are parallel to each other and are more or less perpendicular to the layering. The wider the pyroxenite layer, the larger the fracture spacing; the spacing varies from about a quarter to three quarters of the width of the layer. A 10 cm wide pyroxenite layer has fractures that are approximately 3-4 cm apart (U7.3), while fractures in a 1 cm layer are 2-7 mm apart (U5.2), as can be seen in figure 5.30. Measurements of the width of pyroxenite lenses and the spacing between the cross-fractures within are shown in figure 5.31. As can be seen, there is a slight directly proportional trend present in the plot, which confirms the observation of a wider fracture spacing in a thicker lens. However, much more measurements are needed to really prove a clear trend.

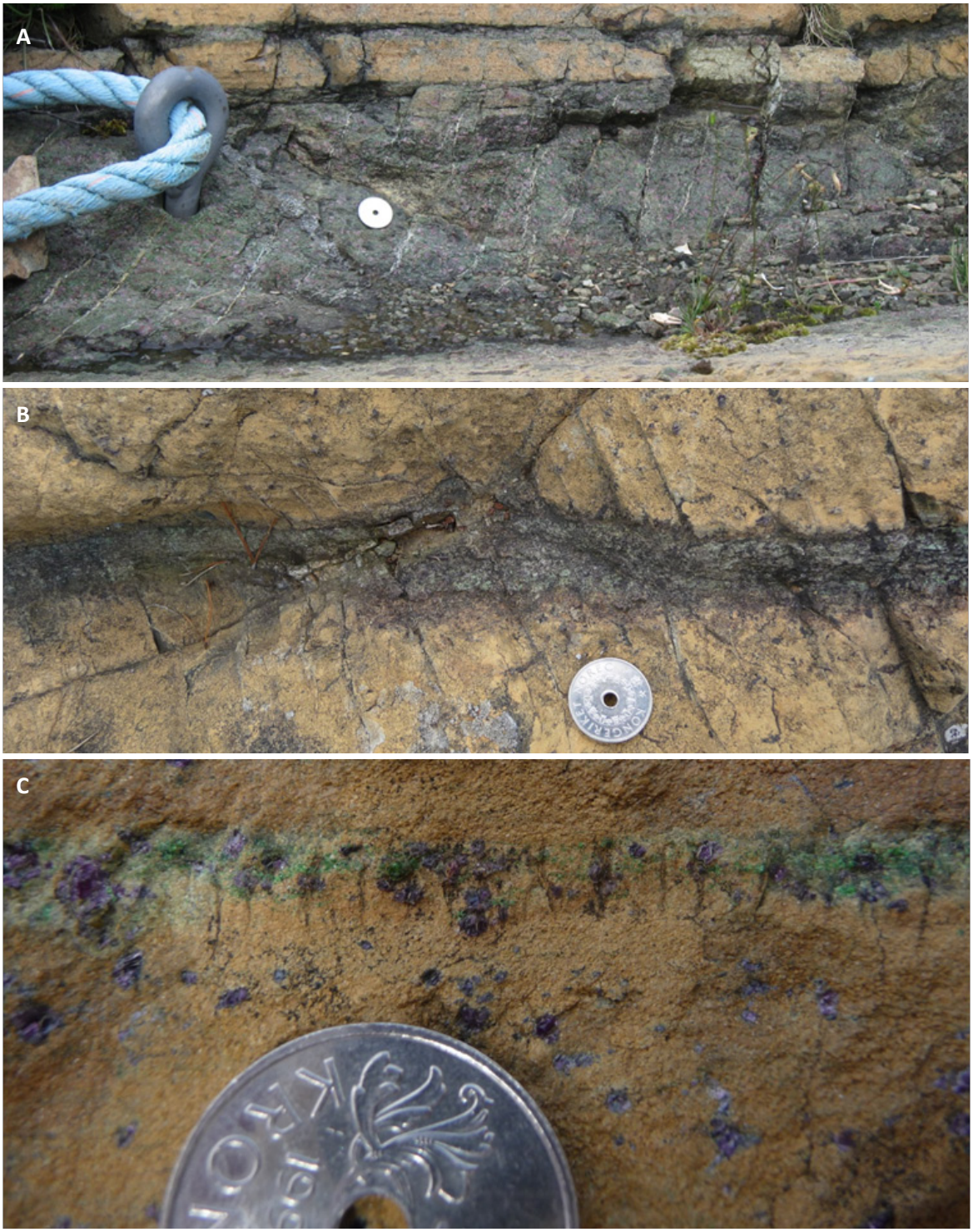

Figure 5.30. *Examples of parallel cross-fractures in a pyroxenite lens at site U7.3 (A), site R4.1 (B) and site U5.2 (C), with regular spacing and angle (perpendicular or oblique).*

At all of the pyroxenite fractures it is observed that most of them stop at the boundary with the surrounding peridotite, but some them cross this boundary for a distance of some mm's or cm's. In the pyroxenite lens at site R4.1, the fractures are not even clearly visible within the lens itself (figure 5.30, middle). At locality U6, the same semi-parallel fractures beneath some pyroxenite lenses, as were observed at site U5.3, can be seen (figure 5.32). Note that both these sites lay in the same area.

Not all fractures are 90° to the layering, they sometimes make an angle with the normal, both regularly and irregularly in one layer.

The width of the fractures is more random and seems to depend more or less on whether it is filled

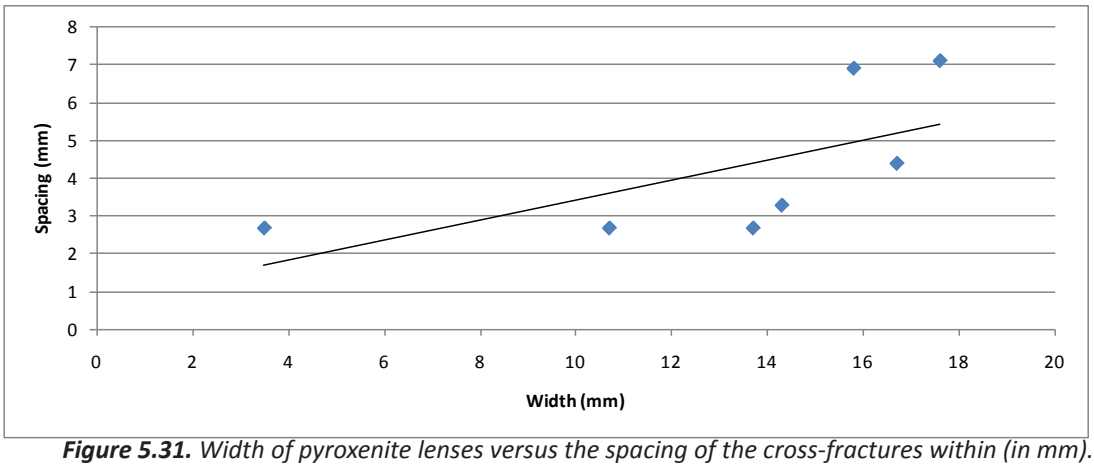

Figure 5.31. *Width of pyroxenite lenses versus the spacing of the cross-fractures within (in mm).*

Figure 5.32. *A view in the direction of a pyroxenite plane and on the parallel fractures within at locality U6.*

or not. In case of the latter, the width of the fracture is up to 2 mm; in case of no filling, fractures are less wide. The filling material is either white or light to dark green.

5.5 FOLDS AND FRACTURES

As is described in the study of Spengler [2006], the compositional banding that is present in both peridotite bodies is folded to a various extent. The observations done here on fracturing with respect to the folding of the compositional banding are not very conclusive. At locality R3, it appears that the folds in the compositional banding hardly contain any fractures. The same holds for locality R9. At some other sites at locality R8, the fractures do run through some slight folds in compositional banding, without changes in direction. And at site U10.1, a very tight fold is seen with also some fractures running through.
These observations are too scarce to give a conclusive result on whether fractures are indeed present in folds or not.

6 MINERALOGY AND MICROSTRUCTURES

6.1 OVERALL MINERALOGY

The samples from the Otrøy peridotite bodies show considerable variation in mineral content and especially in degree of serpentinization. Serpentinization is estimated to be 60–100% in the peridotite, and 20–60% in the pyroxenite lenses. Some samples are almost 100% serpentinized and have only small remnants of primary minerals. Others show a vast network of serpentine mesh that has altered the original mineralogy, but still has relicts of most of the original crystals. In the following two sections, an overview of the mineral content and microstructures in the samples will be given.

6.1.1 Peridotite

In all sampled serpentinized peridotites, the original rock (prior to serpentinization) mainly consists of olivine (forsterite, $Fo_{92\text{-}93}$), together with a substantial amount of orthopyroxene (enstatite) in most of the samples. Minor constituents are clinopyroxene, garnet and spinel. Spinel is often observed close around garnet, or within it; it is thus interpreted as a reaction product due to the breakdown of garnet.

Among the later stage minerals – minerals that have not been part of the 'original' rock composition before hydrous metamorphism took place – serpentine is the most important. This exists in various polymorphs and appearances throughout the rock as mesh, and it also occurs in veins and fractures. Furthermore, chlorite, amphibole (tremolite/actinolite), talc and calcite are observed, though in smaller amounts. Chemical analyses of these minerals are presented in table 6.1.

Chlorite is present in a few samples as a pseudomorph after garnet (sample R321, U1012). In these samples, spinel crystals lay in an original garnet crystal, which implies that spinel has grown within garnet. The rest of the garnet shape is filled with anhedral chlorite, which also surround the spinel crystals and seem to break down some of the rims of the spinels, implying that chlorite grew last (figure 6.1). It may also be that both minerals are intergrown at approximately the same time, as will be discussed in subsection 7.1. In outcrop, these pseudomorphs appear as garnets wrapped in silvery shells (figure 6.2).

Peridotite body	Raudhaugene		Ugelvik				
Sample	R321	R321	U1012	U1012	U1012	U1012	U1012
Analysis	2-2	2-3	2-5	2-4	2-10	2-1	2-9
Mineral	*chlorite (l)*	*chlorite (d)*	*chlorite*	*amphibole*	*amphibole*	*talc*	*talc*
Location	*p-morph*	*p-morph*	*vein*	*vein*	*vein*	*vein*	*vein*
SiO_2	38.005	35.532	33.689	57.165	57.665	59.784	55.212
Al_2O_3	4.910	4.930	14.107	1.565	0.799	0.000	0.000
TiO_2	0.000	0.021	0.000	0.269	0.058	0.000	0.106
FeO	7.654	5.907	3.129	2.351	2.081	6.728	6.724
MgO	34.278	35.186	33.667	23.433	23.764	30.616	28.943
CaO	0.000	0.000	0.053	12.247	12.409	0.384	0.250
K_2O	0.012	0.000	0.078	0.104	0.018	0.000	0.000
Na_2O	0.192	0.116	0.129	0.220	0.239	0.024	0.105
MnO	0.070	0.200	0.000	0.000	0.048	0.104	0.152
Cr_2O_3	0.434	0.972	1.309	0.320	0.484	0.083	0.071
NiO	0.000	0.000	0.000	0.000	0.000	0.000	0.000
Total	85.555	82.864	86.161	97.674	97.565	97.723	91.563

Table 6.1. *Major element compositions of secondary minerals: chlorite, amphibole and talc. p-morph: pseudomorph after garnet; chlorite (l): lighter grey (see figure 6.1); chlorite (d): darker grey.*

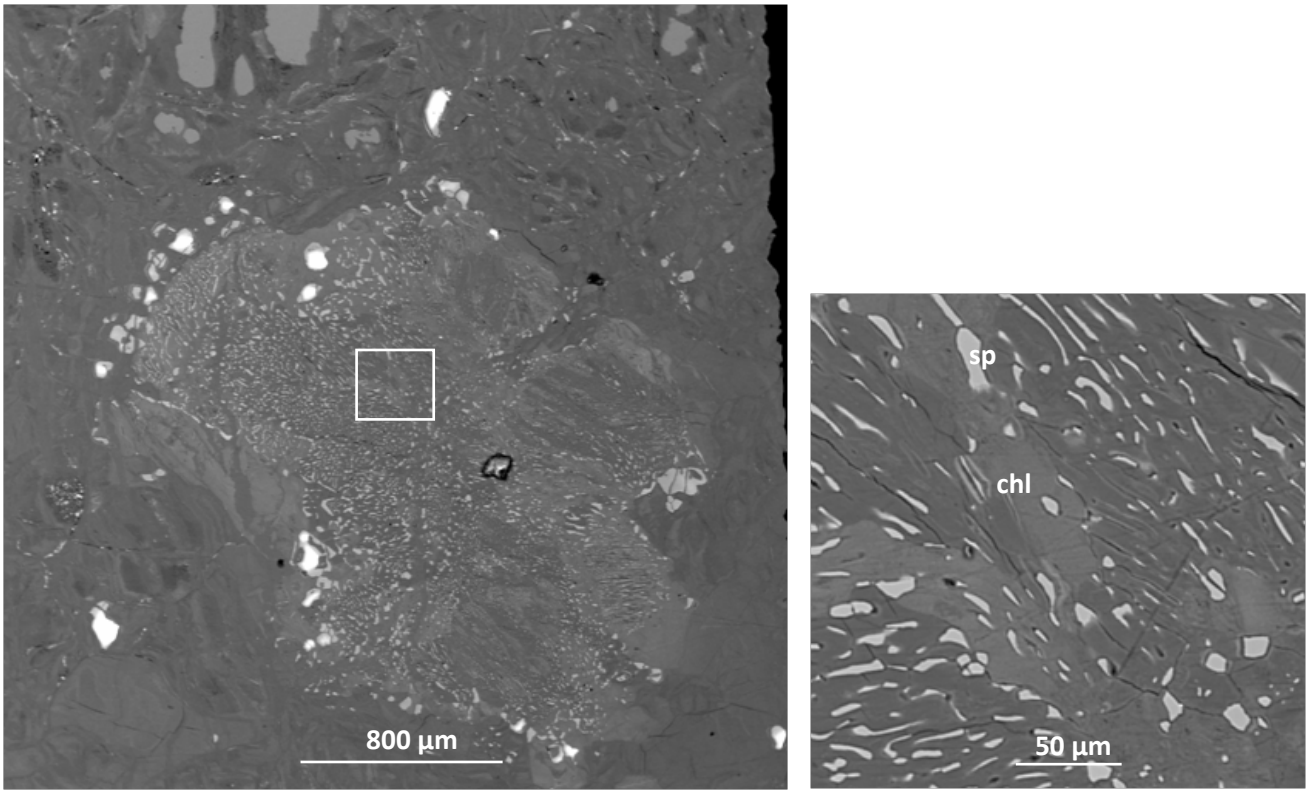

Figure 6.1. *Garnet fully replaced by chlorite (chl, darker matrix) and spinel (sp, lighter flakes within). The two different grey levels in the matrix are produced by slight chemical variations in the chlorite, as can be seen in table 6.1. It is possible that this is caused by a change in composition during formation, due to a changing availability of elements.*

Figure 6.2. *Pseudomorphs after garnet in outcrop, at site U7.2.*

Chlorite is also found as distributed crystals in the peridotite (sample R931), and in some veins in sample U1012. In this sample, amphibole crystals partly surround chlorite – which implies that chlorite has been replaced by amphibole – both in the veins and the pseudomorphs after garnet (figure 6.3). Figure 6.4 shows that amphibole often occurs near garnet, both with or without a kelyphitic rim. This rim consists of a very fine-grained mixture of spinel + enstatite (± diopside ± amphibole) as a consequence of reaction of garnet with olivine upon exhumation [Spengler, 2006]. Talc is present in sample U1012 (from a thick vein) only; it appears as fibrous masses and it surrounds amphibole and chlorite in the vein. It also surrounds chlorite and amphibole crystals in the rest of the sample.

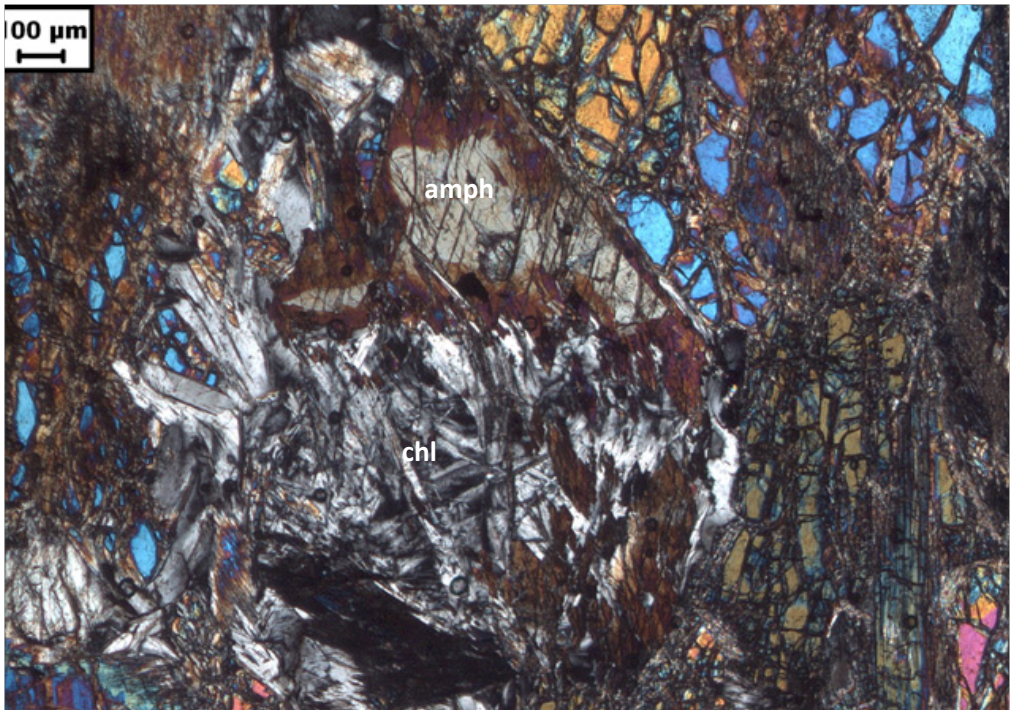

Figure 6.3. *XPL picture of amphibole (amph) partly replacing chlorite (chl, pseudomorph after garnet) in thin section U1012. The scale bar depicts 100 µm.*

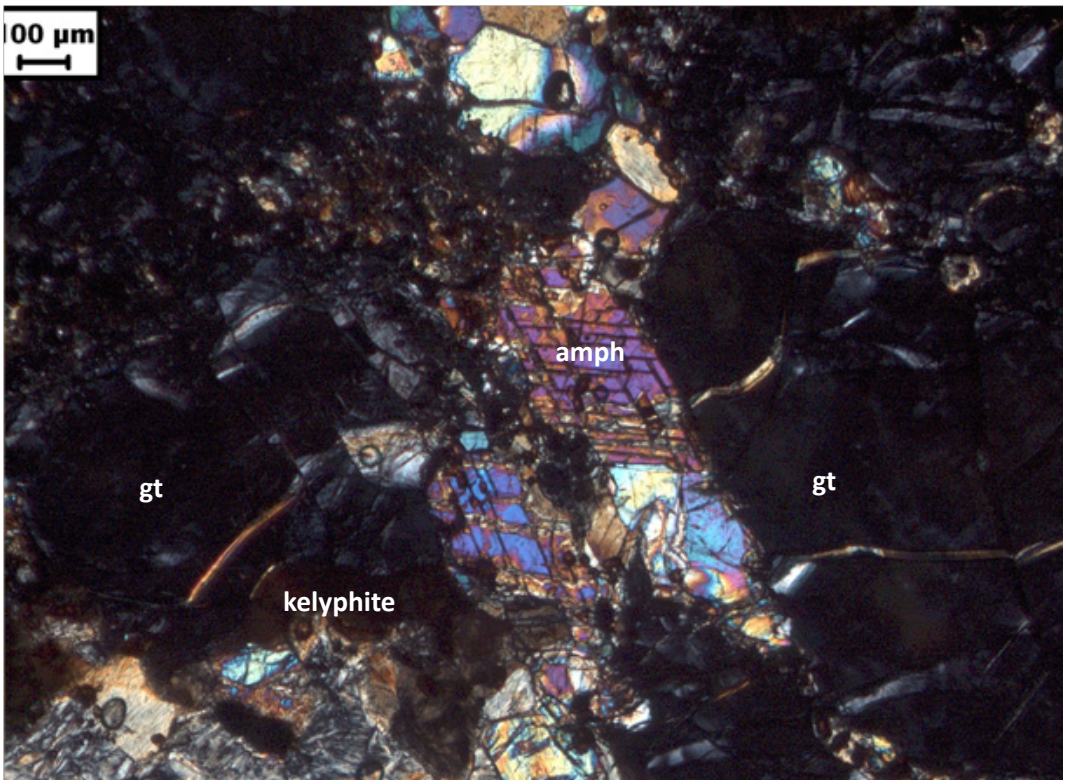

Figure 6.4. *Picture in XPL of amphibole (amph) near a garnet (gt) with a small kelyphitic rim, and one without, in thin section R422A. Scale bar stands for 100 µm.*

In most of the samples, small groups of opaque minerals are present in between the mesh rims and in veins, often growing in narrow strings; these are iron-oxides (magnetite or hematite). In one of the samples (R422), some small crystals of nickel-sulfide are found.

6.1.2 Pyroxenite

The sampled pyroxenite layers have some differences in mineral content. Compositions range from websterite to orthopyroxenite, they thus contain various percentages of mainly orthopyroxene, together with clinopyroxene and minor olivine. Most of them are garnet-rich (up to 20%).
One pyroxenite lens, R422, has a relatively high percentage of olivine. This has caused serpentinization (about 60%, compared to 80% in the surrounding peridotite) in the pyroxenite layer itself (figure 6.5). Related to this is the occurrence of kelyphitic rims around the garnet in sample R422, thus within the pyroxenite lens.
Other pyroxenites are hardly serpentinized. Sample U631 (figure 6.6) shows only minor (20%) serpentinization, caused by a low olivine content and relatively high percentage of clinopyroxene and minor orthopyroxene. Garnets in the pyroxenite do not have a kelyphitic rim whereas they do have that in the surrounding peridotite.
The serpentinization of the pyroxenite lens in this sample is made out of bastite after orthopyroxene.

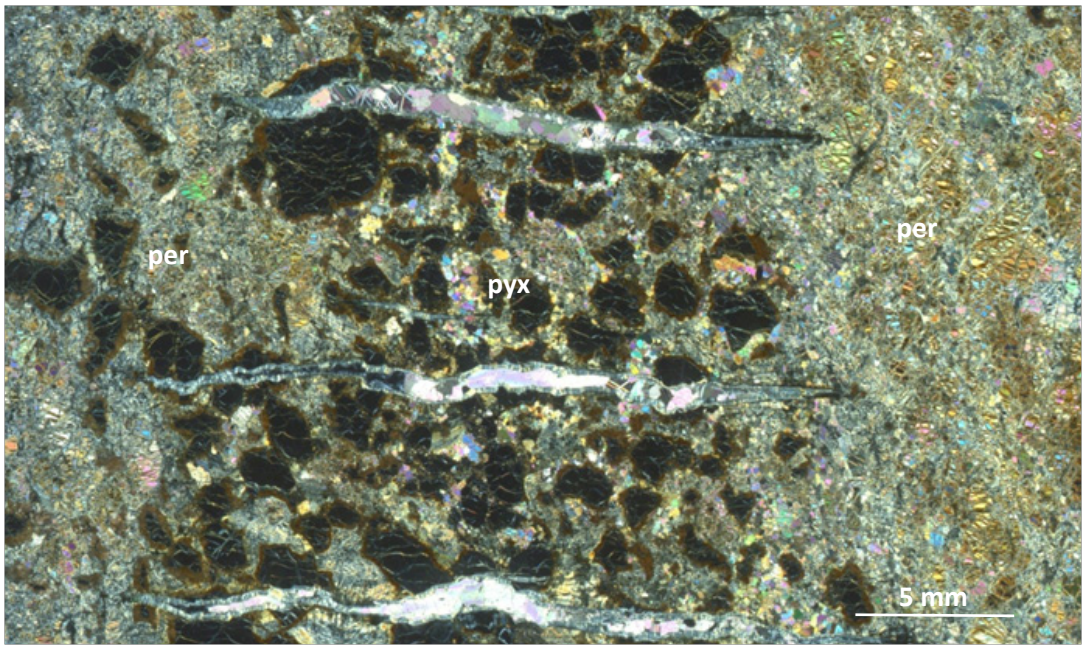

Figure 6.5. *Thin section R422A in XPL: pyroxenite layer (pyx) within peridotite (per). The pyroxenite layer is characterized by a high garnet content and a relatively high olivine content and subsequent serpentinization.*

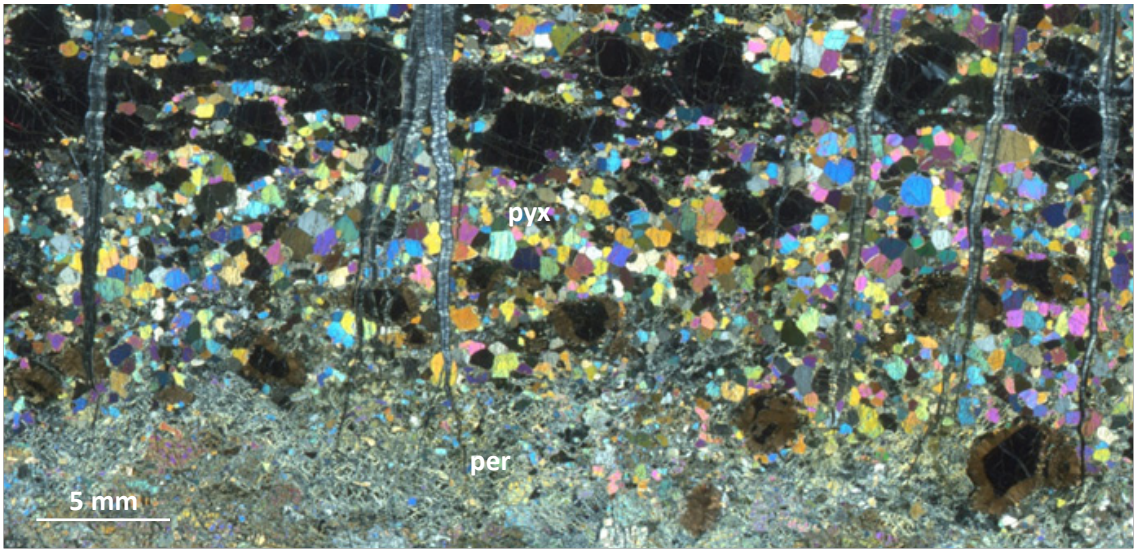

Figure 6.6. *Thin section U631 in XPL. The contrast between pyroxenite layer and peridotite is much clearer.*

6.2 MICROSTRUCTURES AND CHEMISTRY

6.2.1 Mesh

Serpentine

In all samples, the serpentinization of the peridotite is identified as a mesh texture because remnants of original crystals can be observed everywhere. Furthermore, minerals that cannot or can hardly be serpentinized, like garnet or clinopyroxene, are often fractured on the same scale as the mesh network (figure 6.7).

The serpentine in the mesh shows quite some similarity in all samples. The only differences occur due to varying degrees of serpentinization and if the sample is weathered or not. In general, the mesh appears as quite fibrous rims when serpentinization is not complete, which can be seen in figure 6.8. Rims can also show as more fine-grained aggregates. When serpentinization is nearly to fully completed, crystal relicts are completely replaced by serpentine, which is again mainly fibrous. The mesh texture then becomes an hourglass texture, because the individual original grains cannot be recognized anymore (figure 6.9). The serpentines in the mesh most resemble the description of knotted strings or feathers, given by O'Hanley [1996]. The combination of fibrous and feather-like serpentine implies a mixture of lizardite and chrysotile.

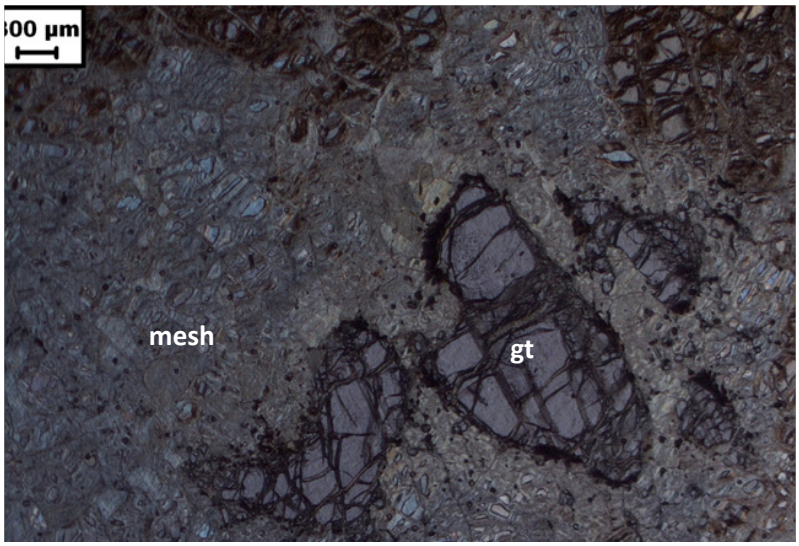

Figure 6.7. *Fractured garnet (gt) in XPL, in sample R412. The scale bar is 300 µm.*

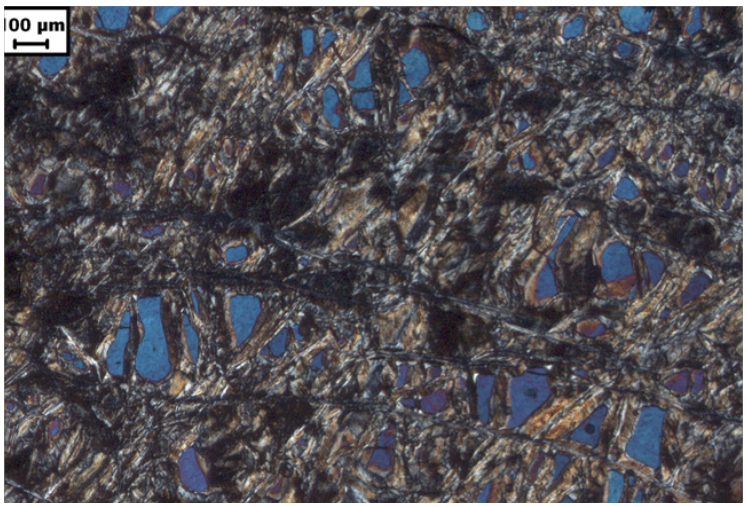

Figure 6.8. *Picture in XPL of mesh texture in sample R412, showing incomplete serpentinization and typical fibrous to feather-like mesh rims. Scale bar is 100 µm.*

Peridotite body	Ugelvik							Raudhaugene				
Sample	U531A	U532A	U611	U631	U631	U632	U1012	R422A	R422B	R931B	R931B	R931B
Serpentinization	98%	80%	99%	70%	70%	70%	50%	80%	80%	80%	80%	80%
Analysis	1-4	1-10	2-3	1-7	2-8	1-15	1-4	1-14	1-5	1-4	1-10	1-12
Mineral	serp	serp	serp	serp	serp	serp	serp	serp	serp	serp	serp	serp
Location	mesh	mesh	mesh	mesh	mesh	mesh	mesh	mesh	mesh	mesh	mesh	mesh
SiO_2	40.698	34.429	41.320	40.156	38.194	40.565	41.222	36.952	41.461	40.300	39.430	34.775
Al_2O_3	0.685	0.020	0.000	0.014	0.000	1.351	0.076	1.611	0.000	0.048	0.118	0.047
TiO_2	0.007	0.000	0.105	0.000	0.000	0.046	0.000	0.039	0.000	0.012	0.000	0.000
FeO	4.332	7.888	3.050	5.360	5.249	5.562	3.390	7.506	4.103	3.475	5.408	4.780
MgO	37.600	38.662	39.270	38.953	38.868	36.854	39.092	37.246	39.611	39.430	38.946	40.507
CaO	0.018	0.051	0.309	0.025	0.000	0.043	0.042	0.132	0.000	0.023	0.012	0.026
K_2O	0.000	0.000	0.000	0.000	0.019	0.000	0.000	0.000	0.077	0.000	0.000	0.000
Na_2O	0.006	0.004	0.057	0.019	0.000	0.012	0.005	0.005	0.083	0.000	0.009	0.014
MnO	0.104	0.102	0.000	0.055	0.000	0.036	0.005	0.095	0.364	0.022	0.089	0.056
Cr_2O_3	0.170	0.000	0.000	0.013	0.061	0.105	0.000	0.164	0.154	0.000	0.009	0.000
NiO	0.098	0.327	0.000	0.433	0.000	0.026	0.335	0.094	0.000	0.397	0.406	0.275
Total	83.718	81.483	84.111	85.028	82.391	84.600	84.167	83.845	85.853	83.707	84.427	80.480
FeO + MgO	41.932	46.550	42.320	44.313	44.117	42.416	42.482	44.752	43.714	42.905	44.354	45.287
FeO/(FeO+MgO)	0.103	0.169	0.072	0.121	0.119	0.131	0.080	0.168	0.094	0.081	0.122	0.106

Table 6.2. *Major element compositions of serpentines in the mesh. Measurements are in weight percentage.*

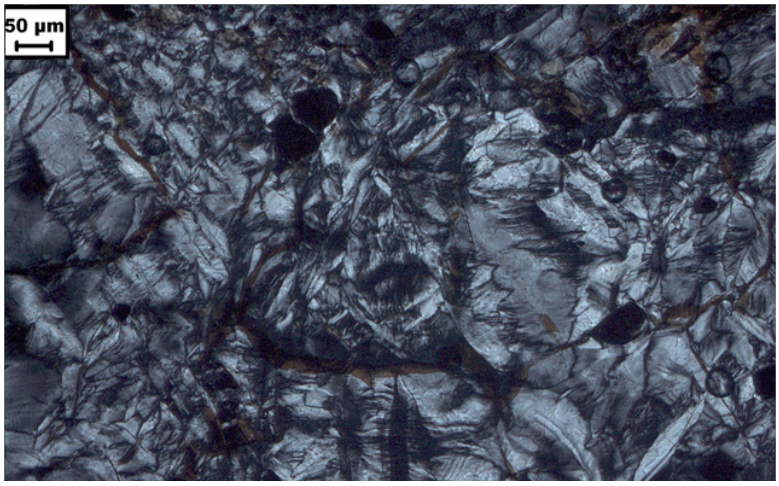

Figure 6.9. *Hourglass texture after (almost) complete serpentinization in sample R321.*

Chemical analyses of serpentine in the mesh of several samples are shown in table 6.2. The measurements in this table show quite consistent characteristics.
Almost all analyses are very low in Al_2O_3, except for sample U531A (analysis 1-4), sample U632 (analysis 1-15) and sample R422A (analysis 1-14). They tend to have a somewhat lower MgO content, which is probably substituted by Al_2O_3. A plot of FeO/Al_2O_3 is shown in figure 6.10A. As can be seen, lizardite has the highest Al_2O_3 values. The data point in between both groups has intermediate Al_2O_3 content, but it is not certain if this is also lizardite.
Figure 6.10B shows a plot of FeO against FeO+MgO, with lines for the fixed values of this proportion (a so-called Fe-number (Fe#)). A slight separation between the measurements below Fe# 0.125 and above that can be seen. The measurements above Fe# 0.125 are lizardite, except one, which is however not the same measurement as the one that lays in between the groups in figure 6.10A. Plot 6.10B shows that lizardite has indeed more MgO substituted by FeO, as was stated in subsection 3.2.
Samples U532A (analysis 1-10) and sample R931B – analysis 1-12 are both relatively low in SiO_2 and H_2O. This does not give implications on the serpentine polymorph, but rather on impurities present in the serpentine [Whittaker and Wicks, 1970]. A high H_2O, high MgO and low SiO_2 content is likely caused by a hydrous impurity, like brucite. Thus, it is probable that brucite layers are present here in between the serpentine layers in the mesh.

Bastite
In highly serpentinized samples, considerable bastite occurs. In pyroxenite layers, often the only serpentine aggregates are formed by bastites after orthopyroxene. Under the microscope these are mainly distinguished from serpentines after olivine by their ability to preserve cleavage from the original crystal (figure 6.11). Serpentine after olivine often has a more varying structure, as was shown in figure 6.9.
Chemically, there is some distinction between bastite after orthopyroxene and serpentine after olivine, as can be seen in table 6.2 and 6.3. Bastite has a lower MgO content and a higher Al_2O_3 content than (most of the) serpentine. Also, their Cr_2O_3 is higher. This is consistent with what is found in literature [Mével, 2003].
As mentioned in section 3.1, bastites after clinopyroxene are rare. This is also observed under the microscope. The clinopyroxenes that are present in the pyroxenite layers are not serpentinized, but somewhat fractured at most.

Iron-oxides
Very fine-grained iron-oxides occur as thin strings of dark red/brown (in PPL) to opaque minerals alongside the mesh rims (figure 6.12). The extent to which these are present differ. Whether these iron-oxides are magnetite (Fe_3O_4) or hematite (Fe_2O_3) was not possible to determine with the mi-

croprobe, since it cannot normally distinguish between Fe^{2+} and Fe^{3+}.

Ni-sulfide

As mentioned in subsection 6.1.1, sample R422 is the only sample in which some small crystals of nickel-sulphide are found in the mesh. This is probably haezlewoodite (Ni_3S_2), which is supposed to be recrystallized from primary sulphides during serpentinization [Mével, 2003].

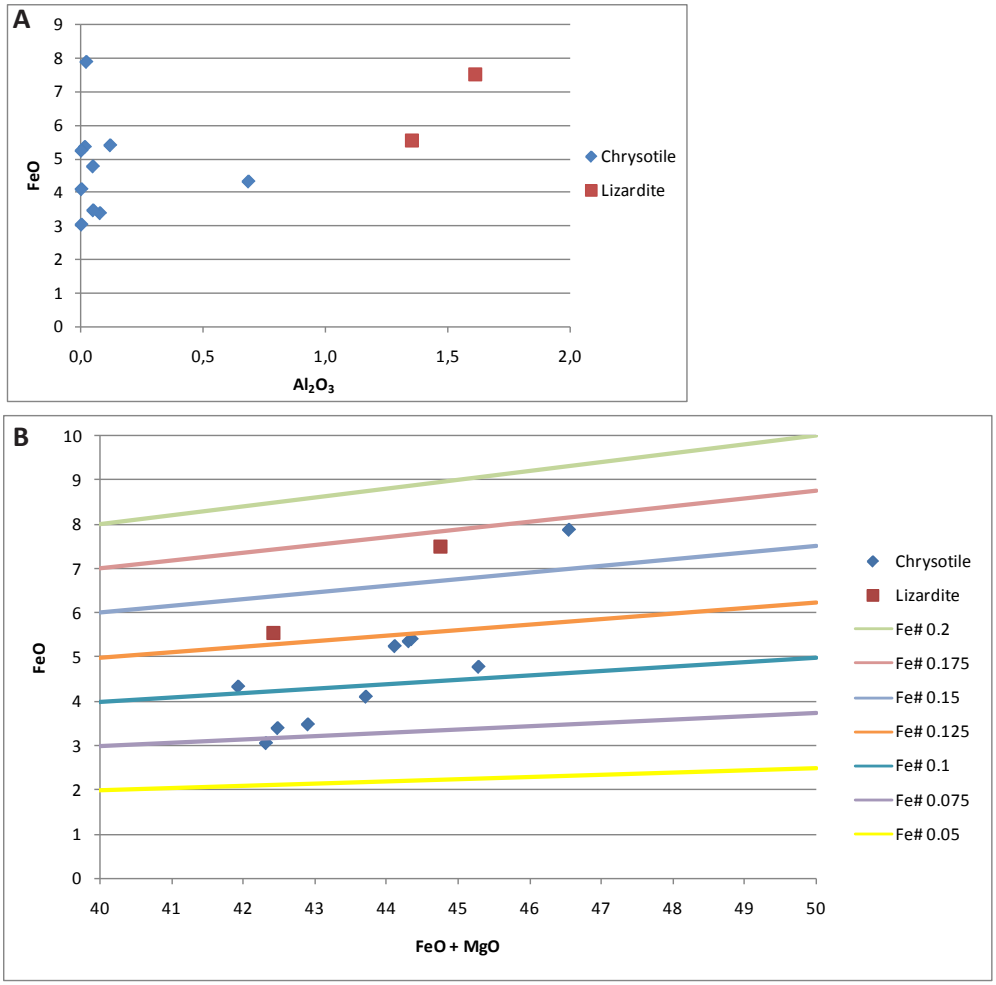

Figure 6.10. *A: Plot of FeO content against Al_2O_3 content. Lizardite clearly plots in a separate area from chrysotile. B: Plot of the proportion of FeO/(FeO+MgO). Lizardite plots above the Fe# 0.125 line, having a higher content of FeO relative to that of chrysotile.*

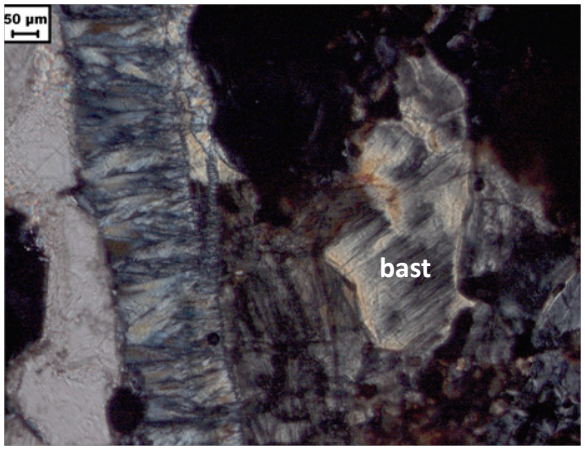

Figure 6.11. *Bastite (bast) after orthopyroxene in a pyroxenite lens, clearly showing the original cleavage of the crystal.*

Peridotite body	Ugelvik	Raudhaugene	
Sample	U631	R422	R931B
Analysis	2-1	2-2	1-11
Mineral	bastite	bastite	Bastite
Location	pyroxenite	pyroxenite	Mesh
SiO_2	41.190	38.405	40.282
Al_2O_3	2.030	1.385	1.131
TiO_2	0.000	0.123	0.010
FeO	6.550	5.525	8.297
MgO	31.031	35.666	33.061
CaO	0.073	0.043	0.105
K_2O	0.000	0.000	0.000
Na_2O	0.113	0.000	0.011
MnO	0.071	0.289	0.089
Cr_2O_3	0.212	0.141	0.155
NiO	0.000	0.000	0.178
Total	81.270	81.578	83.319

Table 6.3. *Major element compositions of bastites in both pyroxenite lenses and mesh.*

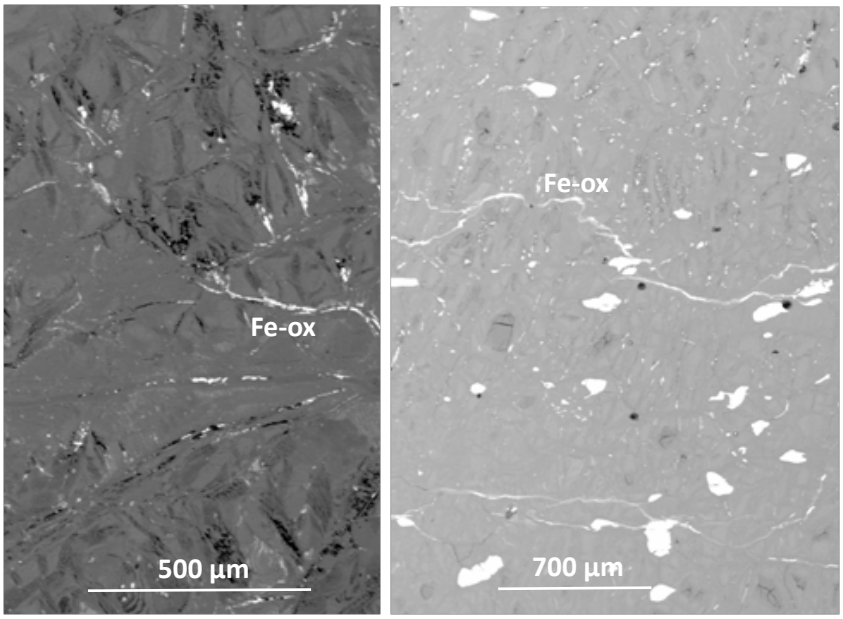

Figure 6.12. *Microprobe picture of strings of iron-oxides (Fe-ox) in between the mesh rims, in thin section R321 (left) and U611 (right). Differences in grey shade are due to the resolution of the picture, not to differences in chemistry.*

Weathering

In much of the thin sections, the serpentine in the mesh has a red-brown weathered colour. It mainly occurs in distinct areas: around the serpentine fractures/veins and at the former surface of the rock, as can be seen in figure 6.13. This weathering of serpentine can be explained by the oxidation of magnetite or hematite that occurs along the mesh rims, due to the presence of water and/or air. Oxidation is less in pyroxenite layers, due to the lower iron-oxide content.

A striking exception appears in thin section U412. Here, the brown oxidation colour of the serpentine mesh is present throughout the sample, but hardly around both serpentine veins that run through (figure 6.13C). This may be caused by a local lack of free iron-oxides along these fractures, because they are locked within the serpentine filling.

Thick fracture rims

The thin sections that were made to investigate the rims around fractures do not give very clear observations. In none of the samples, the degree of serpentinization, structure, mineral content or

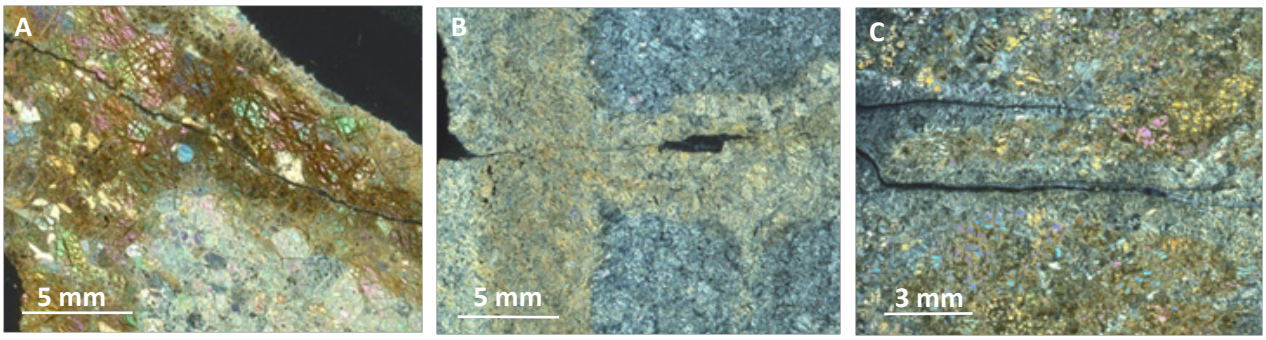

Figure 6.13. *Thin sections of sample R931A (A), U611 (B) and U412 (C) in XPL. A and B clearly show a brown weathered rim around fractures and the former surface. C shows the opposite, the rim around the fractures is not brown, whereas the inner part of the sample is.*

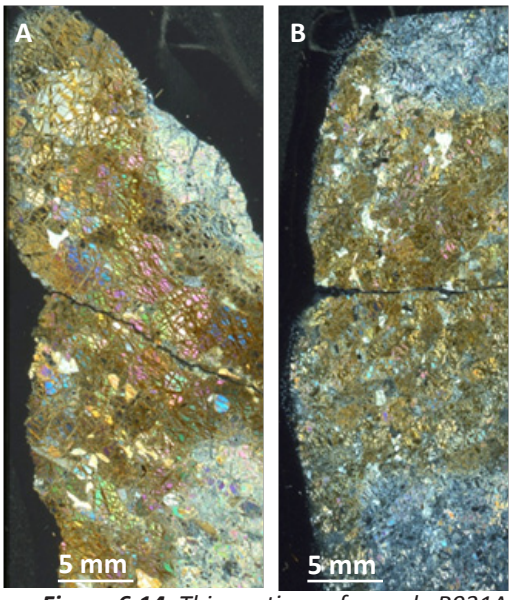

Figure 6.14. *Thin sections of sample R931A (A) and R931B (B) in XPL, showing a thickened rim at the surface around the fractures.*

else is different for the rim of the fracture than for the rest of the section, as is shown in figure 6.14. It can be concluded that there are no signs here of locally coarsened (recrystallized) olivine, interpreted as a fluid pathway, as depicted by Spengler [2006]. Thus, nothing can be said about whether these are reaction rims or not.

6.2.2 Fractures and veins

Fractures or veins occur in various forms and thicknesses and have various fillings, as mentioned earlier. This variety in growth forms, and the presence of several generations becomes even more clear at thin section-scale.

Serpentine is the main fracture-filling material. Some fractures are filled with only one form of serpentine. However, in some samples, serpentine occurs in different growth forms in one fracture, showing different generations, or at least different stages of serpentine growth. Furthermore, calcite is observed in several fractures. Chlorite and talc are present in one thin section as a vein-filling material.

Microprobe measurements from different fractures in some of the samples are presented in table 6.4, in which also the interpretation of the serpentine polymorph is shown. The data shows more variation than the data for the mesh, however, when comparing the data in table 6.2 and 6.4, there are no striking differences between serpentines in the mesh and in fractures.

A plot of FeO/Al_2O_3 is presented in figure 6.15A, but this does not show a clear grouping of the serpentine polymorphs. The only thing that comes up from the plot is that most lizardites indeed have a relatively high Al_2O_3 content, which is mentioned earlier on (in subsections 3.2 and 6.2.1).

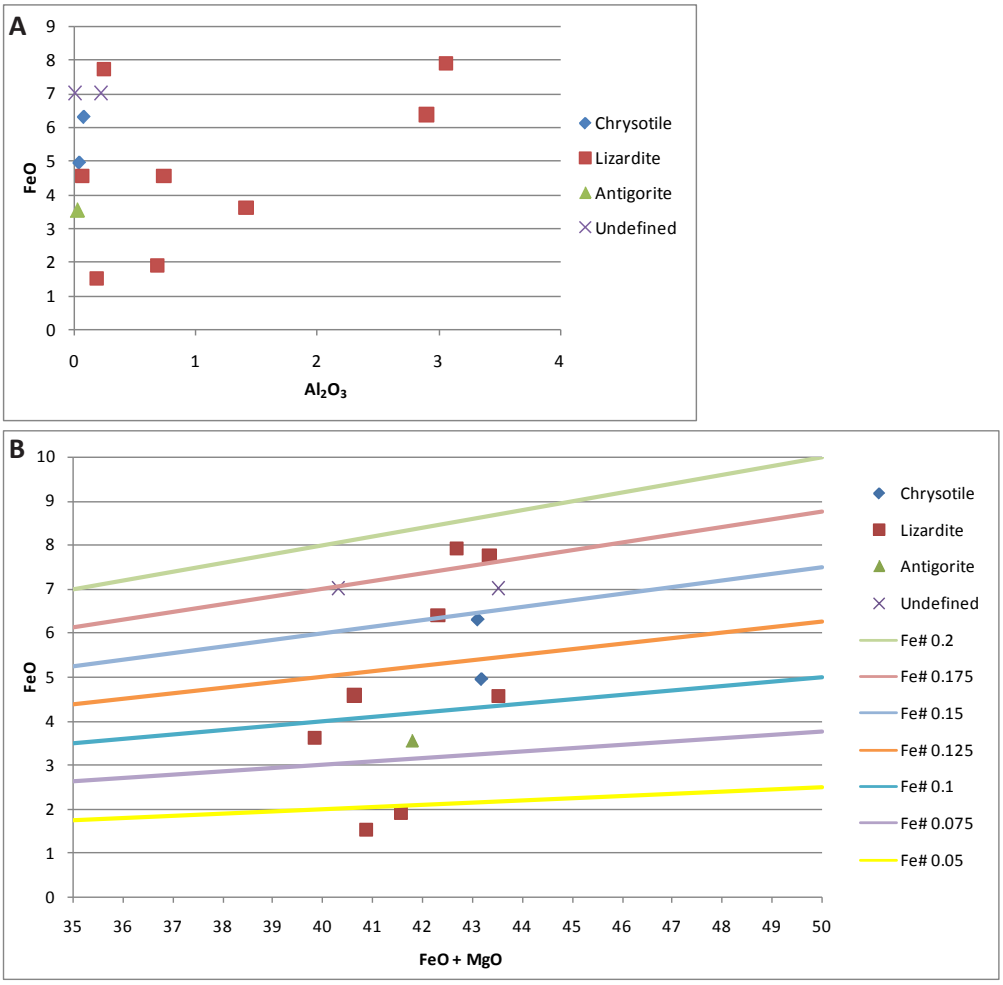

Figure 6.15. *Plots for fracture-filling serpentine analyses. A: FeO/Al_2O_3, only lizardite shows some distinction. B: FeO/(FeO+MgO), there is no clear separation to be seen between different serpentines.*

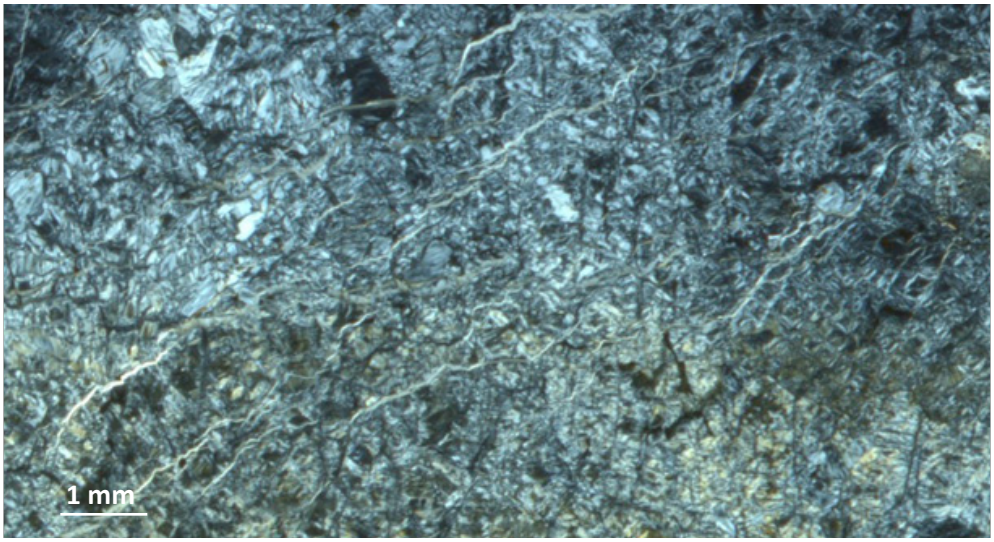

Figure 6.16. *XPL picture of thin section R321 shows small network of serpentine fractures all having more or less the same orientation.*

The plot for FeO/(FeO+MgO) in figure 6.15B does not show a clear distinction between the different serpentines either. The results from these plots in figure 6.15 are probably due to an influence of local differences in element availability. It is also possible that there has been more recrystallization between different serpentines in fractures than was previously assumed in this study, which causes

Sample	R422A		U531A				U532A			U532B	U631	U632	
Analysis	1-5	1-4	1-1	1-5	1-6	1-8	1-1	1-3	1-5	2-1	1-1	1-1	1-2
Mineral	liz	liz	liz	liz	ant	chr	chr	liz	serp	serp	liz	liz	liz
Location	outer	inner	inner	inner	outer	cross	cross	vein	vein	vein	inner	inner	outer
Appearance	triangular	triangular	granular	granular	ribbon	fibrous	banded	star	fibrous	fibrous	granular	granular	triangular
SiO_2	39.961	38.685	41.390	43.865	43.857	36.422	41.229	43.044	41.998	40.636	42.239	41.650	42.588
Al_2O_3	2.895	3.054	0.068	0.187	0.018	0.037	0.076	0.246	0.210	0.000	1.411	0.686	0.736
TiO_2	0.000	0.002	0.011	0.000	0.000	0.008	0.000	0.000	0.012	0.113	0.013	0.014	0.021
FeO	6.397	7.900	4.572	1.548	3.554	4.936	6.299	7.751	7.008	6.997	3.622	1.924	4.586
MgO	35.906	34.773	38.931	39.323	38.227	38.244	36.807	35.578	36.502	33.324	36.222	39.647	36.042
CaO	0.016	0.022	0.005	0.013	0.000	0.011	0.033	0.020	0.064	0.000	0.107	0.011	0.075
K_2O	0.000	0.000	0.000	0.000	0.000	0.000	0.000	0.000	0.000	0.030	0.000	0.000	0.000
Na_2O	0.013	0.005	0.004	0.000	0.006	0.002	0.000	0.006	0.010	0.088	0.000	0.003	0.033
MnO	0.074	0.100	0.005	0.004	0.022	0.044	0.208	0.126	0.191	0.274	0.087	0.036	0.084
Cr_2O_3	0.025	0.005	0.000	0.001	0.007	0.000	0.000	0.129	0.031	0.083	0.025	0.000	0.000
NiO	0.016	0.014	0.032	0.054	0.202	0.000	0.037	0.054	0.033	0.000	0.000	0.021	0.014
Total	85.303	84.561	85.018	84.995	85.893	79.704	84.689	86.956	86.059	81.545	83.726	83.992	84.179
FeO+MgO	42.303	42.674	43.503	40.871	41.781	43.180	43.106	43.329	43.510	40.321	39.844	41.571	40.628
FeO/(FeO+MgO)	0.151	0.185	0.105	0.038	0.085	0.114	0.146	0.179	0.161	0.174	0.091	0.046	0.113

Table 6.4. *Major element compositions of different serpentines in fractures and veins. Measurements are in weight percentage. Liz = lizardite, chr = chrysotile, ant = antigorite, serp = undefined serpentine.*

the chemistry of the serpentines to mix up a bit.

6.2.2.1 *Peridotite fractures*

Thin section R321 is the only sample that shows a micro-scale fracture network (figure 6.16). In this sample, a network of narrow and short fractures is observed; they are up to 3 mm long and 10-100 µm wide. All fractures have the same orientation and they cut through all other structures (mesh). Furthermore, the fractures are not perfectly straight; they are somewhat kinked. No generations or cross-cutting relationships are observed between separate fractures. They are filled with serpentine, which is fibrous perpendicular to the long direction (figure 6.17). Pictures of the microprobe show hardly any difference in grey-scale for the mesh and the fractures, which implies that both have (almost) exactly the same chemistry. Unfortunately, no chemical analysis of the fractures are done (partly because they could not be recognized under the microprobe, because of their similar colour), but when comparing them to veins discussed in other studies, their structure and infill most resembles chrysotile [Andreani et al, 2007], as is shown in figure 6.18.

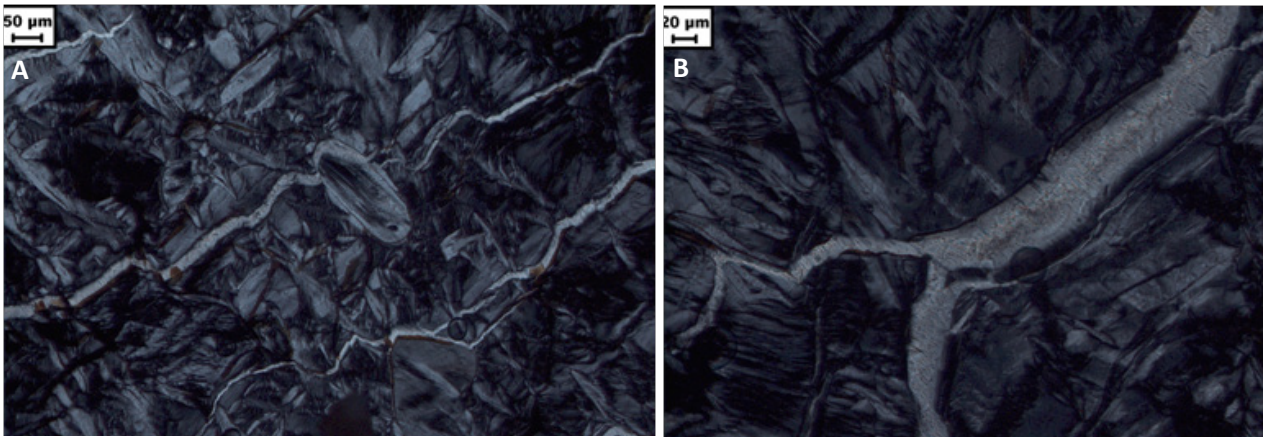

Figure 6.17. *Pictures in XPL from fibrous chrysotile fractures in sample R321.*

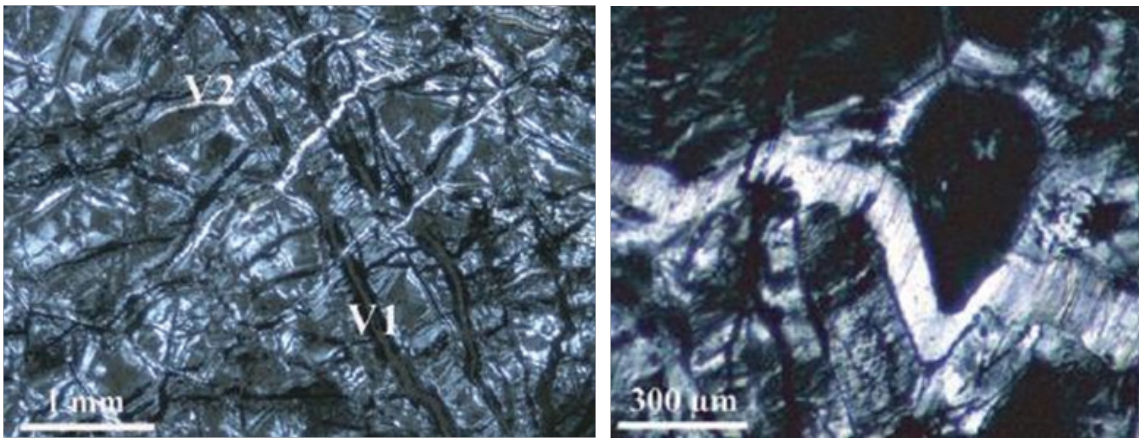

Figure 6.18. *Pictures from Andreani et al. [2007] showing 'V2' serpentine veins.*

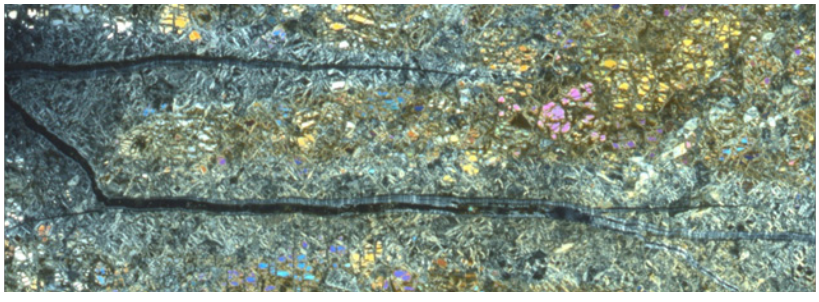

Figure 6.19. *Two parallel banded fractures in XPL in thin section R412.*

In thin section R412 (figure 6.19), two parallel fractures from a pyroxenite layer that continue in the surrounding peridotite are present. These are approximately 1 mm wide and 1.5 cm and 3 cm long, the longest with two thinner side-branches close to its tip. Both fractures are filled with serpentine, which shows a banded structure parallel to the long direction. There is some differentiation between the outer and inner part of the fractures. The outer rim consists of thinner laminated kinked bands, whereas the inner part has wider bands, which are only a bit kinked. Furthermore, the serpentine that grows in this inner part shows a semi-parallel/triangular structure (perpendicular to the long direction of the fracture), as shown in figure 6.20. The outer kinked bands show the same characteristics as those discussed in Andreani et al [2007] (V3, see figure 6.21A), which are composed of mainly chrysotile. The inner triangular serpentine is most probably lizardite, consistent with the V4a type in Andreani et al [2007] (figure 6.21B).
In the centre of the fractures, some thin strings of very fine-grained crystals are present, which are calcite by the look of their lively colours.

Figure 6.20. *Outer banded/kinked chrysotile and inner triangular lizardite in a fracture in sample R412. In the centre of the fracture, very fine-grained calcite has grown.*

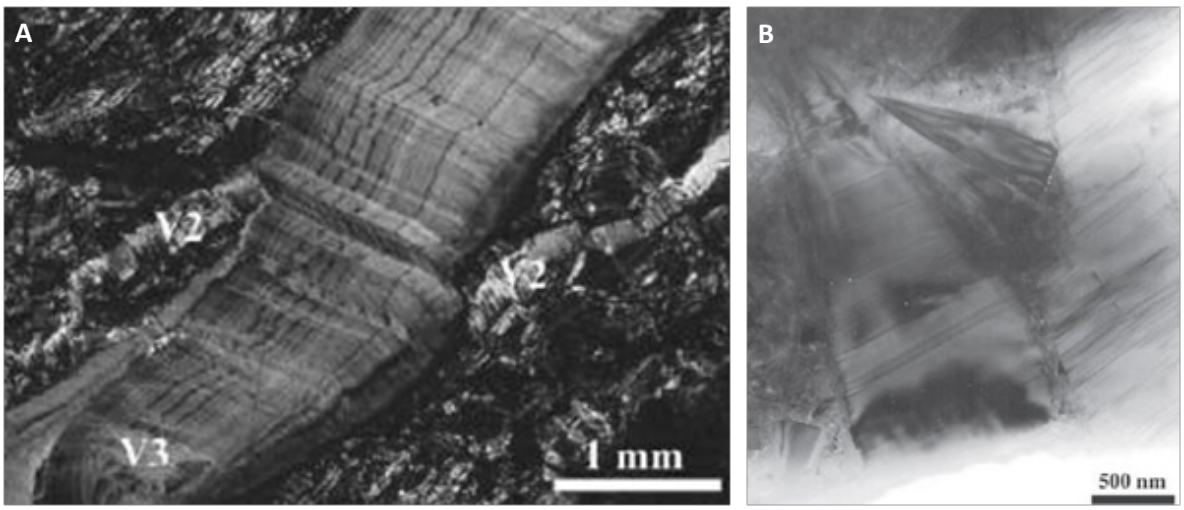

Figure 6.21. *Pictures from Andreani et al. 2007, with examples of banded, kinked V3 fractures (A) and triangular lizardite, the V4a type (B).*

At least two generations of fracturing are observed in thin section U531A and U531B (figure 6.22). This is a sample from the semi-parallel fractures from just under a pyroxenite layer at site U5.3, as described in subsection 5.3. As mentioned, the fractures run along the whole sample and are 0.5 to 1 mm wide; they are filled with serpentine. Under the microscope, a separate outer and inner band can be seen in the fractures (figure 6.23). The outer filling consists of a fibrous serpentine, which exactly looks like ribbons formed by antigorite in a fracture described by O'Hanley [1996], shown in figure 6.24. The inner band is formed by very fine-grained serpentine aggregates. These are probably spherical lizardites, equal to the V4b type in Andreani et al [2007] (figure 6.25). In the centre of this inner filling, strings of hematite or magnetite are formed.

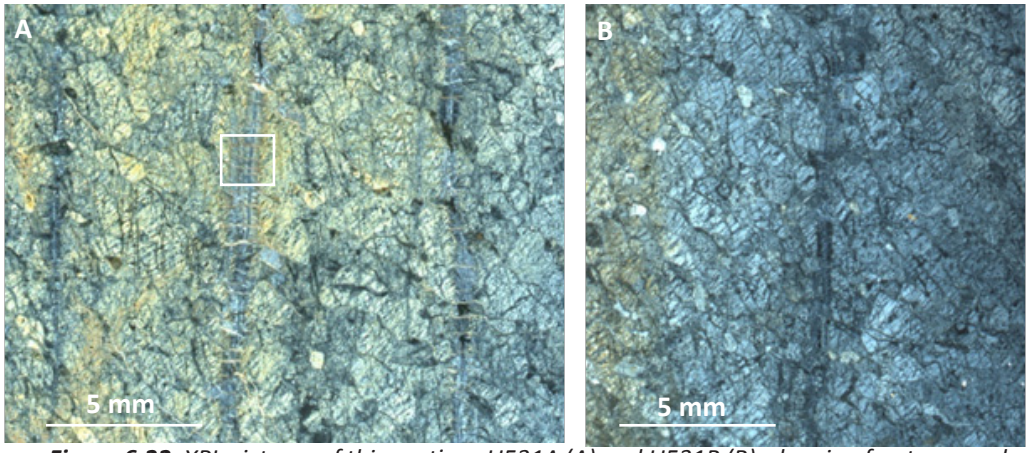

Figure 6.22. *XPL pictures of thin sections U531A (A) and U531B (B), showing fractures and cross-fractures. Square in A depicts the close-up in figure 6.23.*

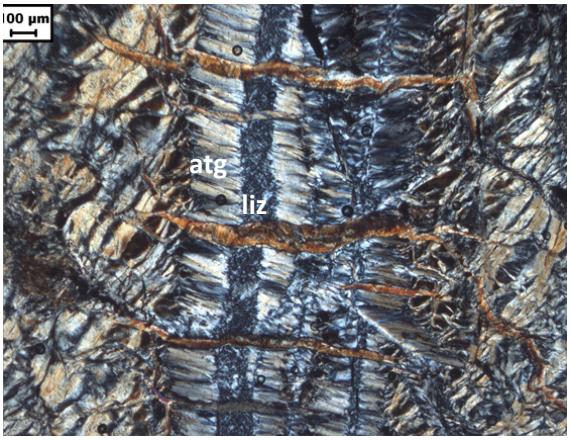

Figure 6.23. *Close-up from thin section U531A (figure 6.22A), showing a fracture with an outer filling of ribbon antigorite (atg) and an inner filling of fine-grained lizardite. Scale bar is 100 µm.*

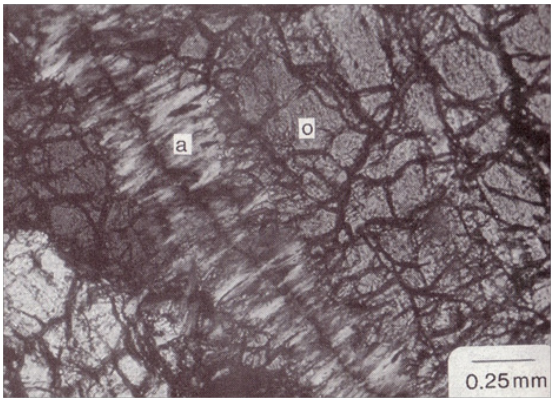

Figure 6.24. *'Ribbon' antigorite, a picture from O'Hanley [1996]. a = antigorite; o = olivine.*

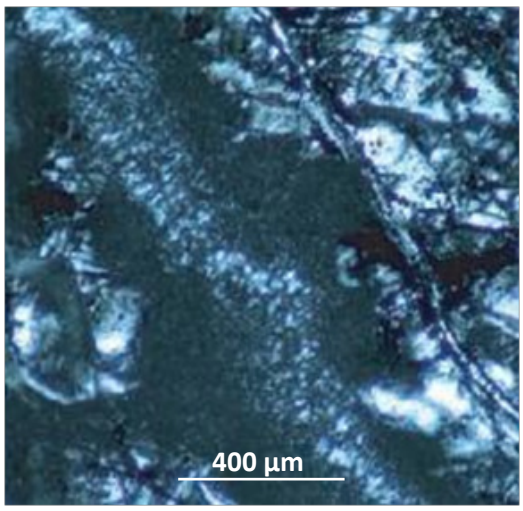

Figure 6.25. *Example of V4b vein consisting of granular lizardite. From Andreani et al. [2007].*

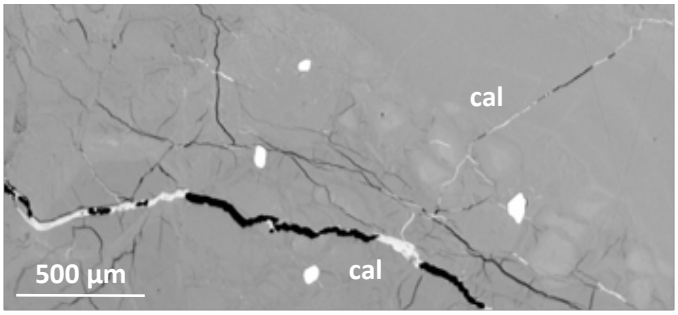

Figure 6.26. *Microprobe picture of thin calcite (cal) -filled fractures within serpentine mesh and fractures.*

A second set of fractures has formed within the first. This set consists of parallel and quite regularly spaced (up to 0.5 mm) cross-fractures, perpendicular to the first set. Some of them continue in the surrounding peridotite. These fractures are also filled with fine-grained to fibrous serpentine; it most resembles that of the fractures in thin section R321.
Furthermore, a couple of thin (about 10 µm wide) (fine-grained) calcite-filled fractures are found within the mesh, close to the serpentine fractures (figure 6.26). They cut through all other structures and the mesh.

Thin section U532A and U532B show no less than four or five types of fracture-filling; of which at least three are serpentines, and one is calcite (figure 6.27). This is a sample from one of the thick veins with visible cross-fractures at site U5.3. The thick vein shows as a fibrous serpentine mass oblique to the long direction of the vein. It is not sure which polymorph is present in the vein, its chemical characteristics do not give conclusive results (see table 6.4). Along the rims of the vein, and throughout the vein, 100 µm long serpentine crystals grow. These crystals are composed of two triangles that grow with one of their tips from one core. Microgranular serpentine grows over the fibrous vein as well. These are both probably lizardite, as recognized in fractures mentioned earlier. Another type of serpentine forms in fractures perpendicular to the large vein – as is also shown at outcrop-scale. These fractures are up to 100 µm wide, start off in the large vein and some of them continue in the mesh. They cut through or grow over the other two serpentines. The filling is composed of banded (parallel to the long direction), kinked serpentine, thus chrysotile. As in thin section R412, some of these fractures are terminated with some side-branches.
Calcite is present as very fine-grained strings running through the centre of the fibrous vein and along the rims of some of the banded serpentine fractures.

The fracture in thin section U611 is part of a small scale (narrow-fractured) network from just under a pyroxenite layer. Although the largest part of the filling of the fracture has disappeared –just

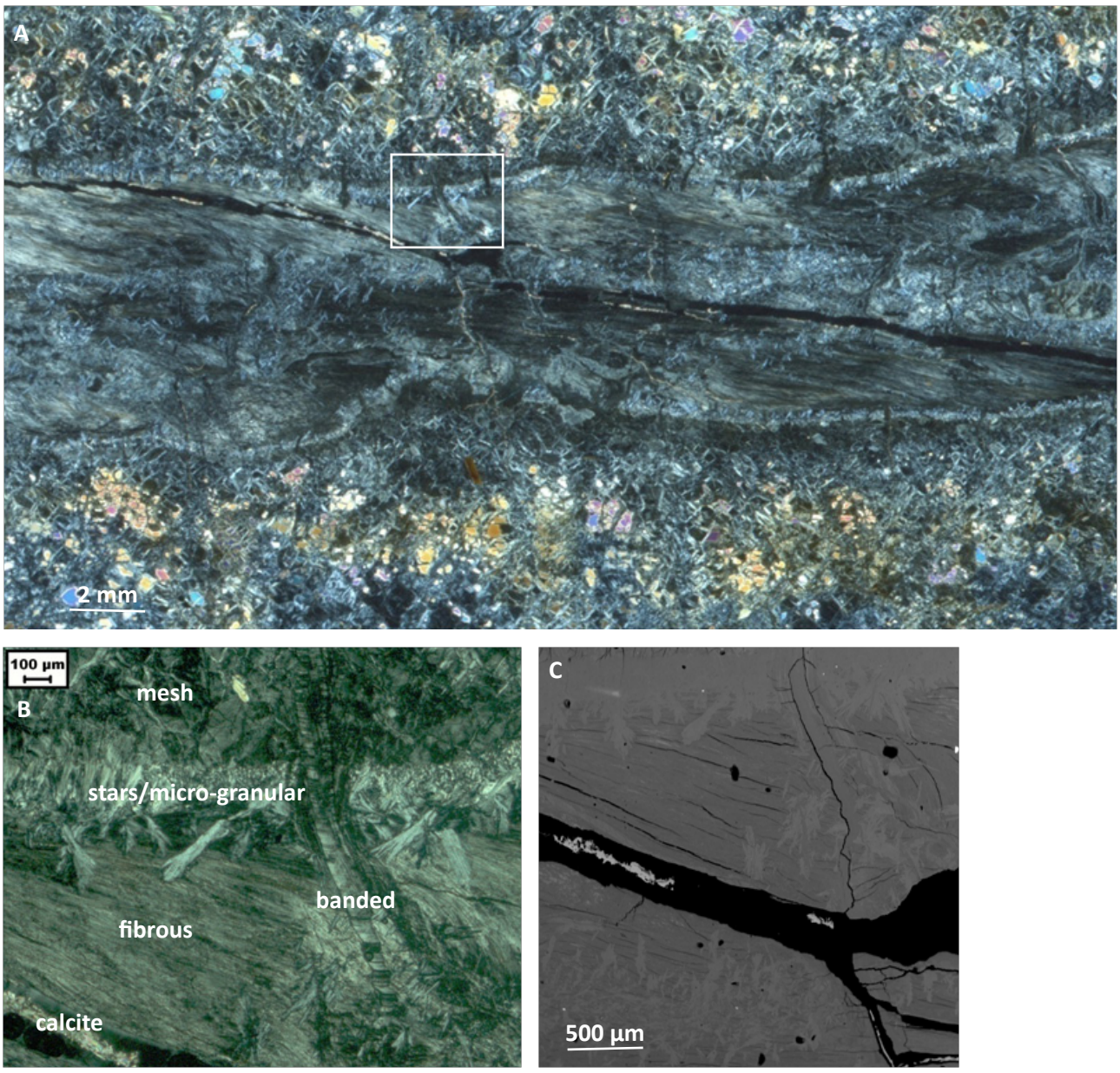

Figure 6.27. *XPL picture of thin section U532A (A) with box depicting magnification (B) in black/white. (B) shows fibrous vein, 'stars' on the rim with some micro-granular serpentine as well, a banded/kinked fracture cutting across, and calcite filling within the fibrous vein. (C) is a scan from the microprobe of the same area.*

because of erosion – some material in it is left. It mainly consists of very fine-grained calcite, which also forms needles growing towards the empty middle of the fracture (figure 6.28). Alongside the wall of the fracture, within some thicker calcite-filled areas, a few fine-grained serpentine patches occur. Calcite also occurs in smaller side-fractures. Furthermore, magnetite/hematite is observed alongside some of the mesh rims, as was shown in figure 6.12B.

Thin section U1012 (figure 6.29), has a fracture/vein that is somewhat different than the rest. This is a sample of the 1-1.5 cm wide long veins at site U10.1, which are filled with pinkish, fibrous material. The material is a mixture of very fibrous talc and chlorite, with minor amphibole. The vein consists of chlorite, and amphibole crystals surround and lay on top of this, thus replacing chlorite, as was shown in figure 6.3 as well for amphibole growing over chlorite throughout the sample. Talc is the latest-stage mineral growth, it surrounds both chlorite and amphibole crystals in the vein as a very fibrous mass (figure 6.30). Throughout the rest of the thin section, some small (up to 100 µm) chlorite veins are observed. In those veins, talc and minor amphibole also replace chlorite, talc being the latest stage. Chlorite also occurs as pseudomorphs after garnet.

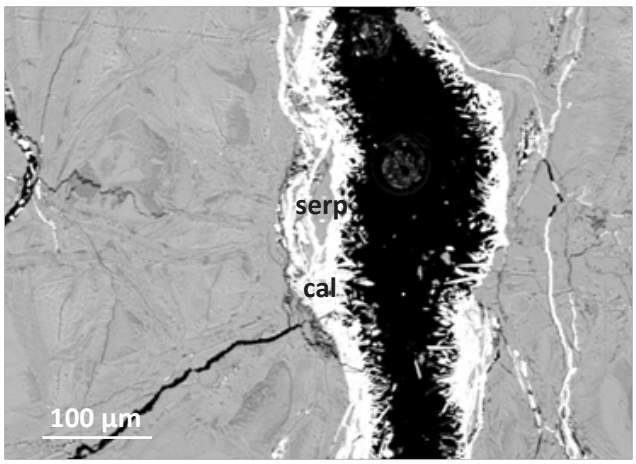

Figure 6.28. *Calcite-filling within fracture, and surrounding some serpentine patches, in thin section U611. Some thin side-fractures with calcite are also visible.*

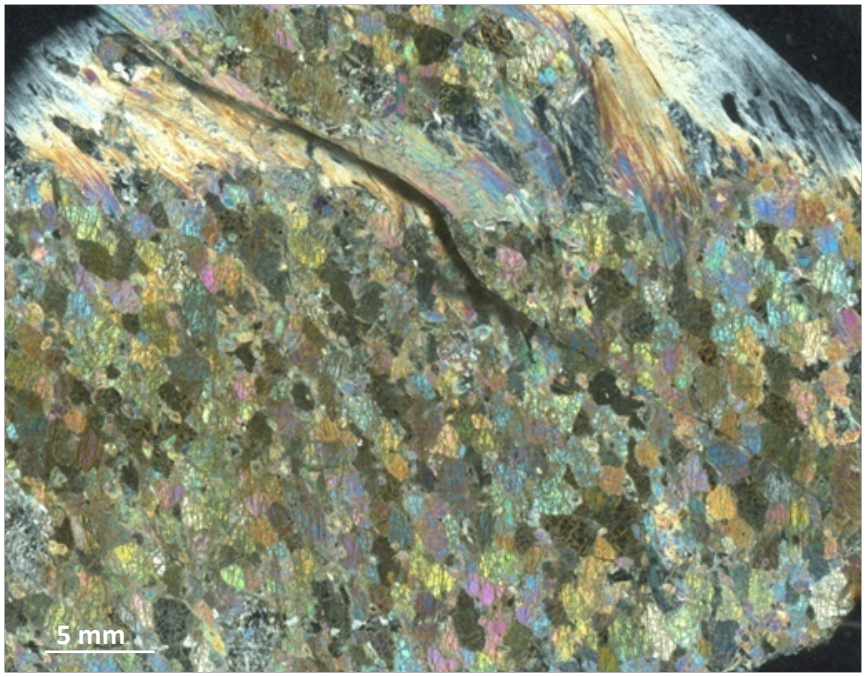

Figure 6.29. *Thin section U1012 in XPL, with talc vein in the top part. (The black shadow crossing the thin section is a crack in the glass.)*

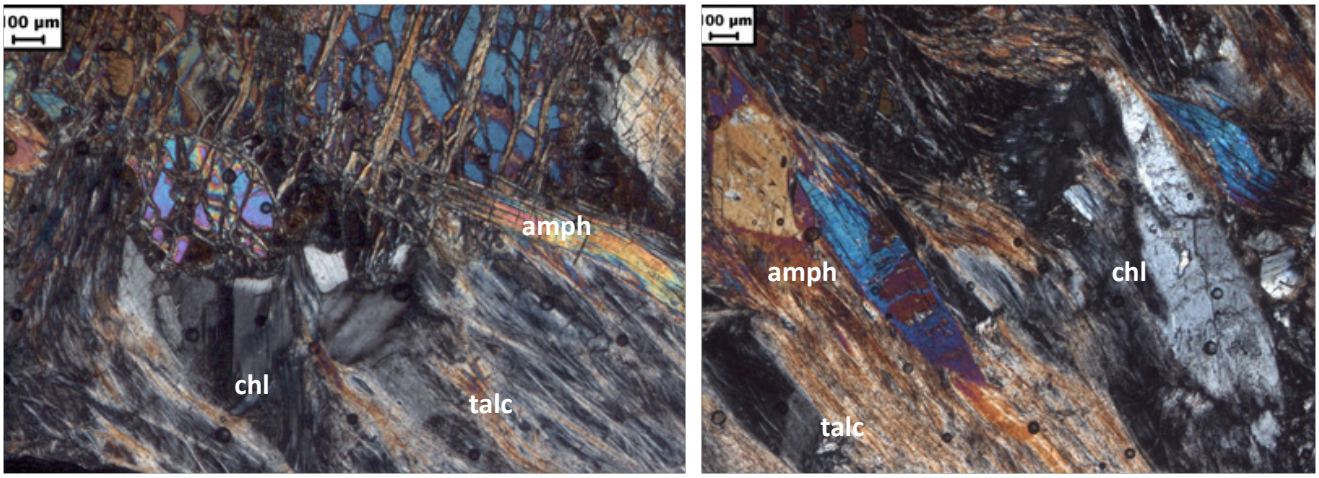

Figure 6.30. *Talc surrounding amphibole and chlorite and thus replacing them in the vein in sample U1012.*

It is important to mention that the fibres of the talc-mass in the veins are somewhat bent around the serpentinized mesh adjacent to the veins. Apart from this folding of the talc-fibres, there are no signs of fracturing or deformation in the vein.

6.2.2.2 *Pyroxenite fractures*

The fractures in the pyroxenite layer in sample R422A and R422B show at least three generations of fracture filling. Under the microscope, it can be seen that the fractures are filled with two types of serpentine: an outer rim of banded/kinked serpentine (chrysotile) and one (or two) inner rims of the semi-parallel/triangular lizardite perpendicular to the long direction of the vein (figure 6.31A). Groups of very fine-grained hematite/magnetite are present along the centres of the fracture-filling serpentine.

Furthermore, in some wider fractures (all in thin section R422A) calcite makes up the innermost filling of the fracture (figure 6.31B). Though the same two earlier (serpentine) fillings are present, but a latest stage is formed by calcite. This calcite is easily recognized under the microscope by its large crystal size, and thus it's corresponding specific twinning.

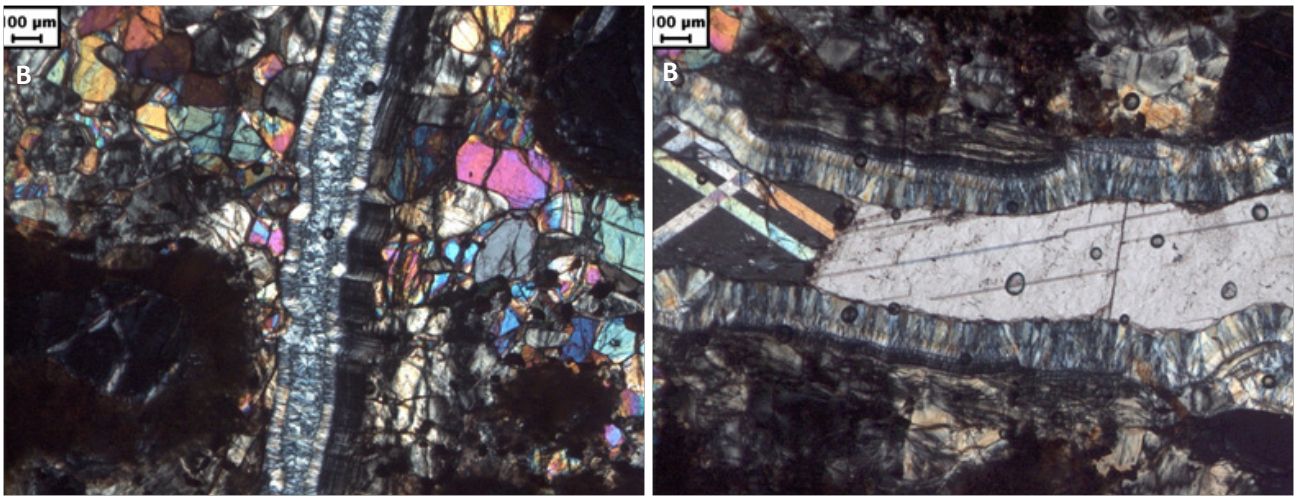

Figure 6.31. *Three generations of fracture-filling in thin sections R422B (A) and R422A (B), the latter having an inner filling with calcite.*

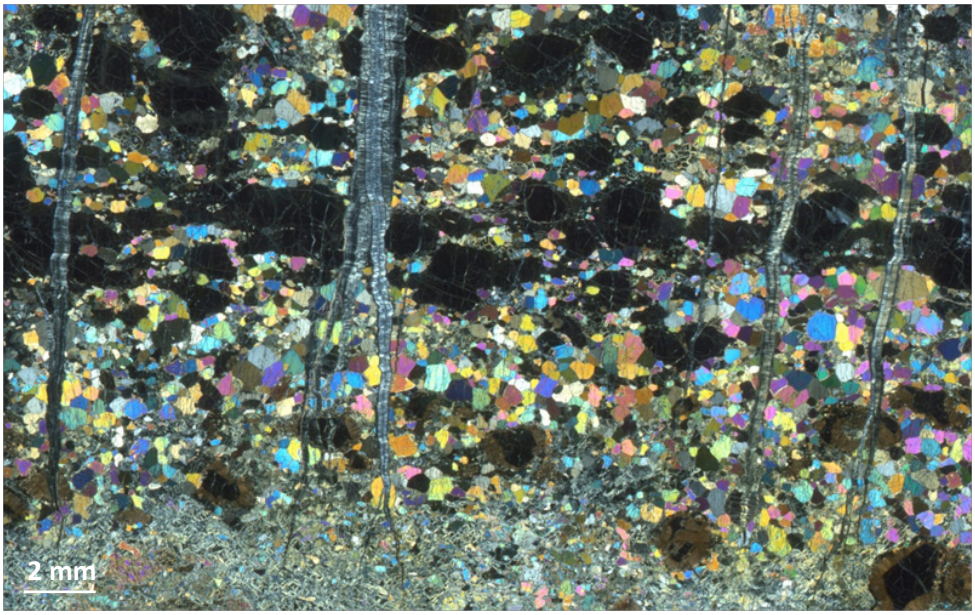

Figure 6.32. *Overview of fractures in the pyroxenite lens in thin section U631.*

Thin sections U631 (figure 6.32) and U632 are quite similar to the thin sections from sample R422. Again, several generations of fracture filling are observed, an outer rim of banded/kinked serpentine (chrysotile) and one or two (in some fractures) inner rims of semi-parallel/triangular serpentine (lizardite), see figure 6.33. These later growth forms often cross-cut the earlier banded serpentine, and sometimes even each other. This results in new fracture tips, thus there is not strictly a continuation of the earlier fracture (only in the central, wider part). The innermost filling of some fractures in thin section U632 is granular lizardite, as is shown in figure 6.34.

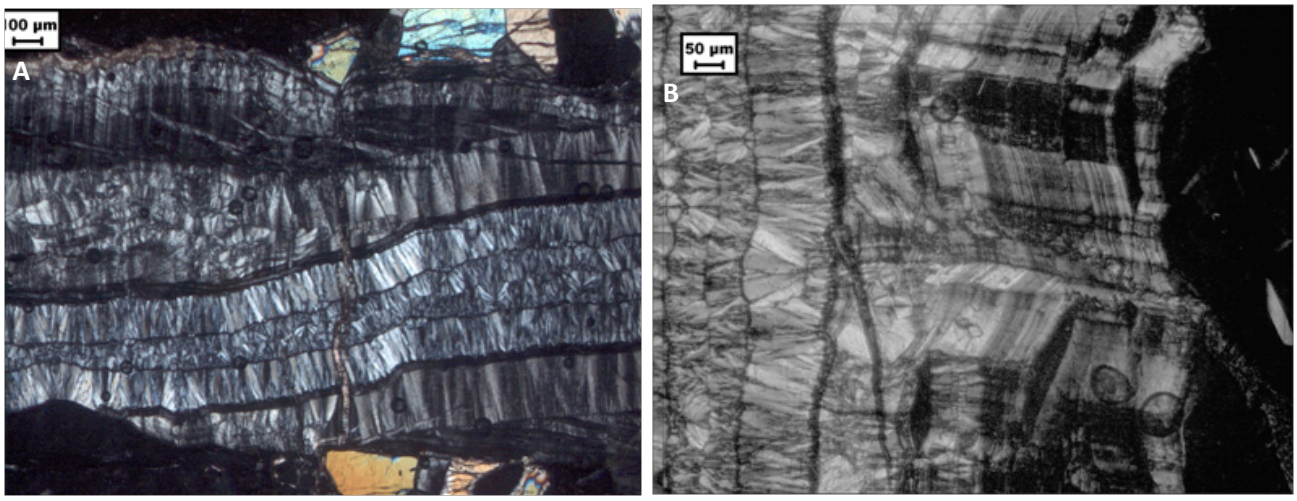

Figure 6.33. *Several stages of inner filling with triangular lizardite (A), and outer filling of banded/kinked chrysotile (B) in thin section U631. Scale bar in (A) is 100 µm.*

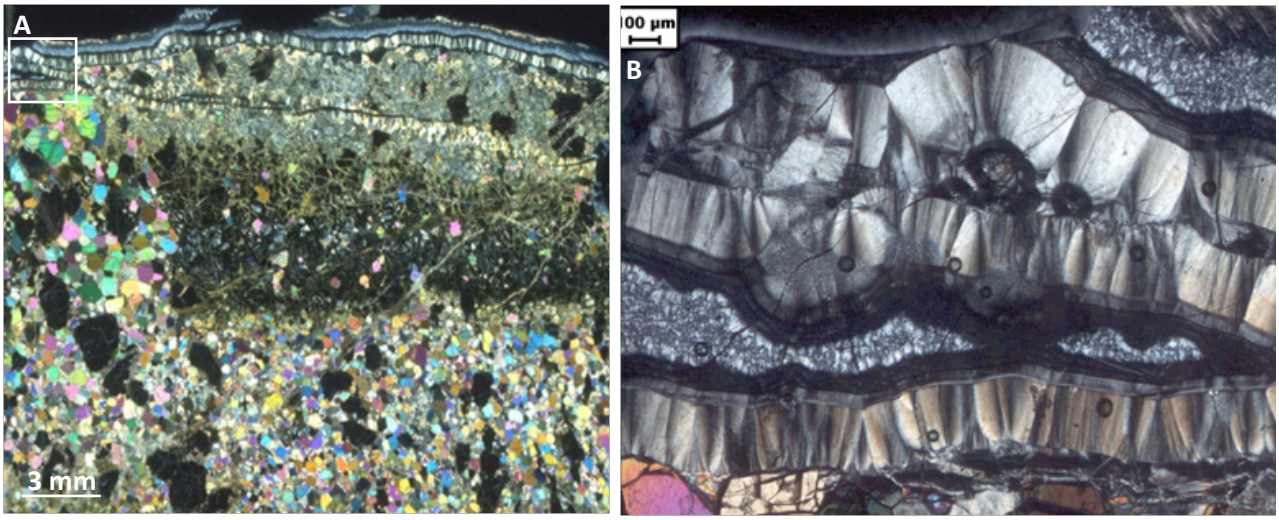

Figure 6.34. *Fracture in thin section U632 (A) and magnification (B), showing several generations of serpentine growth. Scale bar in (B) is 100 µm.*

7 RETROGRADE METAMORPHIC REACTIONS

7.1 EARLY STAGE

On the basis of the observations from the thin sections, reactions that have occurred in the early stages of exhumation (before serpentinization) of the peridotite bodies have been determined. This is done with the help of a basic and extensive petrogenetic grid in the (C)MASH system from Jenkins [1981] and Schmädicke [2000], which are shown in figure 7.1 and 7.2. The reactions that have been interpreted on the basis these diagrams are shown in figure 7.3 and 7.4.
The grids in this system assume olivine (forsterite) and water to be present in excess, which serves as a necessity for the metamorphism of peridotite rocks. All reactions mentioned here are derived from the presented diagrams.

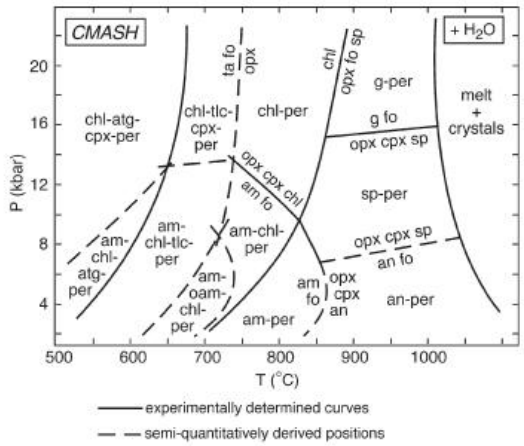

Figure 7.1. *PT phase diagram in the CMASH system from Schmädicke [2000], after Jenkins [1981].*

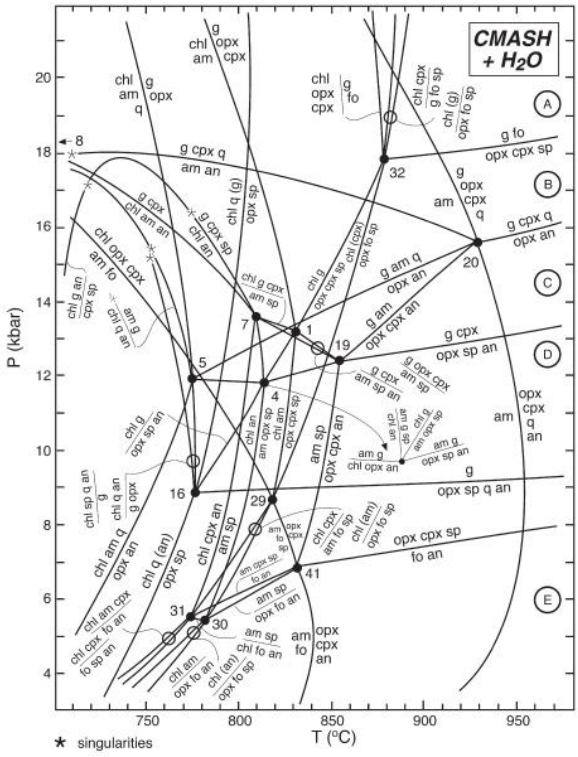

Figure 7.2. *Extensive PT phase diagram in the CMASH system, from Schmädicke [2000].*

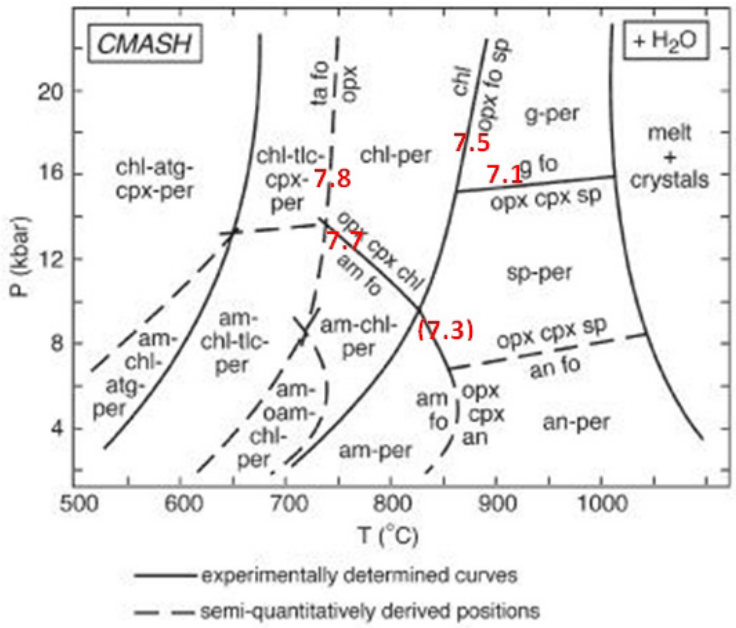

Figure 7.3. *Reactions and proposed PT path in the phase diagram in figure 7.1. From Schmädicke [2000], after Jenkins [1981]. Reaction 7.3 between brackets less likely to have occurred.*

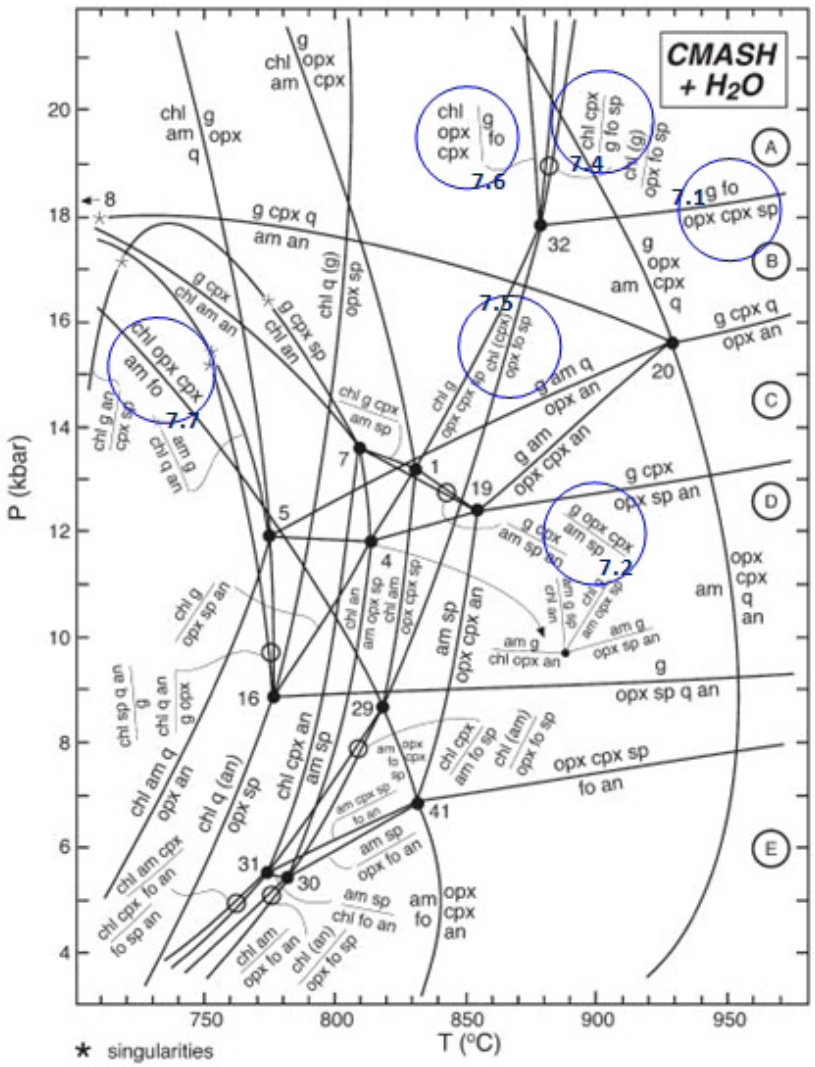

Figure 7.4. *Likely reactions and proposed PT path in the extensive phase diagram in the CMASH system; after Schmädicke [2000].*

At the start of the exhumation, the peridotite bodies have a composition of garnet-peridotite, it thus places in the garnet-peridotite stability field. The earliest reactions involve the breakdown of garnet. In most of the thin sections, the presence of many spinels around garnet imply that it is a reaction product. On the basis of the petrogenetic grids, the reaction that must have occurred is

garnet + forsterite = orthopyroxene + clinopyroxene + spinel. (7.1)

This reaction also holds for the formation of kelyphitic rims around garnets in many of the thin sections; it involves the same reactants and products. The only difference is the Cr-content in garnet and spinel in the latter; this varies, causing different forms of kelyphite. For low-Cr garnet, reaction 7.1 holds; whereas reactions of high-Cr garnet with olivine produce high-Cr spinel + garnet + clinopyroxene (±orthopyroxene ± amphibole) [Spengler, 2006]. Probably, both reactions have occurred here, but there is not enough microprobe data to say which was dominant.
In some thin sections, amphibole is present as well in the vicinity of garnets with kelyphitic rims. This can be due to the following reaction from Schmädicke [2000], which occurs mainly in more calcium-rich rocks or in pyroxenite lenses:

garnet + orthopyroxene + clinopyroxene (+ H2O) = amphibole + spinel. (7.2)

In these rocks, fine-grained amphibole is part of the kelyphitic rim as well [Spengler, 2006]. Another possibility for amphibole to form in the pyroxenite lenses is from the following reaction:

orthopyroxene + clinopyroxene + spinel (+ H_2O) = amphibole + forsterite. (7.3)

As can be seen in figure 7.3, reaction 7.3 is less likely to have occurred, because the pressure of this reaction is relatively low when comparing it with the other reactions. Pseudomorphs after garnet, with spinel involved, can occur through

garnet + forsterite + spinel (+ H_2O) = chlorite + clinopyroxene. (7.4)

Bucher and Fry [2002] state that chlorite and Mg-rich spinel have a shared stability field, caused by the presence of additional (non-pure MASH) components like iron. This would explain the possibility of growth of spinel and chlorite at approximately the same time in sample R321, as was shown in subsection 6.1.1.
The chlorite/amphibole/talc vein in sample U1012 can be formed by reaction 7.4 as well. Though, there is hardly any spinel found in the sample, but this can also be fully reacted away. In this case, the following reaction can also be true:

orthopyroxene + forsterite + spinel (+ H_2O) = chlorite (+ clinopyroxene), (7.5)

Without spinel involved, the most likely reaction to have happened is

garnet + forsterite (+ H_2O) = chlorite + clinopyroxene + orthopyroxene, (7.6)

because there is much chlorite present in the sample, thus there also must have been much reactant, which is extensively present in the form of garnet and olivine. However, at this point, there is not enough information available to really determine which of both reactions has actually occurred to form the chlorite in the vein.
The growth of amphibole over chlorite in this sample (both in the veins as in the matrix) is probably caused by the following reaction:

chlorite + orthopyroxene + clinopyroxene (+ H_2O) = amphibole + forsterite. (7.7)

And the latest overgrowth of chlorite and amphibole by talc can occur through

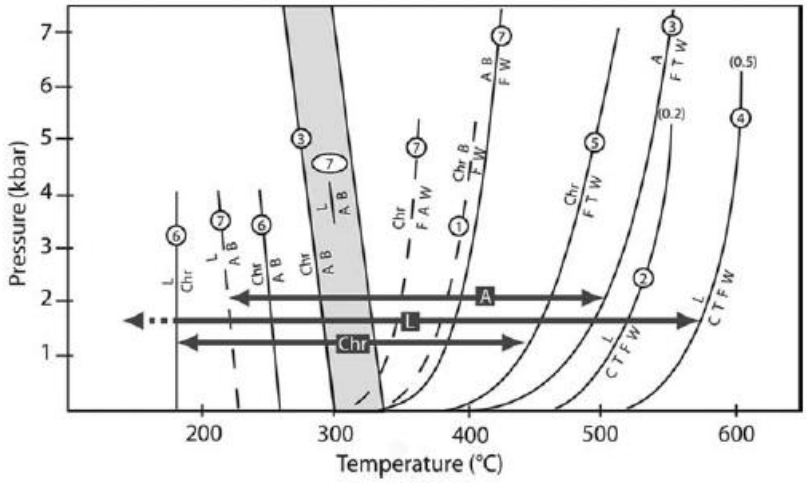

Figure 7.5. *Phase diagram in the MSH system for the three serpentine polymorphs. The stability field for lizardite is enlarged through a higher Al content; (0.2) = 3.7 wt% Al_2O_3 and (0.5) = 9.2 wt% Al_2O_3. L = lizardite, A = antigorite, Chr = chrysotile, B = brucite, C = chlorite, T = talc, F = forsterite, W = water. After Andreani et al. [2007].*

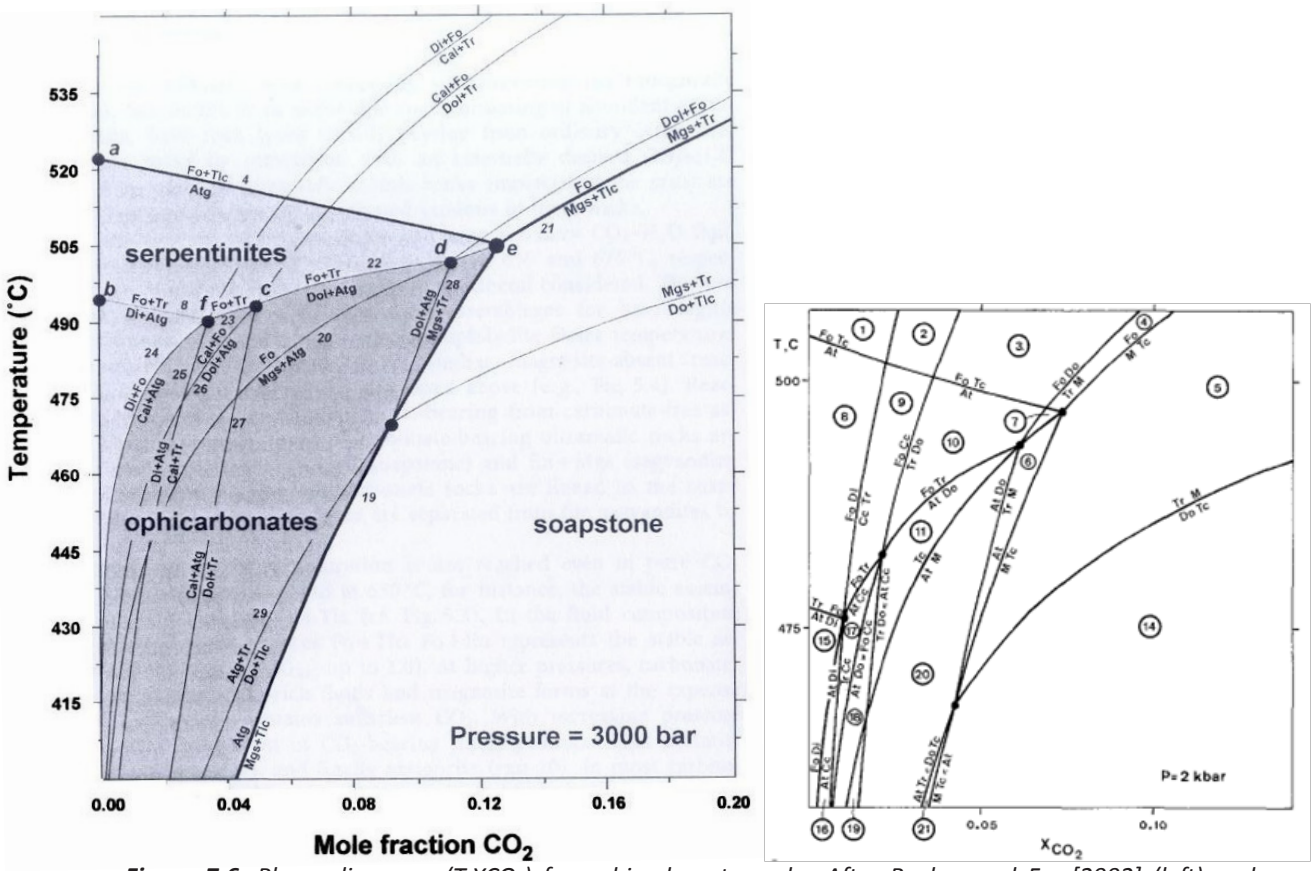

Figure 7.6. *Phase diagrams (T-XCO_2) for ophicarbonate rocks. After Bucher and Fry [2002] (left) and Trommsdorff and Connolly [1990] (right). Difference between both diagrams is the pressure at which the reactions take place. Di = diopside, Fo = forsterite, Tr = tremolite, Cal/Cc = calcite, Atg/At = antigorite.*

orthopyroxene + H_2O = talc + forsterite. (7.8)

7.2 LATE STAGE

The late stage reactions during exhumation are characterized by large scale serpentinization of the peridotite body, fracture formation and latest stage calcite formation in the rock. Some of the

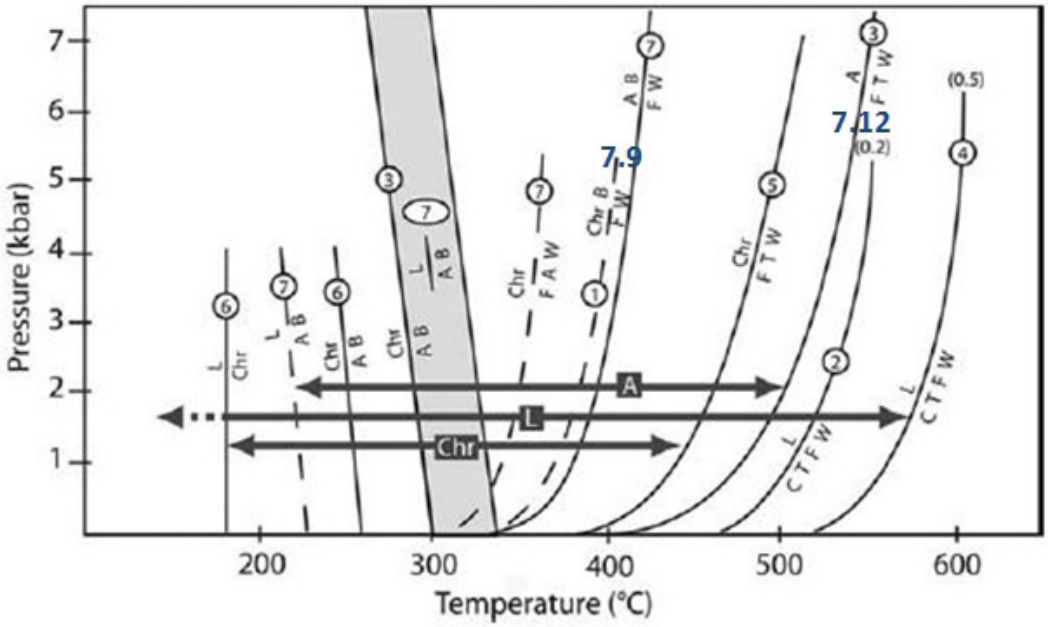

Figure 7.7. *Reactions 7.9 and 7.12 depicted in the MSH PT phase diagram from Andreani et al. [2007].*

serpentine formation went together with the formation of iron-oxides in mesh and fracture rims. Most of the following reactions are derived from literature, as well as from the PT phase diagram as presented by Andreani et al. [2007] (figure 7.5). Reactions for latest stage calcite formation are derived from phase diagrams from Bucher and Fry [2002] and Trommsdorff and Connolly [1990] (figure 7.6). When present, the reactions discussed here are depicted in these phase diagrams in figure 7.7 (for serpentines) and in figure 7.8 (for calcite).

The most basic reaction for the formation of serpentine in the mesh occurs by the reaction of olivine and water:

$$2\,(Mg,Fe)_2SiO_4 + 3\,H_2O = (Mg,Fe)_3Si_2O_5(OH)_4 + Mg(OH)_2. \qquad (7.9)$$

olivine + water = serpentine (mesh) + brucite

As was observed from the microprobe results (see subsection 6.2.1), it is probable that brucite is present in the samples, which is consistent with this reaction.
The same reaction can hold for the formation of serpentine in fractures. However, there are more possibilities for serpentine formation. These include the transport of SiO_2 to the system, or MgO and SiO_2 away from the system during the reaction, as already mentioned in subsection 3.3.5 [O'Hanley, 1996]:

$$3\,(Mg,Fe)_2SiO_4 + SiO_{2\,(aq)} + 4\,H_2O = 2\,(Mg,Fe)_3Si_2O_5(OH)_4, \qquad (7.10)$$

olivine + Si in fluid phase + water = serpentine

$$6.15\,(Mg,Fe)_2SiO_4 + 6\,H_2O = 2\,(Mg,Fe)_3Si_2O_5(OH)_4 + 2\,Mg(OH)_2 + 4.3\,MgO_{(aq)} + 2.15\,SiO_{2\,(aq)}. \qquad (7.11)$$

olivine + water = serpentine + brucite + Mg and Si in fluid phase

Reaction 7.9 is the most likely here. There are no indications that there is transport of MgO or SiO_2 away from the system during the reactions, as is also explained in Spengler [2006]. The gneisses surrounding the Otrøy peridotite bodies do not show metasomatism by MgO or SiO_2. This indicates that serpentinization (at least the first stages) must have occurred in a closed system. It can also be that there is more SiO_2 going into the formed serpentine, which would explain some of the SiO_2 richer samples.

Serpentine can also form with other minerals involved. Talc is common in these reactions, often

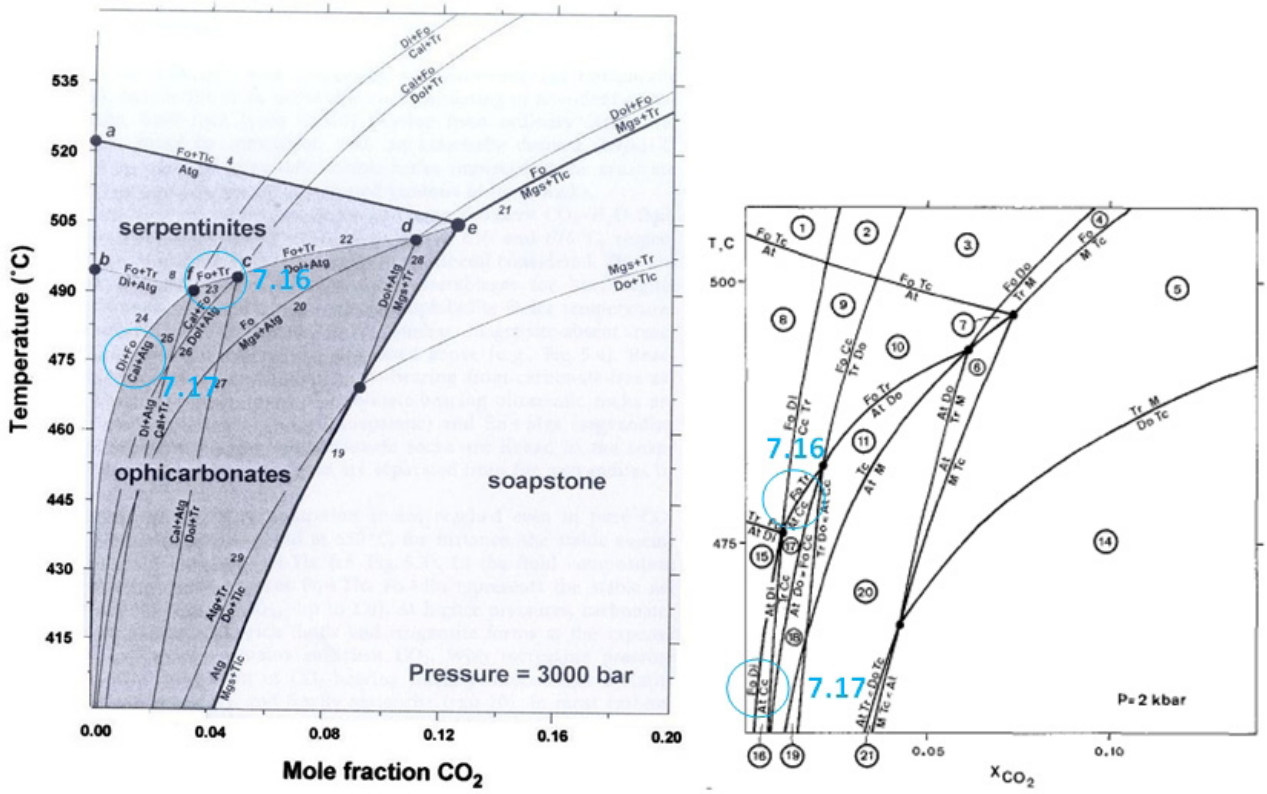

Figure 7.8. *Reactions 7.16 and 7.17 for calcite formation in phase diagrams (T-XCO2) for ophicarbonate rocks. After Bucher and Fry [2002] (left) and Trommsdorff and Connolly [1990] (right).*

with antigorite as a reaction product. The following reaction is from Bucher and Fry [2002]:

$$18\ Mg_2SiO_4 + 4\ Mg_3Si_4O_{10}(OH)_4 + 27\ H_2O = Mg_{48}Si_{34}O_{85}(OH)_{62} \quad (7.12)$$

olivine (forsterite) + talc + water = antigorite

As is shown in the phase diagram from Andreani et al. [2007], lizardite and chrysotile can also form from reaction 7.12. Chlorite is also included as a reactant in the formation of lizardite.
However, the samples discussed here do not contain talc, except one (U1012). Thus, there are two possibilities: 1) no talc was present, and these reactions did not occur; 2) all talc has reacted away during the reaction. The most likely case will be discussed further in subsection 8.1.2.

There are various reactions that cause the alteration of orthopyroxene during infiltration of water and thus the formation of bastite. From Andreani et al. [2007] is the following reaction:

$$3\ (Mg,Fe)SiO_3 + 2\ H_2O = (Mg,Fe)_3Si_2O_5(OH)_4 + SiO_{2(aq)} \quad (7.13)$$

orthopyroxene + water = serpentine (bastite) + Si in fluid phase

in which Si is released in the fluid phase; or

$$(Mg,Fe)_2SiO_4 + (Mg,Fe)SiO_3 + 2\ H_2O = (Mg,Fe)_3Si_2O_5(OH)_4 \quad (7.14)$$

olivine + orthopyroxene + water = serpentine (bastite)

for which olivine is needed [Mével, 2003].
It is very likely that the first reaction occurred in pyroxenite layers that are olivine-poor. This is observed in thin section U631: there is much bastite present whereas the olivine-content in the pyroxenite is very low. The second reaction is likely to take place more often in the peridotite.

Mével [2003] states that magnetite is a common reaction product in the mesh during serpentinization, which grows around the concentric layers of the serpentine mesh rims. This is also observed

in several samples. The corresponding reaction formula from olivine to serpentine and magnetite is as follows:

$$6\,(Mg,Fe)_2SiO_4 + 7\,H_2O = 3\,(Mg,Fe)_3Si_2O_5(OH)_4 + Fe_3O_4 + H_2 \quad (7.15)$$
olivine + water = serpentine + magnetite + hydrogen

It is possible that there is more magnetite/hematite formed when olivine is relatively rich in iron, thus when there is a surplus in iron in the reaction. Another possibility is that the serpentine formed here contains less iron while more iron-oxides are formed. However, there are not enough analyses of serpentine and the exact iron-oxide concentration in samples to make a real conclusive result out of this.

Reactions that form calcite are very diverse. These occur in the ophicarbonate system, and they often involve talc, dolomite and/or magnesite [Bucher and Fry, 2002]. Since there is no dolomite and magnesite in the system, and amphibole (tremolite) clearly formed during an earlier stage, the number of possible reactions is quite limited. Two possibilities, derived from Bucher and Fry [2002] and Trommsdorff and Connolly [1990], are

$$214\,Mg_2SiO_4 + 20\,Ca_2Mg_5Si_8O_{22} + 40\,CO_2 + 321\,H_2O = 11\,Mg_{48}Si_{34}O_{85}(OH)_{62} + 40\,CaCO_3, \quad (7.16)$$
forsterite + amphibole (tremolite) + CO_2 + water = antigorite + calcite

and

$$62\,Mg_2SiO_4 + 20\,CaMgSi_2O_6 + 20\,CO_2 + 93\,H_2O = 3\,Mg_{48}Si_{34}O_{85}(OH)_{62} + 20\,CaCO_3. \quad (7.17)$$
forsterite + clinopyroxene (diopside) + CO_2 + water = antigorite + calcite

Both reactions are possible here. Another option is that calcium from the Ca-rich garnet is dissolved in the system, and takes place in the reaction. This will be discussed further in subsection 8.2.1.

8 DISCUSSION

8.1 RETROGRADE METAMORPHISM

8.1.1 Stages of serpentinization

As is shown in subsection 6.2, all three serpentine polymorphs are present in the mesh and in fractures of the Otrøy peridotite bodies, in various growth forms.

Relative timing of mesh and fracture formation
Based on the observations from the thin sections on relative timing of fracture filling, combined with the mode of fracture filling, the following generations in serpentinization (and later stage) history can be recognized.

M1 - mesh formation: lizardite
M2 - mesh formation: chrysotile
- fibrous vein 'formation'/recrystallization
F1 - banded/kinked chrysotile in fractures
F2 - ribbon antigorite in fractures
- triangular lizardite in fractures/'star' overgrowth in fibrous vein
F3 - micro-granular lizardite in fractures/micro-granular overgrowth
F4 - fibrous chrysotile in cross-fractures
- banded/kinked chrysotile in cross-fractures
F5 - calcite in fractures

Serpentinization in the mesh went on during most of the latest part of retrograde metamorphism of the peridotite, because the degree of serpentinization is very high. Thus, the mesh- and fracture-formation occurred simultaneously. An overview of the several stages of serpentine formation is presented in figure 8.1.
The timing of the formation of the fibrous vein in sample U532 is not certain. This must at least have occurred before recrystallization by star- and micro-granular lizardite. Also, the timing of the ribbon antigorite and triangular lizardite, and that of fibrous chrysotile and the second banded/kinked chrysotile is not certain. No clear cross-cutting relationships were observed to put them in a relative succession. What is certain is that the filling of several fractures with different forms of serpentine shows deformation under changing conditions. Less certain is whether different stages of fracture filling are reactivation of the earlier fractures (thus, if the deformation was not purely ongoing). Probably, both ongoing deformation and some reactivation of structures occurs, as will be discussed in subsection 8.2.1.

8.1.2 Late stage temperature conditions

Late stage PT conditions are quite difficult to determine. As can be seen in the phase diagram presented from Andreani et al. [2007] (figure 8.2 and 7.5), serpentines are not so much dependent on pressure for their formation.
Serpentinization of peridotites can occur between about 180 to 600°C. This depends on the presence of other minerals, which influence the stability of forsterite and serpentine. When talc is present, the stability of serpentine is raised to about 520-600°C. Without talc, forsterite is stable to 300-350°C. During retrograde metamorphism, lizardite is the mineral stable under the highest temperature, and thus the first forming. Orthopyroxene is only stable to somewhat higher temperatures, maximum hydration and alteration of orthopyroxene to bastite occurs at temperatures that are at least 400°C. Below this temperature, it turns out that the reaction kinetics of the reaction of forsterite with water is higher [Andreani et al., 2007; Iyer et al., 2008].

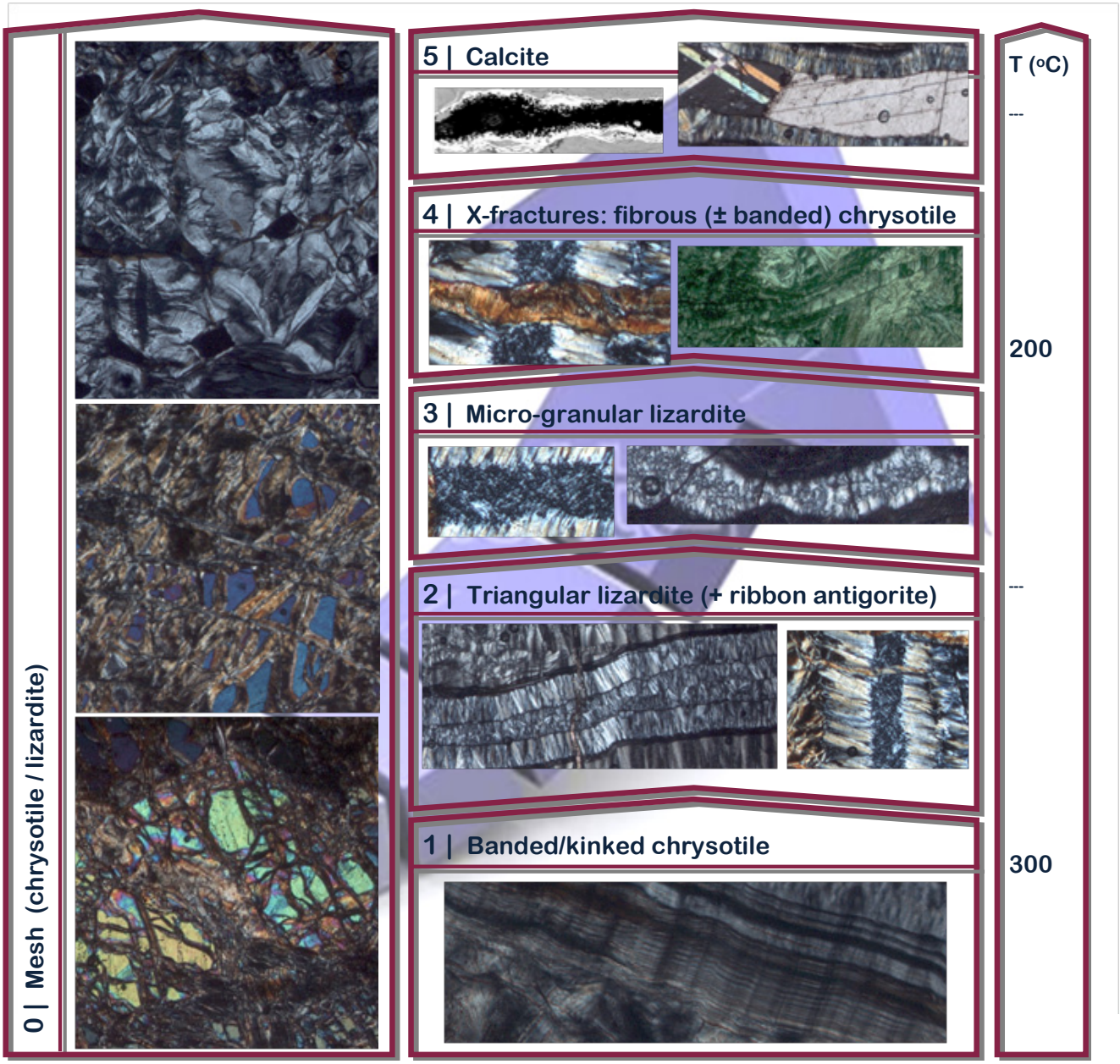

Figure 8.1. *Scheme showing the several stages of serpentinization in the Otrøy peridotites. Temperature constraints are discussed in subsection 8.1.2.*

Since it is not certain whether there was talc present initially (see reaction 7.12), there are two possibilities for the onset of formation of lizardite and chrysotile during retrograde metamorphism: a high temperature variant (1) and a low temperature variant (2).
1) The first lizardite forms from forsterite, talc, chlorite and water at 480-600°C. The first chrysotile forms between 400 and 500°C from forsterite, talc and water. And/or, at 330-400oC together with brucite, from forsterite and water.
2) The first chrysotile forms with brucite from forsterite and water at 330-400°C. The first lizardite forms from chrysotile at around 180°C.

The first case is the most likely here. This is because there are several generations of recrystallization, which would not be possible when the first serpentinization is only just formed at such low temperatures. Thus, for the complete serpentinization history, the whole temperature range that is depicted in the phase diagram is passed through. This implies that it is probable that lizardite first formed in the mesh, and is later overgrown by chrysotile. Another argument that supports this case

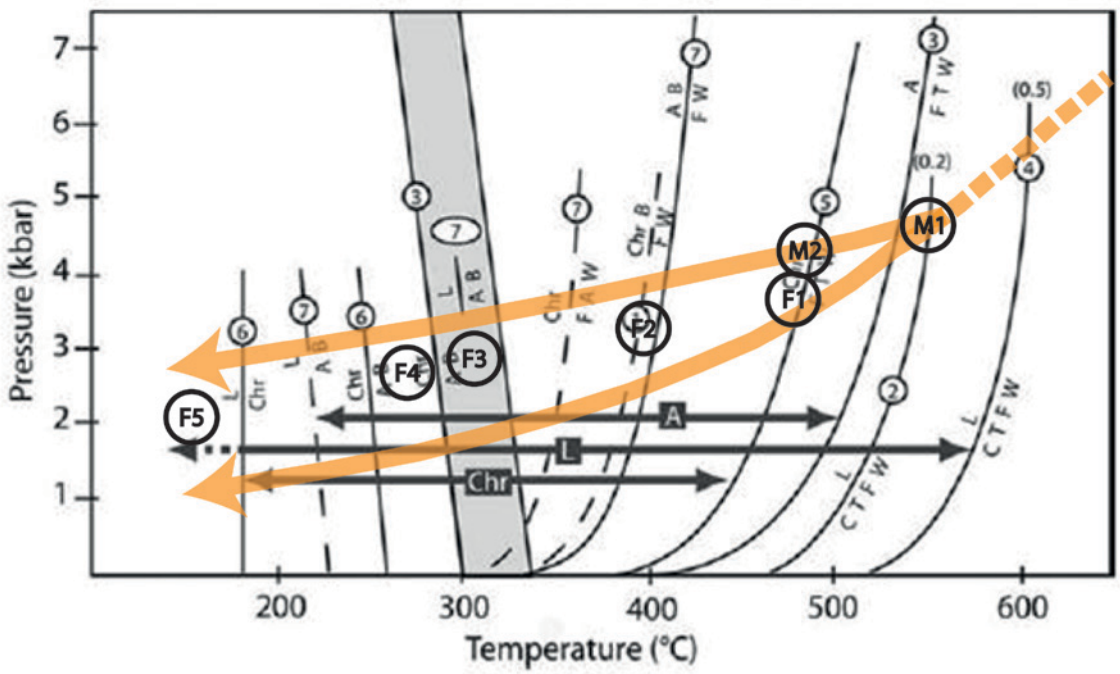

Figure 8.2. *Late stage PT path (range) for serpentinization. Stages of mesh formation (M1,2) and fracture formation (F1-5) are depicted. M1 = lizardite formation; M2 = chrysotile formation. For F1-5, see text. Modified figure from Andreani et al. [2007].*

is that there is hardly any antigorite found throughout the samples, where the first forming serpentine without talc would be antigorite (reaction-curve 7 from Andreani et al. [2007] in figure 7.7). Temperatures accompanying these reactions are 480-530°C for lizardite formation in the mesh (M1), because the Al-content is not that high that the outer right reaction curve is reached (figure 8.2). Chrysotile formation in the mesh (M2) occurs at 400-480°C, together with the first phase of fracturing (banded/kinked chrysotile, F1). Also, bastite from orthopyroxene in the mesh must have formed above 400°C. The second phase of fracturing, thus the formation of ribbon antigorite and triangular lizardite (F2) occurs between 300 and 400°C. Probably, lizardite went on forming during this stage, but it changed into granular lizardite as innermost fracture-filling (F3).
The latest stage is the formation of cross-fractures (F4): fibrous chrysotile in U531 and a second stage of banded/kinked chrysotile in U532. This most likely occurred below 300°C. According to this phase diagram, chrysotile at this temperature can only be formed from antigorite and brucite. This fits with the presence of the fibrous cross-fractures within the ribbon antigorite fractures.

Latest stage calcite must have formed under 180°C, when assuming the latest serpentine to form around that temperature. From phase diagrams for ophicarbonate rocks, it does not become very clear at which pressure this could have been. This is because most of those diagrams have a fixed pressure and are based on the CO_2 content and the temperature. When looking at both diagrams (as were shown in figure 7.8), for a pressure of 3 and 2 kbar, it becomes clear that the pressure maybe must have been even lower to be able to take place at such low temperatures.

Talc

Because talc is not present (anymore) in most of the samples, this 'high temperature' variant of serpentinization cannot really be proved. Chlorite is present in some of the samples though, and it is very well possible that this played a role in the formation of the first lizardite in the mesh. Also, most of the samples are that heavily serpentinized that all talc has probably fully reacted away during the reaction. This is strengthened by the observation that in sample U1012, where talc is still present. In this sample, the degree serpentinization is not that high, which would imply that there is still some talc left to take part in further serpentinization.
Sample U1012 shows another difficulty in the PT evolution of the peridotite. As was mentioned in

subsection 6.2.2.1, talc fibres in the vein are folded around the serpentine mesh and do not seem to be recrystallized or overgrown by this. This would imply a later stage of talc formation, after the formation of the mesh. An explanation for this would be that because of impurities in the system (for instance, from a relatively high iron content), the reactions of talc formation (7.8) and subsequent serpentine formation (7.12) are somewhat brought together. Both minerals would then be able to form together. A similar process is mentioned in Bucher and Fry [2002], where the stability field of spinel and chlorite occurs over a range of pressures/temperatures, because of impurities in the system.
Another possibility is a drop in pressure after crossing the reaction curve for serpentine formation. This would cause the reaction curve to be crossed again, resulting in the formation of talc. This possibility is not likely however, because this would mean that the serpentine reacts away again. More research is needed to draw conclusions on this matter.

8.1.3 PT path

The metamorphic path that can be determined when listing all the reactions presented in chapter 7 is shown in figure 8.3 (early stages) and figure 8.4 (overall PT path).
The rock has started from eclogite/granulite facies, at pressures of at least 2 GPa and temperatures above 900°C. As is stated in Spengler et al. [2009] and Scambelluri et al. [2008] – also shown in subsection 2.2, the rock underwent much higher pressures. However, these results are based on extensive research on high-pressure majoritic garnet microtextures and chemistry, which is beyond the scope of this study.
The peridotite subsequently underwent amphibolite facies metamorphism. Pressures must have been between 1.2 and 0.5 GPa, with temperatures of 850 to 550°C. Serpentinization occurred under greenschist facies metamorphism, from about 0.5 GPa and 530°C downward [Spengler, 2006].
The PT path from Spengler et al. [2009] has a lower peak temperature than is interpreted in this study. The second part of the PT path that is presented by Scambelluri et al. [2008] is quite consistent with the path in this study, though. These differences between both studies are probably due to a different geothermobarometer that is used to determine the PT conditions. It can also be due to slight (compositional) differences that have been found in mineral assemblages, which make the pressure and temperature conditions to vary.

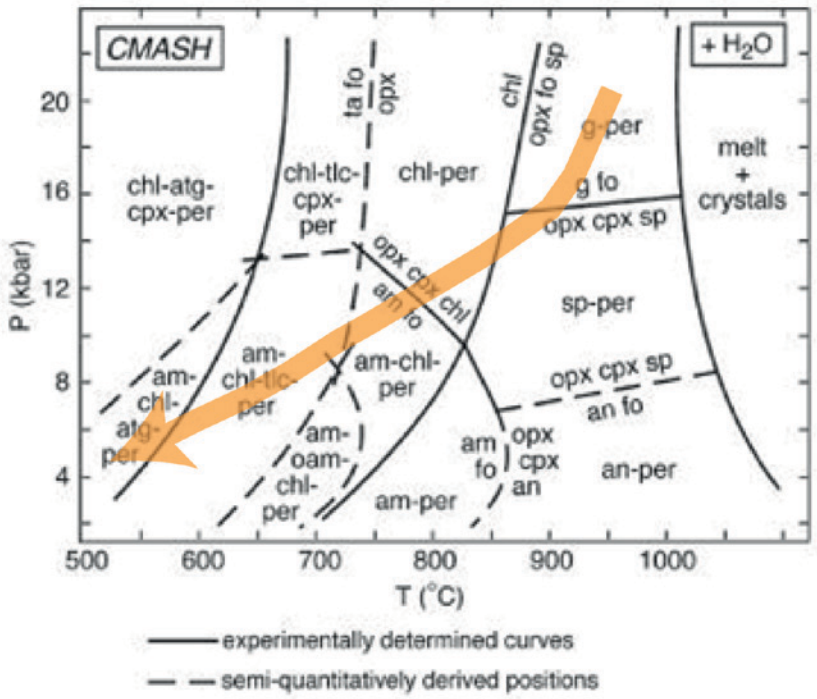

Figure 8.3. *Proposed PT path in the phase diagram in figure 7.1, based on the most likely reactions in subsection 7.1. Modified figure from Schmädicke [2000].*

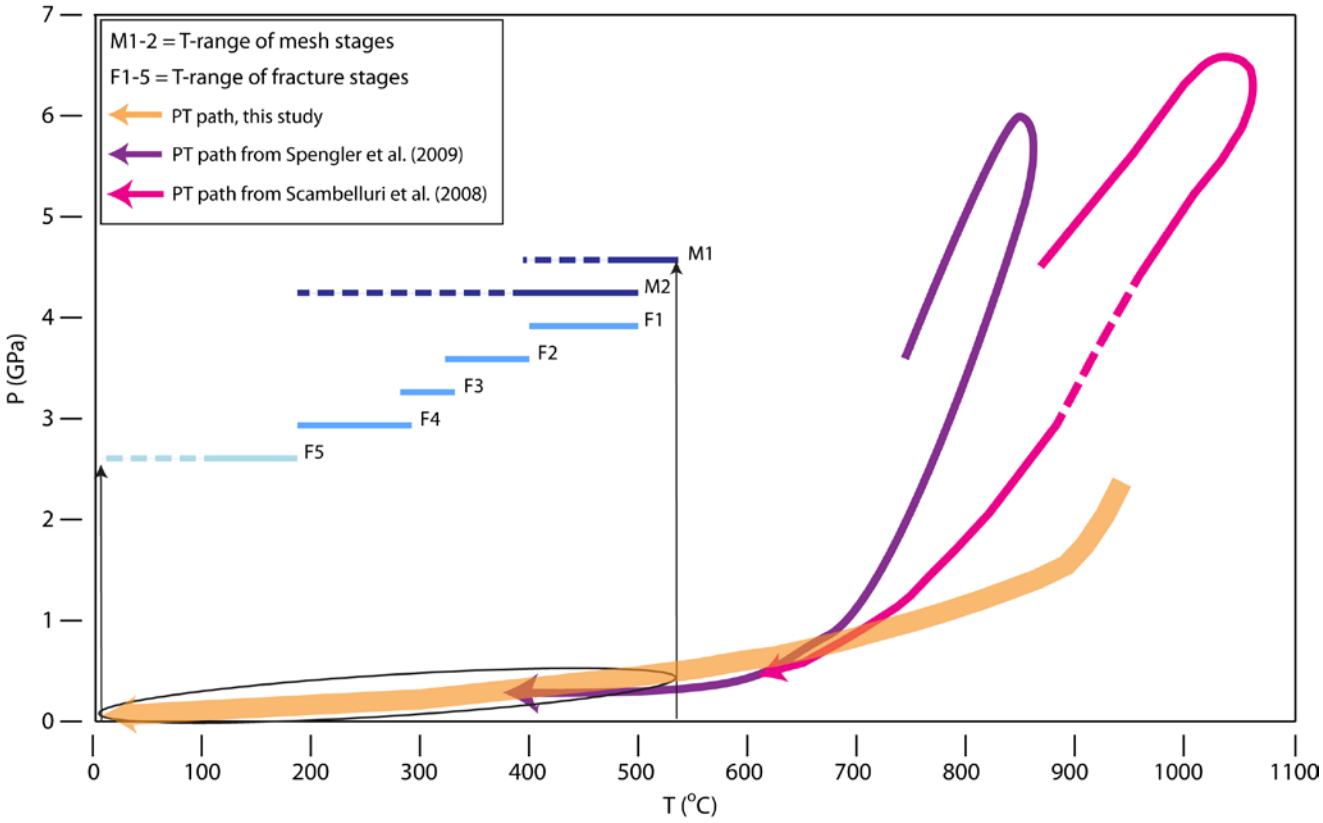

Figure 8.4. *Proposed PT path for retrograde metamorphism of the Otrøy peridotite bodies, derived from the mineral assemblages determined in this study. PT paths for Otrøy and neighbouring Fjørtoft peridotites from Spengler et al. [2009] and Scambelluri et al. [2008] are shown as well. The temperature range for the different stages of mesh and fracture formation are depicted by M1 to F5 (see also figure 8.2).*

The proposed metamorphic path is consistent with retrograde metamorphism, as occurs during exhumation. Results presented in the studies mentioned here, and in other studies from Spengler [2006], and from Labrousse et al. [2004] confirm this conclusion. Labrousse et al. state that exhumation rates in the amphibolite and greenschist facies are quite fast (more than 2 mm/year). This is consistent with the theory of Brueckner and Van Roermund [2004] of dunk tectonics, and the observations that there is much preserved from earlier metamorphic facies, and that not all 'logical' subsequent minerals from stability fields in between the start and ending of exhumation have been produced.

8.2 Micro-scale fracture mechanisms

Besides the fracture pattern on outcrop scale, which will be discussed in subsection 8.3, fracture patterns, chemistry and growth form at micro-scale tell much about the conditions under which fracturing occurred.

8.2.1 Mechanisms of fracture filling

Andreani et al. [2007] state that the formation of fractures in the mesh, not in the vicinity of a pyroxenite lens, is related to the overall brittle deformation and stresses in the rock. These are caused by volume changes during serpentinization, and subsequent chemical reactions in the rock. Circulation of fluids is involved in this process. The chemical reactions can cause fractures to propagate further into the rock than they would have done due to only the brittle deformation. The mode of fracture infill is controlled by the velocity of crack opening, the deformation mechanism and the amount of water and free elements in the system. The latter is controlled by whether the system is

closed or open, thus, whether fluid circulation is only local, or more regionally controlled. Elements provided by the first alteration of the surrounding matrix can be 'used' in the fracture infill.

F1) Banded/kinked serpentine
Chrysotile with a banded and kinked appearance is caused by crystallization during small increments of opening, and thus discontinuous opening, of a fracture [Andrani et al., 2007]. The velocity of vein opening is larger than that of crystallization, and the serpentine within has poorly crystallized. Since the fractures are not interconnected, they are not fluid-pathways and mass transfer occurs through diffusional transfer.
Kinking of the fracture is maybe because of compressive stress in the long-direction of the fracture (as can also be observed in figure 8.5, which will be discussed further in subsection 8.2.2).

F2) Well-crystallized serpentines
These are the semi-parallel triangular lizardite and ribbon antigorite, nucleating perpendicular to the long direction of the fracture. The nucleation of these crystals occurs from the fracture walls toward the centre of the fracture, which implies that elements were provided at the centre of the vein, from the fluid therein. In some of the samples, several generations of triangular lizardite bands are found within each other. These imply several stages of ongoing brittle fracture opening.

F3) Granular serpentine
This lizardite has a higher nucleation rate than the previous triangular lizardite, not only localized at the fracture wall. This implies a progressive supersaturation of the fluids within the fractures, and convection of fluids throughout the fracture, which can be caused by the decrease in temperature (by exhumation) and pressure (by fracture opening).

F4) Fibrous serpentine
The chrysotile that is fibrous perpendicular to the fractures has grown continuously in the length of the fibres, during a constant fracture opening velocity and during constant supersaturation. The fracture opening velocity must have been equal or slower than the process of crystal growth. The parallel character of the fractures is probably caused by a constant extensional stress perpendicular to their long direction.

The first three generations mentioned here (as found in the thin sections) are one stage of progressive open space circulation and higher nucleation rates due to less pressure. This could be due to fracture opening, or due to decreasing tectonic pressure. Maybe there is some reactivation of fractures involved when switching between the several generations.
The fourth stage is somewhat different, especially because there has a second stage of banded/kinked chrysotile formed, which does not really match the mechanism of fibrous chrysotile growth at the same moment. My conclusion is that both chrysotiles from the fourth stage must have formed at different times, but at this point it cannot be said which of the two was earlier or later, or relative to which other stages they would have formed.

F5) Calcite
The latest stage calcite filling within fractures is not related to the earlier phase of fluid infiltration. This time, a CO_2-rich fluid infiltrates the system, which binds with calcium to form calcite within open fractures. The calcium is most probably (partly) provided by the surrounding minerals. A good example is the pyroxenite lens in sample R422, in which much calcite has filled up the innermost part of the fractures. The calcium is provided by the Ca-rich garnet and amphibole in the pyroxenite lens. However, it is unlikely that all calcium needed for the filling of the fractures came from the surrounding garnets.
Other samples have less calcite within fractures. It is possible that those samples were less well fractured, by which less open space has been created. Therefore, it was more difficult for fluids to infiltrate. It is striking though that all calcite is present within seemingly open spaces, which im-

plies that these spaces where really open during infiltration. This must have occurred very close to the Earth's surface. A possibility that accompanies this theory is the infiltration of seawater, which could have provided the CO_2 needed for the formation of calcite.
In addition, seawater has a higher concentration of calcium than freshwater, and this also tends to precipitate more quickly from it. This could have been an additional source for calcium in the fractures.
Overall, there is little calcite present in the peridotites, compared to the rate of fracturing. This implies that the rock would not be very useful for CO_2 sequestration.

Fibrous vein
The large vein and its overgrowths in sample U532 are a somewhat separate story from the main course of fracturing. One possibility is that this vein was initially a large talc vein as in sample U1012 – in which the talc is probably derived from stretched orthopyroxene megacrystals – that is later completely overgrown by a form of fibrous serpentine, which preserves the initial fibrous appearance of the talc. This theory is strengthened by the somewhat higher order colours (in XPL) of the vein, which propose indeed a recrystallization from talc. However, there are more causes for higher order colours in serpentine (weathering for instance), and also chemistry cannot confirm this theory.

Chemistry of serpentine polymorphs
The conclusions drawn here on the type of serpentine in fractures are based mostly on the appearance and somewhat less on chemistry of the serpentine minerals. As is shown several times before, the chemistry of one polymorph can differ quite a lot. This is possibly affected by the availability of elements in the system.
The chemical resemblance that some of the fractures have, while they are clearly distinct in appearance, is caused by recrystallization and advection of elements in a closed system. As mentioned earlier, the fractures do not form an interconnected network, which makes it more difficult for fluids and dissolved elements to be transported. Therefore, serpentines within fractures must have 'local' chemical characteristics. Thus, the polymorph that grows is partly determined by the local availability of elements in combination with the temperature during growth. In addition, the growth form partly depends on the mechanism of fracture opening (velocity, stress). However, the different polymorphs do have some restrictions for their growth form, i.e. triangular lizardite and ribbon antigorite.

8.2.2 Volume change in pyroxenite fractures
Hydration and serpentinization of peridotite takes place at temperatures that are significantly lower than temperatures at which pyroxenite lenses are hydrated, as mentioned in subsection 8.1.2. This means that when peridotite expands due to serpentinization (see subsection 3.3.5), the pyroxenite is already maximally hydrated, and cannot expand any further. Furthermore, pyroxenite contains much less olivine (thus less 'expanding' material during the serpentinization reaction). This gives much less volume change in pyroxenite lenses compared to peridotite.
During serpentinization and volume increase of the peridotite, compressive stresses are produced at the peridotite-pyroxenite contact, with a normal direction to it. The pyroxenite cannot accommodate for the volume change and must fracture, with opening directions normal to the compressive stress, thus parallel to the boundary. This is shown figure 8.5.

The only strange thing about this is that field observations and thin sections only show fracturing in one direction. In 'real' volume-expansion fracturing, two sets of parallel fractures at 90° angles would be expected. This may have something to do with the direction of stress release during expansion, and that this stress release in one direction was enough to accommodate for the expansion.
However, in thin section U531, which shows fractures from just beneath a pyroxenite layer, there are indeed perpendicular cross-fractures present. Though not wide, these can explain the volume

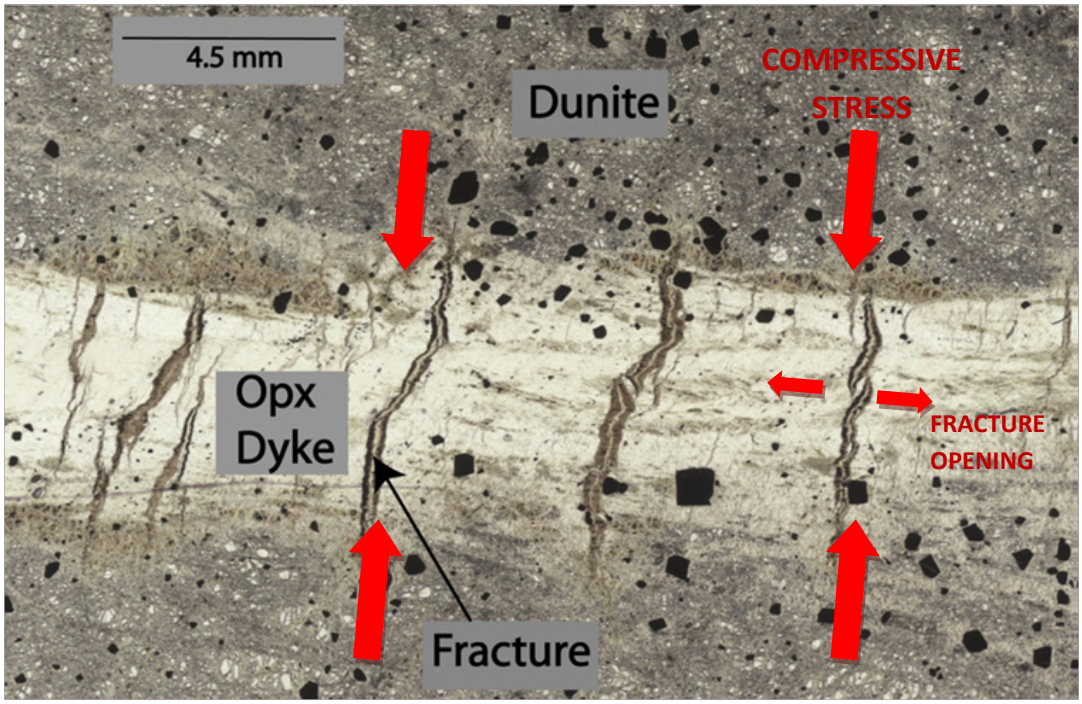

Figure 8.5. *Fracturing in a pyroxenite lens due to compressive stress perpendicular to the lens. Modified after Iyer et al. [2008].*

expansion acting in two subsequent directions, as mentioned in Iyer et al. [2008]. The first direction is set by the largest stress, and determines the second direction.
Thin section U532 also shows cross-fractures, that appear as banded/kinked chrysotile. This setting has a somewhat different cause, though. The large vein that is crossed by the banded/kinked chrysotile is related to large-scale recrystallization of a vein that is similar to the talc vein in sample U1012, as was mentioned in subsection 8.2.1.
The same process of differences in volume change between peridotite and pyroxenite lenses on a smaller scale occurs in kernel pattern formation on outcrop scale. This will be discussed in subsection 8.3.

8.3 Large scale fracture patterns

8.3.1 Fracture pattern formation

Large scale fracture networks within the Raudhaugene peridotite body are quite consistent in abundance throughout the entire body, whilst they are not in the Ugelvik peridotite body. This is easily explained by the fact that there are a lot more (large) outcrops present in the first.
The large scale fracture pattern that is observed in both bodies, with a dominance in Raudhaugene, can be formed in two ways: by kernel formation, or by hierarchical fracturing. Both processes are mainly driven by the volume changes that accompany serpentinization of the peridotite, as explained in subsection 3.3.5. See text box on page 79 for a description of both patterns.

I propose that the large scale fracture pattern on Otrøy is caused by a combination of the two patterns, with a dominance of a hierarchical pattern. As comes up from the results that have been plotted in stereographic projections, the dominant directions make angles to each other in the range of 60 to 100°, which is consistent with the results from Iyer et al. [2008] (figure 8.7).
Though there are no generations of fractures found in the field, there are certainly some dominant directions present in the large scale fracture pattern, the most dominant being the ones at (very) low angle, and at approximately 90° to the compositional banding. Measurements in the histograms are somewhat more scattered, but this is because the number of measurements is too mea-

Kernel pattern

A kernel pattern – described by O'Hanley [1992] – consists of a core of partly serpentinized peridotite, bounded by a rim of fully serpentinized peridotite. Upon further hydration, the core of the kernel must expand, whereas the rim cannot expand anymore. This yields fracturing of the rim, perpendicular to the surface between peridotite and serpentinite, to accommodate for the expansion (figure 8.6A). Upon widening, fractures become a space wherein serpentine can grow, thus a serpentine vein is produced (figure 8.6B).

Fracturing occurs in three directions around the kernel core, because volume expansion is in three directions. Thus, fractures cross each other at the surface of the kernel at approximately 90° angles (figure 8.6C).

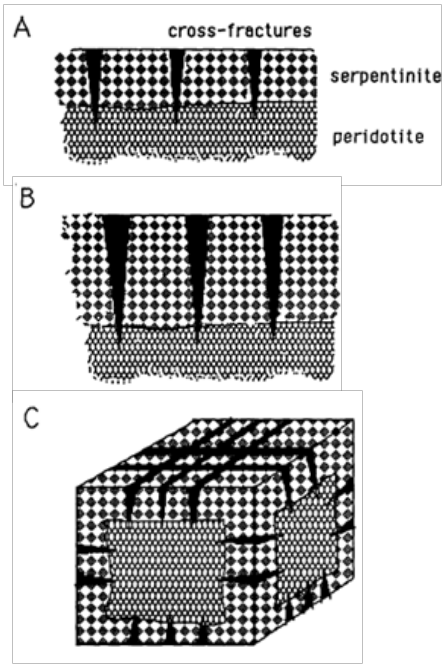

Figure 8.6. *The formation of a kernel pattern. After O'Hanley [1996]. A: Fractures form perpendicular to the serpentinite-peridotite boundary; B: fractures extent (in length and width) due to ongoing serpentinization and filling with serpentine is possible; C: fractures form in three directions around kernels.*

Hierarchical fracture pattern

Also assisted by volume changes, the theory of a hierarchical fracture pattern – as extensively described by Iyer et al. [2008]; though earlier mentioned as well by Hustrulid and Johnson [1990] – is based on a slow buildup of a stress field. The fracture pattern is caused by anisotropy of this stress field and the material properties. In this process, a first set of fractures is formed in a certain direction, and all later fractures form in directions that are determined by the first set and its corresponding stress field. Thus, the fracturing history is reasonably fixed after the first parallel set has formed. Fractures have a tendency to form at approximately 90° angles to each other (figure 8.7). Figure 8.8 shows the build-up of the pattern. Hierarchical fracturing can occur at several scales, thus at outcrop scale, but also at micro-scale, for instance in the mesh.

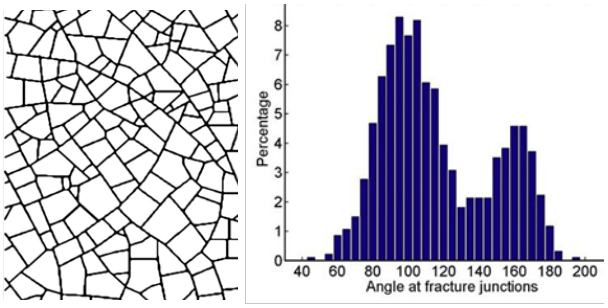

Figure 8.7. *Hierarchical fracture pattern and angles between fractures at their junctions. Most angles are around 90° and 160-180°. From Iyer et al. [2008].*

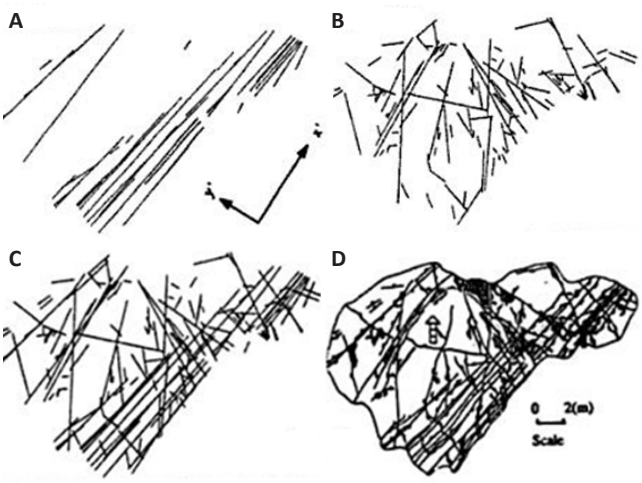

Figure 8.8. *Hierarchical fracture pattern formation, after Hustrulid and Johnson [1990]. A: Formation of fractures in one direction; B: a second set of fractures forms mostly perpendicular (and oblique) to the first set; C and D: total fracture set and appearance in outcrop.*

ger for this purpose. A more extensive discussion on the implications of these dominant directions is presented in subsection 8.4.

What pleads for a hierarchical fracture pattern as well is the different scales on which it can occur. As was observed in several sites, large scale fractures are interchanged with smaller scale fractures which have similar characteristics in terms of relative spacing and angles to each other (see subsection 5.2).

8.3.2 Dependence on compositional banding

It is certain that the folding of the compositional banding occurred before serpentinization and subsequent fracturing of the peridotite bodies. This is not extensively proven by observations from the field (subsection 5.5), but it would be logical to have found more proof in the field if the opposite was true. In that case, fractures would have been folded together with the compositional banding. This was never observed though. Also, Spengler [2006] states that the compositional banding was already folded before exhumation of the peridotites, at around 431 Ma, thus during continental collision and subduction.

The compositional banding that is widely present in the peridotite bodies may have caused the anisotropy in the material, which is the key initiator of a hierarchical fracture pattern. Differences in rock composition cause differences in degree of serpentinization, thus volume change, and thus a local stress field. This can onset the first direction of fracturing, as is also observed in pyroxenite lenses within the peridotite. It would explain the fractures having a dominantly parallel or perpendicular angle to this compositional banding.

However, I have some doubts on whether this compositional anisotropy is large enough through the whole body to produce such an extensive fracture set. Also, since there is no real evidence from the observations in this study for the dominance of one direction compared to the compositional banding, it is possible that a kernel pattern also played a role in the formation of the fracture sets, thus, with fractures forming in three perpendicular directions more or less at the same time.
A kernel pattern would explain the 90° fracture angles and the blocks that they form in outcrop (the kernels) as well. However, one of the most important features of a kernel pattern, i.e. a less serpentinized centre of a kernel relative to the rim, has not been found in the field. It can be that because of the high degree of serpentinization, the centre has also been serpentinized to a quite high level, and that the rim is therefore thicker and deeper under the surface. But even so, it seems likely that there would have been some signs of differentiation between fully serpentinized and less serpentinized rock in the field. Therefore, a kernel pattern is not likely here.

The comparison of rotated data between both bodies also argues against a strong dependence of fracture formation on the compositional banding. This is because is there are only similar orientations (poles form a WNW-ESE range), in the case that their compositional bandings are 40° apart. The stereographic projection of all data from both bodies rotated to one compositional banding gives much more scatter (figure 5.18).
Thus, it seems logical that a possible anisotropy in the rock caused by compositional banding may give a direction to the formation of the fracture pattern. However, with the results presented here, this does not show very clearly. Another factor that can have produced anisotropy (in the stress field) in the rock is tectonic decompression during exhumation of the bodies. This theory will be discussed in subsection 8.4.

8.4 Implications on tectonism

As discussed earlier on, the first fractures came into being due to differences in volume change due to anisotropy in the rock, and subsequent formation of stress fields. This process was possibly aided by the tectonic stresses that were caused by orogenic extension, by which the exhumation of the bodies was caused. Thus, the orientation of (at least some of) the fractures could have been caused by this extensional stress during exhumation, as will be shown here.

The convergent plate motion between Baltica and Laurentia caused mineral lineations in the subducted crust to form during eclogite facies metamorphism. These lineations are in the direction of subduction of the plate, and it is stated by Spengler [1996] that they actually have the same di-

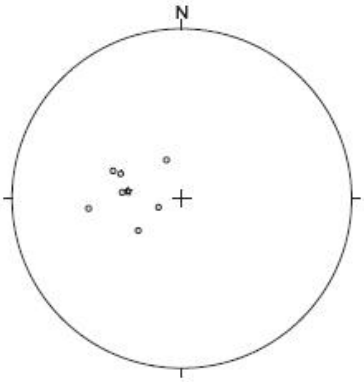

Figure 8.9. *Stereographic projection of mineral lineations in the gneiss surrounding the Otrøy peridotites. Mean direction is 278/64. From Spengler [2006].*

rection as the later phase of (W)NW-(E)SE exhumation, by which the subducted slab with intruded SCLM peridotites was relatively quickly brought to the surface. This would favor the theory of dunk tectonics, as mentioned in subsection 2.2. Because the slab subducted to the (W)NW, the plunge of the lineations must be similar, which is indeed shown in a stereographic projection of the lineations in Spengler [1996] (figure 8.9).

I suggest that when (hierarchical) fracturing in the peridotites is indeed for a substantial part caused by extensional stresses due to tectonic decompression, the normal vectors to a first forming fracture set must be equal to the direction of the surrounding lineations (figure 8.10).
When looking at the poles to the fracture planes in the Ugelvik peridotite body (figure 8.11A), this trend is present indeed. The set with poles to the (W)NW would be formed first, and the set with poles at about 90° angles to this would be the second-formed set. Although the poles are more scattered and have a less steep plunge than the lineations, this can very well be caused by some slight rotation of the body during it's late stage exhumation evolution.
In the Raudhaugene peridotite body, a good comparison with the lineations can be made as well (figure 8.11B). The 'first' set of fracture plane poles plots quite nicely in the same area as the lineations do. The orientation of the second set is not certain, however. This can be either one of both the other sets, the last set then being a third-formed fracture set, possibly.

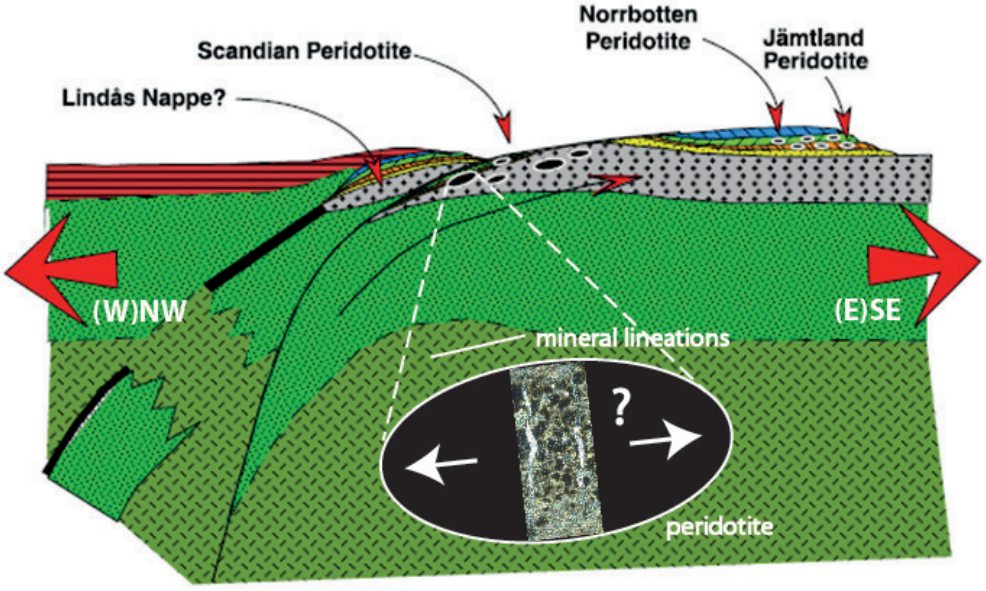

Figure 8.10. *The direction of extensional stress is the same as the orientation mineral lineations in the surrounding gneiss. Is this also the same as the normals to the fracture planes in the peridotite? After Brueckner and Van Roermund [2004].*

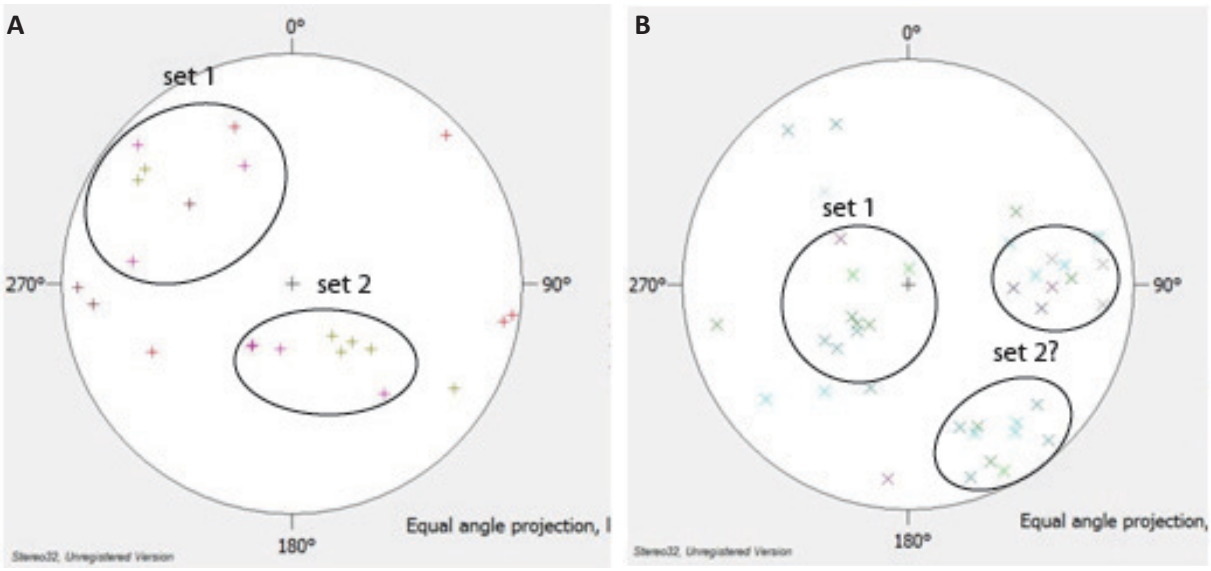

Figure 8.11. *Stereographic projection of two sets of poles to fracture planes, that can be linked to the direction of tectonic extension. A: Ugelvik; B: Raudhaugene.*

The difference with the Ugelvik body is that the sets plot in somewhat different areas, which would mean that both bodies have rotated independently from each other. Spengler [2006] mentions some late stage deformation which slightly refolded some existing structures in the bodies, but this is before serpentinization took place. In that case, it does not become clear what causes the discrepancy between these plots. Maybe this is the influence of the difference in orientation of compositional banding between the bodies, then. However, it is also likely that there have been just too few measurements for this purpose, as mentioned earlier.

In short, I propose that large scale fracture formation is caused by volume change in the rock due to serpentinization during exhumation. The direction of the formation of a first fracture set is mainly controlled by decompression (stress release) caused by tectonic extension in a (W)NW-(E)SE direction. This is probably aided by a more local anisotropy caused by compositional banding in the rock, though it is not certain to what extent.

8.5 Recommendations for future research

Some critical notes were made during this study, and these can have great value for future improvements and extensions to this research. The two most important difficulties that came up during the research were the determination of serpentine polymorphs and the analysis of the fracture plane measurements.
Because serpentine polymorphs all have such similar chemical characteristics, other analyses in addition to only microprobe results need to be done to add to the microscope analyses. For instance, high-resolution transmission electron microscopy (HRTEM) and (to a lesser extent) X-ray diffraction techniques would be very useful, because these can visualize the microstructure of the crystal surface on a nanoscale.
The analysis of measurements of fracture planes was uncertain because there were just too little measurements. It is necessary to collect and work with much larger datasets during future research, in order to give a more balanced interpretation of the data and to be able to make a better comparison with larger scale tectonics. Also, more information is needed on relative timing of the fracture sets. This can be determined by more detailed analyses of cross-cutting relationships between fractures in thin sections and in outcrop.

CONCLUSIONS

Hydration of mantle peridotites during exhumation causes serpentinization of the rock and fracturing as a consequence of volume change. Goal of this study was to determine the influence of other – larger scale – processes, like tectonic extension, on fracture formation. For this, research was performed on two peridotite bodies on the island of Otrøy, WGR, Norway. Spatial analysis of fractures was done and the mode of fracturing was determined, as well as the pressure and temperature conditions of their formation.

Microscope observations show at least five generations of serpentine formation, in both the mesh and in fractures. In the mesh, first lizardite forms, and is later overgrown by chrysotile. In fractures, a first stage of banded/kinked chrysotile is followed by triangular and later micro-granular lizardite. Cross-fractures are filled with chrysotile (banded/kinked or fibrous). The several fracture fillings show one stage of progressive open space circulation and higher nucleation rates, caused by a lowering in the pressure because of fracture opening and exhumation of the rock. Latest stage calcite filling in some fractures is not linked to this phase, but occurred close to the surface, if not at the surface.

Early hydration of the rock occurred at about 530°C, by reaction of olivine + talc (± chlorite) + water to serpentine (lizardite) in the mesh. Talc is not present anymore in most of the samples, but has probably all reacted away during serpentinization, which means that serpentinization indeed can have occurred at such high temperatures. The first fractures (chrysotile, also in the mesh) formed between 400 and 500°C. The total phase of serpentinization occurred between 530 and 180°C and between 0.5-0.1 GPa; pressures cannot be determined exactly because the serpentinization reactions hardly have a pressure dependence. Calcite filling of fractures occurred below 180°C and below 0.3GPa.
The rock underwent eclogite, amphibolite and greenschist facies during its retrograde path, which must have gone quite fast because there are much minerals of these facies preserved in the rock. This is in agreement with other studies [Spengler, 2006; Labrousse et al., 2004; Spengler et al. 2009; Scambelluri et al., 2008]. The PT path determined on the basis of mineral assemblages for the early retrograde metamorphism most resembles that of Scambelluri et al. [2008].

Spatial analysis of fracture patterns in outcrop show the presence of three fracture sets in the Raudhaugene peridotite body, which have 60-100° angles to each other. This is in agreement with a hierarchical fracture pattern. Since there is no relative timing between the sets, it cannot be determined which fracture set formed first. However, the normals of one set have the same (W) NW direction of orogen-normal extension mineral lineations in the surrounding gneiss, as depicted by Spengler [2006]. This implies the influence of tectonic stress release on fracturing during exhumation. The normals to the fractures in the Ugelvik peridotite body show a band, approximately NW-SE directed, with one set to the NW, which is also approximately the same direction as orogen-normal extension. Probably, fracturing first occurred in this (W)NW direction, caused by tectonic extension. The difference in direction of the first set between both bodies is maybe caused by more local anisotropy, due to the compositional banding.
The evidence for this, however, is not overwhelming and further research, in the form of much more measurements of fracture sets and an exact determination of relative timing between them, will be needed.

REFERENCES

Andreani, M., Mével, C., Boullier, A.-M., Escartín, J., 2007. Dynamic control on serpentine crystallization in veins: Constraints on hydration processes in oceanic peridotites. *Geochemistry Geophysics Geosystems*, **8** (2), 24 p.

Brueckner, H.K., Van Roermund, H.L.M., 2004. Dunk tectonics: A multiple subduction/eduction model for the evolution of the Scandinavian Caledonides. *Tectonics*, **23**, 20 p.

Bucher, K., Frey, M., 2002. *Petrogenesis of Metamorphic Rocks*. 7th edition. Springer-Verlag

Caillaud, J., Proust, D., Righi, D., 2006. Weathering sequences of rock-forming minerals in a serpentinite: Influence of microsystems on clay mineralogy. *Clays and Clay Minerals*, **54** (1), p. 87-100.

Carswell, D.A., 1963. Possible primary upper mantle peridotite in Norwegian basal gneiss. *Lithos,* **1**, p. 322-355.

Cocks, L.R.M., Torsvik, T.H., 2006. European geography in a global context from the Vendian to the end of the Palaeozoic. *Memoirs of the Geological Society of London*, **32**, p. 83-95.

Deer, W.A., Howie, R.A., Zussman, J., 1983. *An introduction to the rock-forming minerals*. Printing Press Ltd., Hong Kong.

Drury, M.R., Van Roermund, H.L.M., Carswell, D.A., De Smet, J.H., Van den Berg, A.P., Vlaar, N.J., 2001. Emplacement of deep upper-mantle rocks into cratonic lithosphere by convection and diapiric upwelling. *Journal of Petrology*, **42**, p. 131-140.

Hustrulid, W.A., Johnson, G.A., 1990. Rock mechanics: Contributions and challenges. *Proceedings of the 31st U.S. Symposium, Colorado School of Mines, Golden*.

Iyer, K., Jamtveit, B., Mathiesen, J., Malthe-Sørenssen, A., Feder, J., 2008. Reaction-assisted hierarchical fracturing during serpentinization. *Earth and Planetary Science Letters*, **267**, p. 503-516.

Jenkins, D.M., 1981. Experimental phase relations of hydrous peridotites modeled in the system H_2O-CaO-MgO-Al_2O_3-SiO_2. *Contributions to Mineralogy and Petrology*, **77**, p. 166-176.

Kelemen, P.B., Matter, J., 2008. In situ carbonation of peridotite for CO_2 storage. *Proc. Natl. Acad. Sci. U.S.A.,* **105**, p. 17295–17300.

Labrousse, L., Andersen, T.B., Agard, P., Hébert, R., Maluski, H., Schärer, U., 2004. Pressure-temperature-time deformation history of the exhumation of ultra-high pressure rocks in the Western Gneiss Region, Norway. *Geological Society of America Special Paper*, **380**, p. 155-183.

Medaris Jr., L.G., 1984. A geothermobarometric investigation of garnet peridotites in the Western Gneiss Region of Norway. *Contributions to Mineralogy and Petrology*, **87**, p. 72-86.

Mével, C., 2003. Serpentinization of abyssal peridotites at mid-ocean ridges. *C.R. Geoscience*, **335**, p. 825-852.

O'Hanley, D.S., 1992. Solution to the volume problem of serpentinization. *Geology*, **20**, p. 705-708.

O'Hanley, D.S., 1996. Serpentinites. *Oxford Monographs on Geology and Geophysics*, **34**, 277 p. Oxford University Press.

Scambelluri, M., Pettke, T., Van Roermund, H.L.M., 2008. Majoritic garnets monitor deep subduction fluid flow and mantle dynamics. *Geology*, **6** (1), p. 59-62.

Schmädicke, E., 2000. Phase relations in peridotitic and pyroxenitic rocks in the model systems CMASH and NCMASH. *Journal of Petrology*, **41** (1), p. 69-86.

Spengler, D., 2006. Origin and evolution of deep upper mantle rocks from western Norway. PhD thesis, Utrecht University, The Netherlands. *Geologica Ultraiectina,* **266**, 266 p.

Torsvik, T.H., Smethurst, M.A., Meert, J.G., Van der Voo, R., McKerrow, W.S., Brasier, M.D., Sturt, B.A., Walderhaug, H.J., 1996. Continental break-up and collision in the Neoproterozoic and Palaeozoic – A tale of Baltica and Laurentia. *Earth-Science Reviews*, **40**, p. 229-258.

Trommsdorff, V., Connolly, J.A.D., 1990. Constraints on phase diagram topology for the system CaO-MgO-SiO_2-CO_2-H_2O. *Contributions to Mineralogy and Petrology*, **104**, p. 1-7.

Van Roermund, H., 2009. Mantle-wedge garnet peridotites from the northernmost ultra-high pressure domain of the Western Gneiss Region, SW Norway. *European Journal of Mineralogy*, **21**, p. 1085-1096.

Whittaker, E.J.W., Wicks, F.J., 1970. Chemical differences among the serpentine "polymorphs": A discussion. *The American Mineralogist*, **55**, p. 1025-1047.

ACKNOWLEDGEMENTS

This study would not have been possible without the financial support by Prof. Dr. Chris Spiers and Dr. Martyn Drury, so I would like to thank them very much for that. Without the fieldwork on Otrøy, the project would have looked totally different, and a lot less interesting, in my opinion.
I would like to thank Martyn for his ideas on putting the fieldwork in the right shape, in order to be able to work independently in the field. Your regular advice by e-mail during the fieldwork was of great value.
Auke, thank you for your continuous willingness to help us out with all sorts of things, especially during the fieldwork preparations and analyses afterwards. Thanks for your quick responses when we went on expedition to the Hornsnipa anorthosite. Too bad we haven't been able to reach it after all.
I thank Tilly Bouten for her help in preparing and performing the microprobe analyses at Utrecht University.
Renske, my fieldpartner-in-crime, thanks for all the good times we had in beautiful Norway. I really enjoyed it all! Especially the never-ending rainy days on Otrøy, during which we strolled through the swampy field, dressed in our rainproof suits and a poncho over that: a perfect way to be able to write in our fieldbooks below our poncho, without getting them wet! And, of course, thank you for your part of the analyses, the useful discussions, and the sharing of our pictures; I used some good ones in this thesis.
Last of all, I would like to thank my parents for giving me the opportunity to study somewhat longer than 'normal', and spending three years on training very much and rowing matches. Thanks for always being there for me and helping me out when possible!

Renske and I during one of the few sunny days on Otrøy, and in between showers at our outcrop at the Raudhaugene peridotite body.

Serpentinization and fracture formation in peridotites on Otrøy, Western Gneiss Region, Norway: Late stage PT-conditions and implications for tectonic decompression - Thesis

Karen Oud, 2009-2010
MSc Geology
Utrecht University